Bioinspired solid catalysts
for the hydroxylation of methane

vorgelegt von

M.Eng.

Ha Vu Le

geb. in Quang Ngai, Vietnam

von der Fakultät II – Mathematik und Naturwissenschaften

der Technischen Universität Berlin

zur Erlangung des akademischen Grades

Doktor der Naturwissenschaften

Dr.rer.nat.

genehmigte Dissertation

Promotionsausschuss:

Vorsitzender: Prof. Dr. Reinhard Schomäcker

Gutachter: Prof. Dr. Arne Thomas

Gutachter: Prof. Dr. Christian Limberg

Tag der wissenschaftlichen Aussprache: 19. März 2018

Berlin 2018

Acknowledgements

Abbreviations

Abbreviation	Description
BAS	Brønsted acid sites
bcm	Billion cubic meters
BET	Brauner-Emmett-Teller
DFT	Density functional theory
DME	Dimethyl ether
DRM	Dry reforming of methane
EDX	Energy dispersive X-ray spectroscopy
EPR	Electron paramagnetic resonance
EXAFS	Extended X-ray absorption fine structure
FID	Flame ionization detector
FT-IR	Fourier-transform infrared spectroscopy
GC	Gas chromatography
GTL	Gas to liquid
ICP	Inductively coupled plasma
MFI	Framework type of ZSM-5, silicalite-1
MOR	Framework type of mordenite
MMO	Methane monooxygenase
MMT	Million metric tons
MS	Mass spectrometry
MTBE	Methyl *tert*-butyl ether
MTG	Methanol to gasoline
MTO	Methane to olefins
NADH	Nicotinamide adenine dinucleotide
NLDFT	Non-local density functional theory
NOCM	Non-oxidative coupling of methane
OCM	Oxidative coupling of methane
pMMO	Particulate methane monooxygenase

PXRD	Powder X-ray diffraction
RT	Room temperature
sMMO	Soluble methane monooxygenase
TAME	*tert*-Amyl methyl ether
TEM	Transmission electron microscopy
TEOS	Tetraethyl orthosilicate
TGA	Thermogravimetric analysis
TON	Turnover number
TPR	Temperature programmed reduction
UV-vis	Ultraviolet-visible
wt.%	Weight percent
XANES	X-ray absorption near edge structure
XPS	X-ray photoelectron spectroscopy
XRD	X-Ray diffraction
ZSM-5	Zeolite Socony Mobile-5

Abstract

Abundant and cheap resources including natural gas, methane hydrates, and biogas, whose major component is methane, have been considered as promising alternatives to decline the dependence of chemical and energy industries on crude oil. However, there is currently an underutilization of these resources, especially due to the costly transportation and storage, and high chemical inertness of methane. The one-step conversion of methane to more energy-dense liquid derivatives such as methanol is an economically efficient strategy to utilize the great potential of methane. Over the last decades, great interest and numerous efforts have been devoted to direct methane conversion processes with the aim of improving reactivity and selectivity of catalysts toward desired products. Many synthetic catalysts are inspired by the exceptional performance of Fe- and Cu-dependent enzymes (methane monooxygenases) in methanotrophs for the hydroxylation of methane under ambient conditions. In this contribution, the development and use of bioinspired solid catalysts for the partial oxidation of methane to methanol by either H_2O_2 or O_2 at low temperature are presented.

The first part of the thesis focused on the methanol production over Fe-containing zeolites using H_2O_2 as an oxidant. The catalytic activity of these catalysts was found to be dependent on the protocol used to load Fe species into the zeolite framework. Fe-exchanged ZSM-5 activates H_2O_2 and methane, respectively, at a previously proposed diiron site, yielding methyl hydroperoxide (MeOOH) as an intermediate. To obtain high yields of methanol upon decomposition of MeOOH, the formation of highly reactive hydroxyl radicals, which can further oxidize MeOOH into unwanted products, should be controlled by adding Cu species and performing the reaction under mild conditions. On the other hand, extra-framework Fe species in Fe-silicalite-1, proposed to be isolated sites due to the low overall Fe content (0.4–0.8 wt.%), were obtained via hydrothermal synthesis and subsequent thermal treatment. Such isolated Fe sites are capable of converting methane to methanol via facilitating the formation of the hydroxyl radicals like a Fenton system.

Zeolites loaded with Cu species are inactive in the above mentioned H_2O_2-mediated system but known as the most efficient catalysts for the stepwise oxidation of methane to methanol by O_2. In the next chapter, it is described that the Cu-exchange protocol had a considerably influence on the methanol production. Solid-state ion-exchanged Cu/mordenites exhibited a much higher activity than the ones prepared by a conventional liquid-phase procedure. From temperature-programmed reduction by H_2 and infrared spectroscopy measurements, it was concluded that the

solid-state protocol accelerates the Cu exchange at the small pores of mordenite, where the most active Cu species are preferably located. *In situ* UV-Vis spectroscopy showed that different active Cu clusters are formed in the catalyst upon the treatment in O_2. After the activation of methane, different intermediates seem to be formed and stabilized at the Cu sites. The main intermediate is a methoxy species, which can be further converted to methanol or dimethyl ether (DME) via the reaction with water or methanol, respectively.

Furthermore, within the next chapter it was demonstrated that CuO species supported on SBA-15 are able to react with methane and subsequently produce methanol with a high selectivity (> 84%) via water-assisted extraction. The cluster size of the CuO species can be varied by the Cu-compounds applied for preparing the catalyst, leading to different catalytic performances. It was proposed that highly dispersed small CuO clusters are responsible for the activity.

Table of Contents

Chapter 1

Introduction

1.1 Utilization of methane in chemical industry

1.1.1 Methane potential

When the late-18th-century Italian physicist Alessandro Volta first identified methane as an inflammable gas in the bubbles that were released from waterlogged marshes, he could not foresee the great importance of this gas to human society in the following centuries.[1] Nowadays, methane is not only an energy source applied in both industrial and domestic scales but also a promising carbon feedstock for chemical manufacture.[1]

Methane is the major component of natural gas (55–99.5 % by volume) that is a very abundant fossil resource widely distributed around the globe. Varied amounts of C_2^+ hydrocarbons and other gases such as N_2, He, H_2S and CO_2 are also found in natural gas.[2-4] Natural gas is conventionally recovered as a free gas from the formation of either crude oil or easily accessible rock, namely carbonate, sandstone, and siltstone while non-conventional sources including shale gas, tight gas, coal bed methane, methane hydrate attract increasing attention due to their huge reserves.[5] Currently, advanced drilling and extraction approaches allow natural gas resources to be efficiently exploited. The estimated quantity of technically recoverable natural gas in the US is capable of providing the domestic market with 100 years of natural gas at current usage rates.[6] According to the annually published BP Statistical Review of World Energy, approximately 190 x 10^{12} m^3 of natural gas remain uncaptured in 2013 while the amount of methane stored in hydrates, which is not included in the report, can be up to 15 000 x 10^{12} m^3.[7,8] Another source of methane is biogas with nearly equal concentrations of methane and CO_2 facilely produced from catabolism of organic solids, sludge, and wastewater by methanogenic bacteria (methanogens) in anaerobic environments. The anaerobic production of biogas plays a core role in the treatment of waste and biomass due to the greatly advantageous reuse of methane compared to other biological processes.[9-11] The amount of biogas produced in the European Union in 2010 is corresponding to 1.1 x 10^{10} m^3 of natural gas.[7] Unlike natural gas, which was generated millions of years ago, biogas is considered as a renewable and carbon-neutral source for long-term energy sustainability.[12]

On the other hand, methane is also identified as a greenhouse gas. It was estimated that methane has a 25 times larger potential impact than CO_2 on global warming due to the combined ability of methane to trap heat and absorb infrared radiation.[13] As a consequence, methane contributes about 20% of overall global warming potential each year even though the concentration of

methane in the atmosphere is much lower than that of CO_2 (1.813 ppm and 390.5 ppm, respectively, in 2011).[6,14] Sources of methane emission are generally classified in two categories, including natural sources and anthropogenic sources (Figure 1.1).[13] Human activities are responsible for two-thirds of the total methane emissions, including leakages from the exploitation of coal, oil, and natural gas.[15] Like CO_2, the methane amount released from the anthropogenic sources into the atmosphere has continuously increased since 1978 and this value reached about 6875 million metric tons CO_2 equivalent in 2010.[13,14] Development of technologies to efficiently utilize methane should be therefore pursued to mitigate its negative effect on the earth climate.[6]

(a) Natural methane emissions

Wetlands 72%
Termites 13%
Oceans 6%
Others 9%

(b) Anthropogenic methane emissions

Enteric fermentation 28%
Oil and gas 18%
Rice cultivation 10%
Other argriculture 10%
Landfill 10%
Wastewater 8%
Manure management 6%
Coal mining 6%
Biomass 3%
Others 1%
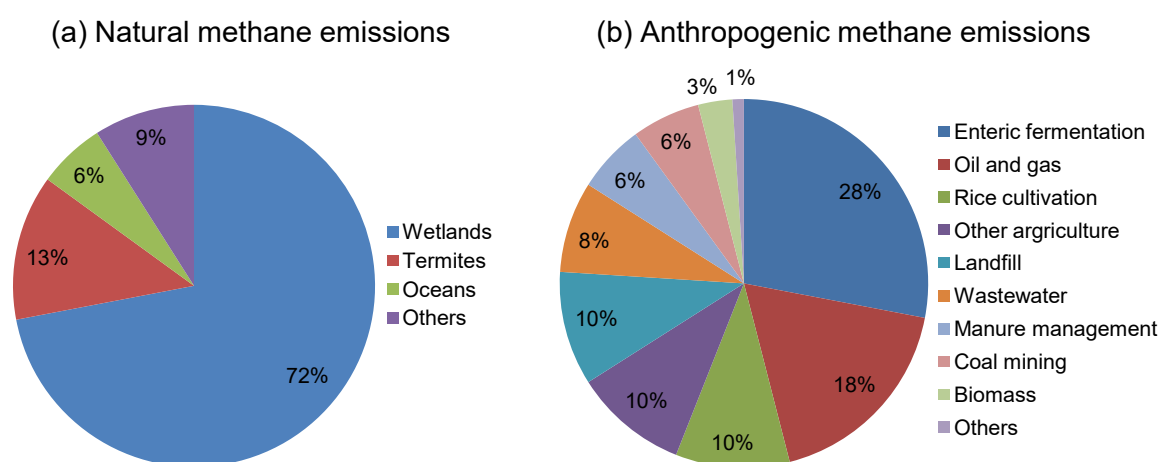
Figure 1.1. Contribution of individual sources to (a) total natural methane emissions and (b) total anthropogenic methane emissions. Reproduced with permission from ref. 13 (Copyright 2016 Elsevier).

Population explosion and rapid industrialization have resulted in a ceaseless increase of energy demand over the years.[14] Despite noteworthy achievements in developing renewable energy sources, production of energy is strongly dependent on carbon-based sources, namely gas, oil and coal, which is forecasted to make up more than 76% of the total consumed energy of the world in 2040.[16] The increasing availability of natural gas has lowered its commercial price and natural gas is generally cheaper than gasoline based on an energy-equivalent basis.[6] Importantly, among three carbon-based sources, combustion of methane generates the lowest amount of CO_2 per unit of energy due to its low C/H ratio.[15,16] In addition, as introduced above, methane can be easily obtained from the renewable organic feedstocks via biogas generation. Possessing the great benefits of both conventional and sustainable energy sources, methane has therefore gained increasing attention in the energy industry. It is estimated that natural gas contributed 22% of the worldwide primary energy supply in 2012 and the natural gas demand for energy generation

grows at the highest average rate of 1.7% per year as compared to those of oil and coal (0.9% per year and 1.3% per year, respectively) (Figure 1.2).[5,16]
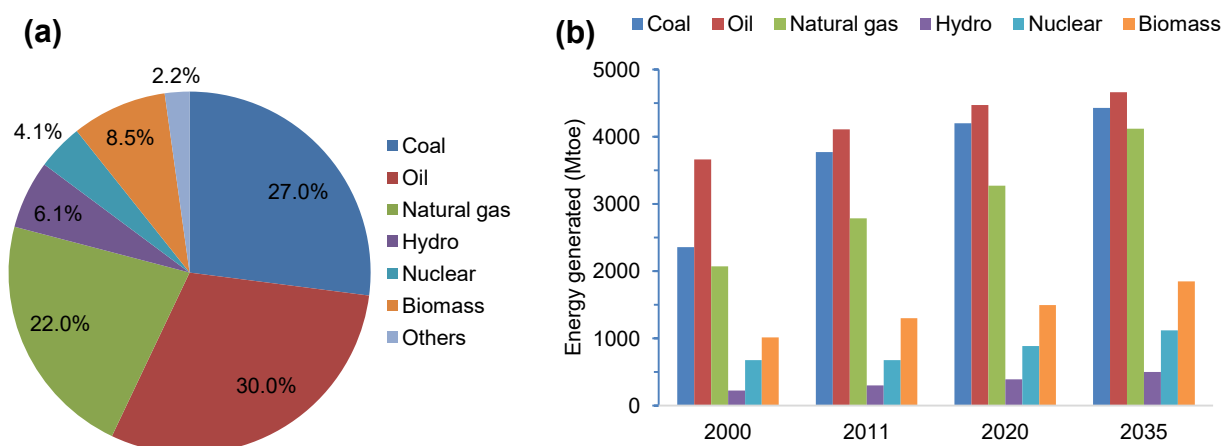
Figure 1.2. (a) Worldwide energy consumption of different fuel sources in 2012. Reproduced with permission from ref. 5 (Copyright 2016 American Chemical Society). (b) World's primary energy demand from 2000 to 2035 based on the data in World Energy Outlook 2013 of International Energy Agency.[17]
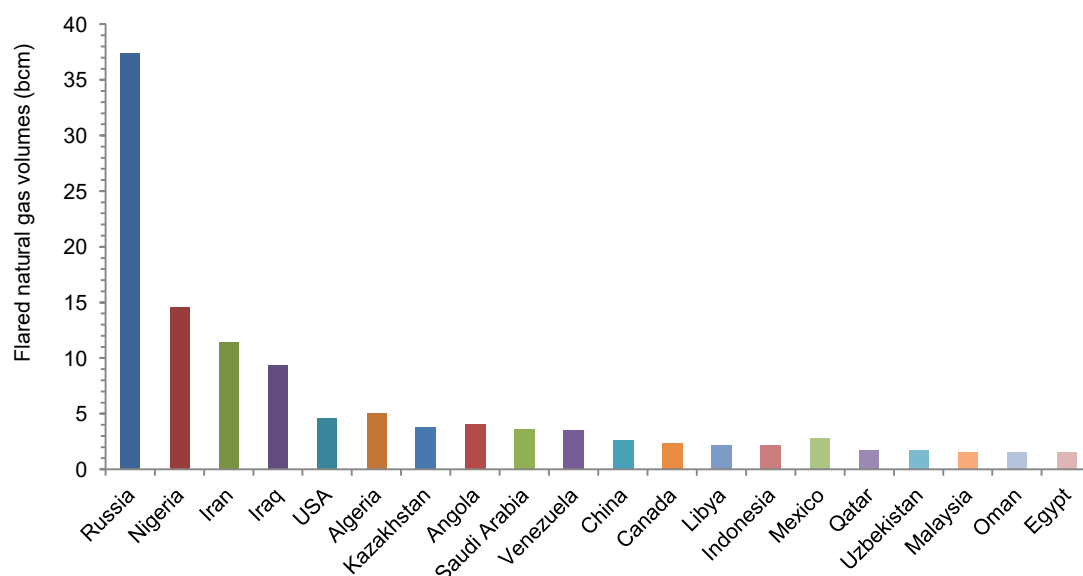
Figure 1.3. Top 20 countries for flaring of natural gas in 2011 based on the data of Global Gas Flaring Reduction Partnership.[18]

From both environmental and economical points of view, natural gas is the most promising alternative to other fossil sources for energy and chemical industries. Currently, the majority of natural gas, more than 90 % of the global production, is simply used to generate energy for heating, cooking and transportation purposes in industrial and residential sectors and for

electricity production.[7] In spite of its vast availability, versatility and smaller environmental footprint, the use of methane as a chemical raw material is still limited.[19] Furthermore, a decreasing but still significant amount of valuable natural gas, namely from 172 billion cubic meters (bcm) in 2005 to 140 bcm in 2011, is uselessly flared in many fields of Russia, Nigeria, Iran, Iraq and others, emitting millions of tons of CO_2 into the atmosphere (Figure 1.3).[7,18,20] The main reason for such wasteful and harmful treatment lies in the high cost of natural gas transportation and storage. Methane is a gas at atmospheric pressure with a low boiling point of - 161.5 °C while most of the natural gas reservoirs are located far from consumers or are in the areas where the gas need is negligible. Therefore, long-distance transportation of natural gas via pipelines to potential markets is impractical and uneconomical (Figure 1.4).[2,14,19] Although it can be converted in either compressed natural gas or liquefied natural gas, high energy inputs and expensive investment and operating costs are required for such processes. In addition, both these forms of natural gas are obviously unsafe as stored and shipped at high pressure (up to 250 bar) and low temperature (-160 °C).[9]
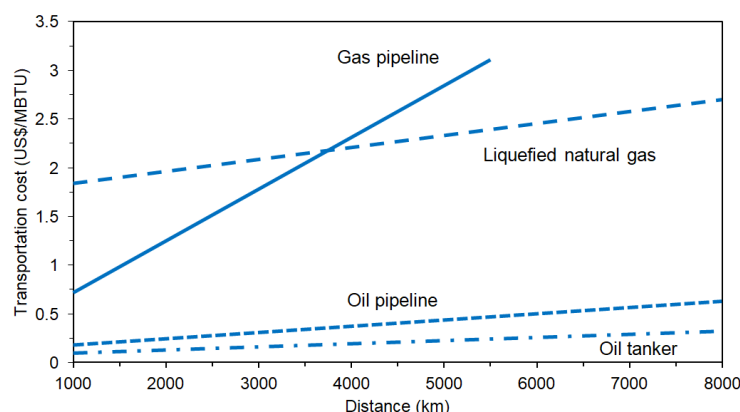
Figure 1.4. Estimated cost to transport natural gas and oil by different means. Reproduced with permission from ref. 2 (Copyright 1998 Springer).

Transformation of methane to more energy-dense liquid derivatives and value-added products would significantly expand the scale of methane consumption and access the great potential of the carbon and hydrogen sources in methane for the chemical industry. The most ideal fuels, such as methanol, DME, longer alkanes, etc., would not only be facilely and uncostly transportable compared to natural gas but also retain nearly all of the energy content of methane. Furthermore, methanol and DME can be further used as efficient and flexible building blocks in place of declining petroleum to produce valuable organic compounds via either direct or indirect routes.[21-23] To date, two indirect approaches for the conversion of methane to liquid fuels have been commercially applied, including methane-to-methanol and Fischer-Tropsch synthesis for

production of hydrocarbons. Both these processes have to undergo an energy-intensive intermediate step of synthesis gas (syngas – a mixture of CO, H_2 and small traces of CO_2) manufacture.[24] The high investment cost and the large scale are required for the syngas route, hindering the utilization of inconveniently located natural gas resources and small-scale biogas plants. Therefore, the direct methane conversion to methanol and hydrocarbons would be more economically attractive, energy-efficient, and environmentally friendly.[15,25]

Table 1.1. Various quantitative measures of reactivity of methane, methanol, and ethylene.[21,25]

Property	Methane	Methanol	Ethylene
Boiling point (^{o}C)	-161.5	64.7	-103.7
Water solubility at 1 atm, 25 ^{o}C (mM)	1	miscible	5
Dipole moment (D)	0	1.69	0
First bond dissociation energy (kJ mol^{-1})	439 (C-H)	402 (C-H)	268 (π bond)
Ionization potential (eV)	12.6	10.8	10.5
Electron affinity (eV)	1.5	1.4	0.5
Proton affinity	553	762	678
pK_a in DMSO (kJ mol^{-1})	50	15	44

Unfortunately, the direct methane conversion routes still remain a major challenge in chemistry. The primary reason is of the high inertness of methane. A methane molecule has a perfect tetrahedral geometry with four C-H bonds upon the sp^3 hybridization of the central carbon atom. With the highest C-H bond strength (the first bond dissociation energy of 439 kJ mol^{-1}), methane is the least reactive hydrocarbon.[25] A relatively high local electric field is required to polarize methane due to the absence of dipole moment and the small polarization of the C-H bond. Also, methane exhibits a high ionization energy, low electron and proton affinities, and a weak acidity, which make reactions involving nucleophilic and electrophilic attacks, electron transfer, and deprotonation unfavorable with methane. These characteristics of methane explain its high stability and the high difficulty in its activation.[25,26] On the other hand, more seriously, the target molecules (e.g., methanol, formaldehyde, and ethylene) are much more reactive than methane (Table 1.1) while aggressive reactants and harsh reaction conditions have to be applied to activate the C-H bond of methane. Thus, undesired reactions of the products (e.g., deeper oxidation, oligomerization, and carbonization) would be simultaneously promoted, leading to

losses in activity and selectivity.[27,28] The efficient conversion of methane is regarded as a ''Holy Grail'' in the chemical community.[28] Therefore, in spite of many favorable factors, methane is not yet competitive to oil in use as a raw material for the manufacture of the chemicals and fuels. Apart from the syngas production, just a small number of direct pathways including radical halogenations, thermal pyrolysis to acetylene, and coupling with ammonia to hydrogen cyanide are developed in small-scale plants (Figure 1.5).[7] Nevertheless, recent advances of methane conversion processes, in which catalysts have been considered as a key of success, are promising for widely industrial implementation in the near future.
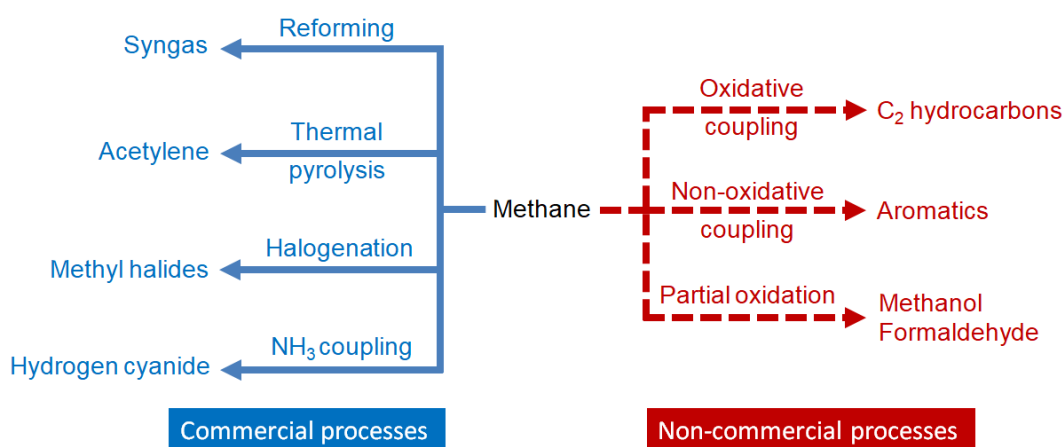
Figure 1.5. An overview of methane conversion processes.

1.1.2 Commercialized methane conversion processes

1.1.2.1 Syngas production
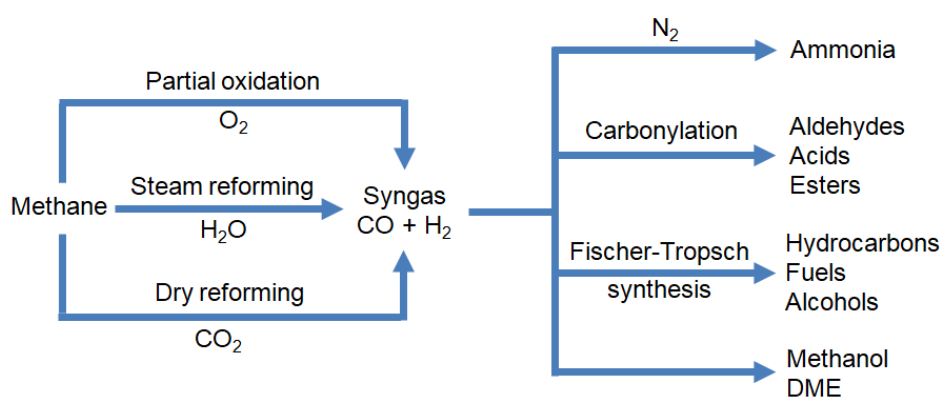
Figure 1.6. Industrial conversion of methane to a range of liquid and gaseous chemicals via the syngas route.[19]

Today, the most commercially viable process using methane as a feedstock is the syngas production, which is called reforming of methane.[23,27] The technology for this conversion is

highly developed and optimized at large scales.[29] Initially, the produced syngas mixture containing CO and H_2 was directly used as to generate electricity and heat.[30] Furthermore, the syngas can also be a versatile and important intermediate in the chemical industry (Figure 1.6). The H_2 source separated from the syngas mixture is forwarded to ammonia synthesis. The majority of methanol is currently made from syngas via a hydrogenation process catalyzed by $Cu/ZnO/Al_2O_3$, which would be described in detail in Section 1.2.1. Importantly, the following Fischer-Tropsch synthesis, in which CO and H_2 are exothermically converted into hydrocarbons and alcohols on Fe, Co or Ru catalysts with a very high selectivity, has significantly contributed to the rapidly growing demand for transportation fuels.[19,23,31] The syngas is processed in Fischer-Tropsch reactors with various designs, depending on the desired long-chain alkane products (approximated as $2(n+1)H_2 + nCO \rightarrow C_nH_{2n+2} + nH_2O$, typically n = 10–20). The Fischer-Tropsch processes are able to produce a variety of liquid fuels, particularly diesel and jet fuel that were proven to possess a significantly higher quality than the ones derived from crude oil.[6,19]

Table 1.2. Principal processes in syngas production from methane.[29,30]

Process	Main reaction	ΔH_{298} (kJ mol^{-1})	H_2:CO ratio	Reaction conditions
Steam reforming	$CH_4 + H_2O \rightleftharpoons CO + 3H_2$	206	3:1	800–900 ^{o}C, 15–30 bar
Dry reforming	$CH_4 + CO_2 \rightleftharpoons 2CO + 2H_2$	24	1:1	> 750 ^{o}C, 1 bar
Partial oxidation	$CH_4 + 0.5O_2 \rightleftharpoons CO + 2H_2$	-36	2:1	> 750 ^{o}C, 1 bar

Basically, methane can be upgraded to the syngas via three different processes including steam reforming, oxy reforming (partial oxidation), and CO_2 reforming (dry reforming) of methane. In general, these techniques of methane reforming differ in the oxidant, the catalyst, the final H_2/CO ratio, and the reaction kinetics (Table 1.2).[11,30,32] The processes of steam reforming and partial oxidation of methane have been commercially practiced while methane reforming with CO_2, which is a very attractive and potential route because it utilizes both major greenhouse gases, has still been under investigation to improve efficiency for the industrial application.[14,23,31]

Steam reforming of methane is the most developed process initially for the production of H_2 from methane. About 48% of the H_2 amount in the world is produced by steam reforming.[23,27] Industrially, the reaction of methane with steam occurs at 800–900 ^{o}C and 15–30 bar over an Ni/Al_2O_3 catalyst, yielding an H_2-rich syngas mixture.[32,33] To achieve a high methane conversion, an H_2O:CH_4 feed ratio of ~ 1:3 is required for this highly endothermic reaction.[31]

The significant challenges in the Ni/Al_2O_3-based process consist of deactivation of the catalyst due to coke formation (Reactions 1 and 2) and sintering Ni particles at the high temperature.[7,27,34] Addition of rare earth oxides or alkaline metals to the catalytic system can prevent such unwanted phenomena, improving the catalyst lifetime.[32] The process is also accompanied by the water gas shift reaction, in which CO reacts with steam into CO_2 and H_2 (Reaction 3).[27] Interestingly, the H_2/CO ratio from the steam reforming reactor which is too high for the Fischer-Tropsch process can be reduced by adding fresh CO_2 for the further reverse water shift reaction.[31]

$$CH_4 \rightleftharpoons C_{(s)} + 2H_2 \qquad\qquad \Delta H_{298} = 75 \text{ kJ mol}^{-1} \qquad\qquad (1)$$

$$2CO \rightleftharpoons C_{(s)} + CO_2 \qquad\qquad \Delta H_{298} = -172 \text{ kJ mol}^{-1} \qquad\qquad (2)$$

$$CO + H_2O_{(g)} \rightleftharpoons CO_2 + H_2 \qquad\qquad \Delta H_{298} = -41 \text{ kJ mol}^{-1} \qquad\qquad (3)$$
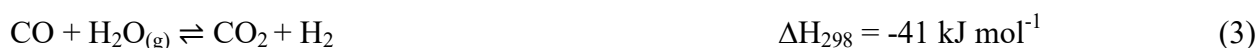
Dry reforming of methane consumes two most abundant and potential greenhouse gases, i.e., CO_2 and methane, to generate CO and H_2 in a 1:1 ratio. This process not only diminishes CO_2 and methane emissions but also guides an efficient approach to utilize low-grade natural gas resources and biogas.[11,14,23] Similar to steam reforming of methane, the reaction is highly endothermic and commonly catalyzed by transition metals supported on oxides.[27] Catalyst deactivation by intense coke deposition still is a great challenge of the dry reforming route. Cheap Ni-based catalysts show a comparable catalytic activity with noble metals but are readily deactivated. There have been many attempts to prolong the catalyst lifetime by improving the resistance to the carbon production, for example, use of noble metal oxides as promoters.[11,34,35] Although it was estimated that this process produces high-purity syngas containing little CO_2 and needs a 20% lower total operating cost compared to the other reforming processes, so far, no technology solely based on dry reforming of methane has enough efficiency for commercialization.[11,29,34]

Partial oxidation of methane to syngas is the only exothermic process of methane reforming giving a CO/H_2 ratio of 1:2, which is suitable for the following production of methanol and Fischer-Tropsch fuels. This route can be conducted either catalytically or non-catalytically (homogeneously).[30] The catalyst-free reaction requires very high temperatures (up to 2000 °C) and always involves decomposition of methane to carbon black.[19,32] As expected, the presence of a catalyst can lower the reaction temperature (< 1000 °C), giving a high methane conversion at very high space velocities.[30,31,36] Major challenges in oxy reforming of methane are related to

safety. A mixture of methane and O_2 is extremely dangerous for the industrial use while the high-temperature oxidation reaction is very difficult to control. In addition, hot spots formed in this autonomous oxidative process are difficult to handle, leading to local overheating.[23] The non-catalytic partial oxidation of methane into the syngas has been well-established while the issue of catalyst stability prevents the catalytic process from being industrialized.[23,36]
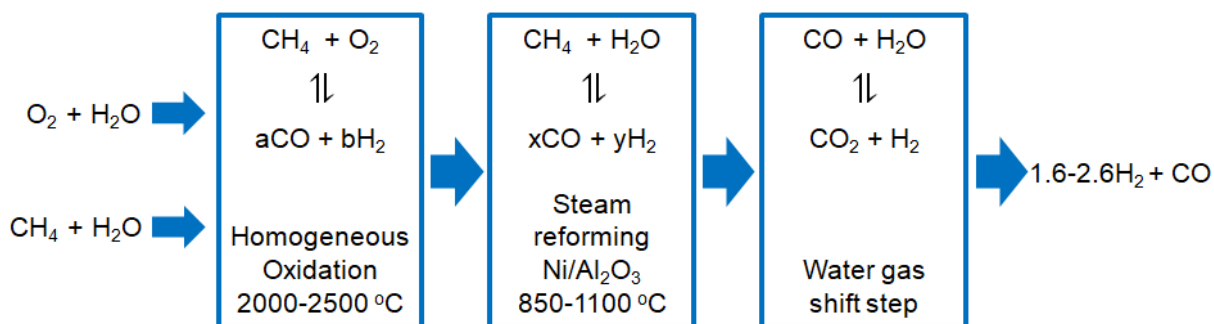
Figure 1.7. Production of syngas based on methane autothermal reforming.[7,32] Adapted with permission from ref. 32 (Copyright 2016 Elsevier).

The technology choice for sygas production is dependent on the downstream application.[37] Therefore, further methane reforming processes have been developed to obtain a higher energy efficiency and an H_2/CO ratio expected toward the subsequent chemical syntheses. Autothermal reforming is a combination of steam reforming and partial methane oxidation, in which steam and O_2 are simultaneously used (Figure 1.7).[7,31,32] This route is more economical and better controlled (overall $\Delta H \sim 0$), yielding CO/H_2 ratios more favorable for methanol synthesis and Fischer-Tropsch processes. Furthermore, combined reforming using $H_2O/O_2/CO_2$ as oxidants is designed to prevent the hot spots and the coke formation.[11,23,30]

1.1.2.2 Synthesis of methyl halides

The activation of methane via halogenation is a well-known process in organic chemistry to convert methane into many organic compounds. The reaction typically proceeds by a free-radical mechanism, yielding a mixture of halogenated methanes ($CH_{4-n}X_n$) and lacking selectivity to a particular product.[23,28] The highly exothermic reaction between methane and F_2 is extremely difficult to control. On the other hand, the equilibrium conversion between methane and I_2 is low (e.g., only 10% at 650 ^oC) and iodomethane readily decomposes to I_2 and hydrocarbons. Therefore, only chlorination and bromination of methane are of practical interest for a large-scale process.[7,23] By controlling the reaction conditions and employing a suitable catalyst, the selectivity to methyl halides (CH_3Cl and CH_3Br) could be enhanced (Reaction 4). Olah *et al.*

showed that the synthesis of monohalogenated methane over a supported acidic catalyst (e.g., $TaOF_3/Al_2O_3$) or supported noble metal catalyst (e.g., Pt/Al_2O_3) at 180–250 $^{\circ}$C led to a selectivity higher than 90%.[27,28]

$$CH_4 + Br_{2(g)} \rightarrow CH_3Br + HBr \qquad \Delta H_{298} = -28.0 \text{ kJ mol}^{-1} \qquad (4)$$

$$CH_4 + HBr + 0.5O_2 \rightarrow CH_3Br + H_2O \qquad \Delta H_{298} = -166.0 \text{ kJ mol}^{-1} \qquad (5)$$

$$2CH_4 + HBr + O_2 \rightarrow CH_3Br + CO + 3H_2O_{(g)} \qquad \Delta H_{298} = -686.0 \text{ kJ mol}^{-1} \qquad (6)$$

$$CH_3Br + CO + H_2O_{(g)} \rightarrow CH_3COOH_{(g)} + HBr \qquad \Delta H_{298} = -89.0 \text{ kJ mol}^{-1} \qquad (7)$$
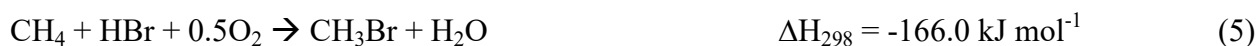
Although methyl halides are valuable intermediates which can then undergo catalytic hydrolysis and coupling reactions to produce methanol, DME, alkanes, olefins, and aromatics under mild conditions with high yields, the corrosive and toxic nature of halogen and hydrogen halide hinders the wide utilization of these chemical processes.[7,23] The oxidative halogenation (also called oxyhalogenation) of methane using noble metal catalysts such as $LaCl_3$, Ru/SiO_2 and Rh/SiO_2 or an $FePO_4/SiO_2$ catalyst, in which reactive halogen species can be *in situ* formed by oxidation of a hydrogen halide with O_2, was therefore developed to avoid the presence of halogen and achieve a higher atom efficiency (Reaction 5).[23,27,28] In this alternative route, CO and CO_2 are major by-products. Interestingly, under controlled conditions, a mixture of methyl halide and CO with a ratio of 1:1 can be obtained, which is a potential feedstock for the production of acetic acid in the subsequent step (Reactions 6 and 7).[23,28]

1.1.2.3 Non-catalytic synthesis of acetylene

The thermal decomposition of methane at high temperatures may yield ethylene, acetylene, benzene, and hydrogen. The chemistry of this reaction is strongly dependent on equilibrium limitations.[29,37] At elevated temperature, radicals including $CH_3\cdot$, $CH_2\cdot$ and $CH\cdot$ generated from methane may be combined to give acetylene. The overall reaction can be described as a stepwise dehydrogenation (Reaction 8).[2,37]

$$2CH_4 \xrightarrow{-H_2} C_2H_6 \xrightarrow{-H_2} C_2H_4 \xrightarrow{-H_2} C_2H_2 \xrightarrow{-H_2} 2C \qquad (8)$$
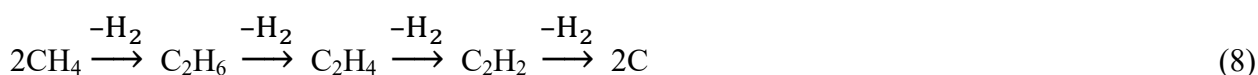
In fact, methane can be converted directly to acetylene by pyrolysis with high yields. Applying short reaction times and low partial pressures of methane preferably by hydrogen dilution of the

feed and rapid quenching of the reaction mixture can reduce the formation of carbon. Holmen *et al.* proved that high yields of acetylene (> 90%) could be obtained at temperatures higher than 1800 $^{\circ}$C and with extremely short reaction times (< 0.01 s) (Figure 1.8).[37,38] The well-established processes to produce acetylene from methane are not attractive anymore due to the emergence of ethylene as an important alternative building block in petrochemistry. Because of the relative rates of the possible reactions, it is difficult to obtain high yields of ethylene by the thermal decomposition of methane.[37] Several reaction schemes to produce ethylene have recently been proposed and even tested in a small pilot plant. Selectivites of 32 and 23% toward acetylene and ethylene, respectively, at an overall methane conversion of 31% were achieved at 1200 $^{\circ}$C; however the process also remarkably yielded benzene (15%) and coke (18%). Furthermore, a combined route that initially cracks methane to form acetylene and then selectively hydrogenates acetylene into ethylene in another reactor has been studied by a US company.[19,37]
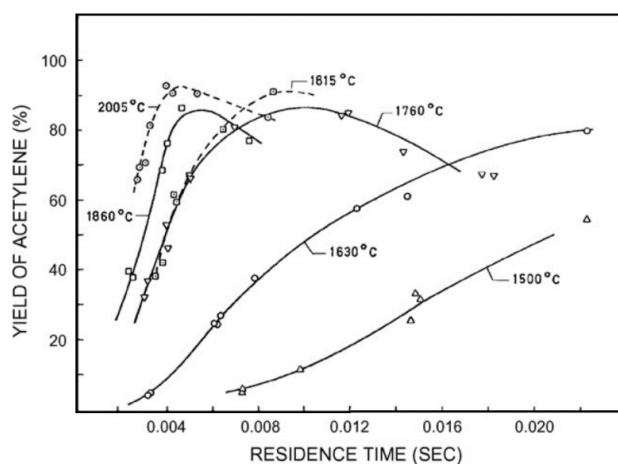
Figure 1.8. Acetylene yields from the pyrolysis of methane (Reaction conditions: CH_4/H_2 = 1:1, P_{total} = 100 mmHg, solid lines: inner diameter of reactor = 7 mm, cold finger quench; dotted lines: inner diameter of reactor = 10 mm, direct water quench). Reprinted with permission from ref. 38 (Copyright 1976 American Chemical Society).

1.1.2.4 Synthesis of hydrogen cyanide

The production of HCN from methane and NH_3 in the absence of O_2 (Degussa or BMA process, Reaction 9) or in the presence of O_2 (Andrussow process, Reaction 10) has been industrially developed for several decades.[28] The O_2-free route is conducted at ~ 1200 $^{\circ}$C over a Pt catalyst coated to the wall of a tubular reactor.[7] Schwarz *et al.* proposed the formation of HCN based on two reaction sequences, both of which start with dehydrogenation of methane by a bare platinum cation to yield a platinum carbine intermediate $[PtCH_2]^+$ (Figure 1.9).[7,39] Addition of O_2 to the

CH_4/NH_3 coupling is able to improve the rate of HCN formation by several orders of magnitude. Therefore, the Andrussow process uses a catalytic Pt/Rh gauze reactor, which is adiabatically operated, at millisecond contact times.[7] Because of being highly exothermic, the Andrussow route is of higher importance compared to the BMA process, contributing the majority of the industrial HCN production.[2]

$$CH_4 + NH_3 \rightleftharpoons HCN + 3H_2 \qquad\qquad \Delta H_{298} = 251 \text{ kJ mol}^{-1} \qquad\qquad (9)$$

$$CH_4 + NH_3 + 1.5O_2 \rightarrow HCN + 3H_2O \qquad\qquad \Delta H_{298} = -481 \text{ kJ mol}^{-1} \qquad\qquad (10)$$
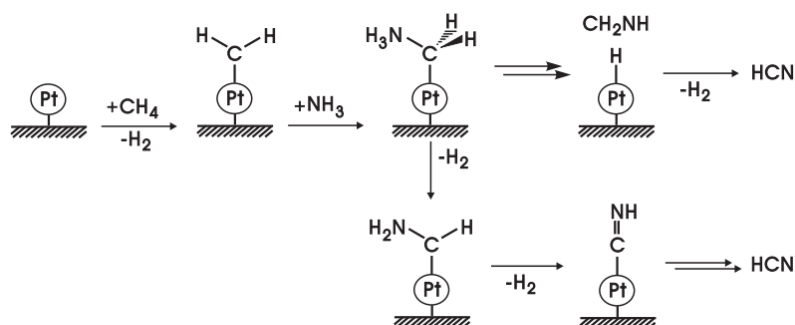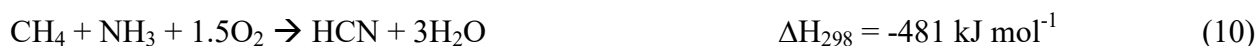
Figure 1.9. Proposed mechanism for the Pt-catalyzed coupling of methane with ammonia. Reprinted with permission from ref. 39 (Copyright 1998 Wiley-VCH).

1.1.3 Promising direct routes of catalytic methane conversion

1.1.3.1 Oxidative coupling of methane (OCM)

$$2CH_4 + O_2 \rightarrow C_2H_4 + 2H_2O \qquad\qquad \Delta H_{298} = -281.8 \text{ kJ mol}^{-1} \qquad\qquad (11)$$

Ethylene is known as one of the most important feedstocks for the chemical industry; therefore, the production of the C_2 hydrocarbons from methane, which provides a promising alternative to traditional processes based on petroleum and syngas, has received much attention in the last decades. Because the oxidant-free and catalyst-free coupling reaction of methane is not favorable to produce ethylene as mentioned above, many efforts have been devoted to developing the catalytic oxidative coupling route that is thermodynamically more advantageous occurs at lower temperatures and therefore avoids the formation of carbon and aromatics.[2,3,23,40] Since the first report of Keller *et al.* in 1982, all aspects of the OCM reaction have been critically studied. In this pathway, methane reacts with O_2 over a solid catalyst to form ethane and ethylene with the latter one being more desired (Reaction 11).[37] Small amounts of C_3^+ hydrocarbons and H_2 can also be detected from the outlet stream.[2] The selective formation of ethylene is proposed to

proceed via three steps: (i) activation of methane to methyl radical through a cleavage of a C-H bond, (ii) homogeneous coupling of two methyl radicals to ethane in the gas phase, and (iii) oxidative dehydrogenation of ethane to ethylene. At each step, non-selective (homogeneous and/or heterogeneous) oxidation to the unwanted products (CO_x) may occur, depending on the reaction conditions and the used catalysts (Figure 1.10).[25,41,42]
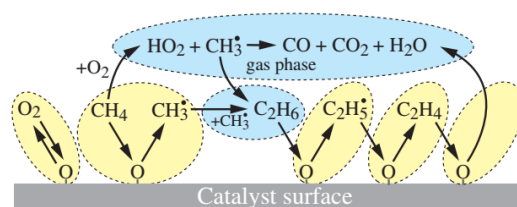
Figure 1.10. Possible reactions proposed for the oxidative coupling of methane with the catalytic conversions highlighted in yellow and the gas-phase ones highlighted in blue. Reprinted with permission from ref. 42 (Copyright 2016 Elsevier).
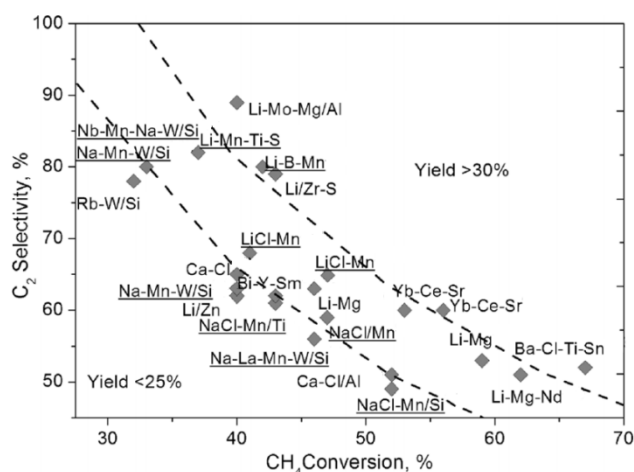
Figure 1.11. Methane conversion and C_2 selectivity data for metal oxide catalysts reported in the literature. Reprinted with permission from ref. 43 (Copyright 2011 Wiley-VCH).

The major problem in the OCM reaction is that the active sites in the catalysts also readily activate the C–H bond in ethane and ethylene at high temperatures, leading to the considerable formations of CO_x and even solid graphitic carbon.[37,44] According to the catalytic data on OCM collected by Zavyalova *et al.*, promising OCM catalysts should contain host basic metal oxides (e.g., MgO, La_2O_3) promoted with metal oxide dopant(s) that can improve C_2 selectivity (e.g., Cs, Na, Sr, Ba) and catalyst activity (e.g., Mn, W) (Figure 1.11).[43,45] Some of these catalysts exhibited performances close to the target for industrial viability of an OCM process, namely single-pass C_2 yield and selectivity of at least 30 and 90%, respectively.[43,44] Recently, an OCM

mini-plant has been constructed within the UniCat cluster to optimize process design, reactor concept and treatment of the products, in which reaction engineering, thermal separation engineering aspects, and safety issues are seriously considered.[40,46,47]

1.1.3.2 Non-oxidative coupling of methane (NOCM)
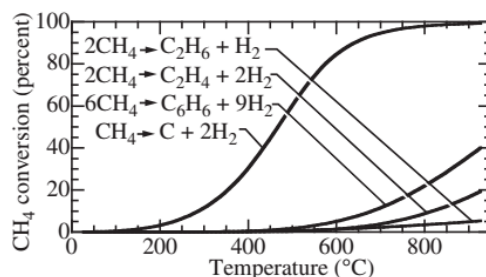
Figure 1.12. Equilibrium thermodynamics of non-oxidative conversions of methane. Reprinted with permission from ref. 42 (Copyright 2016 Elsevier).

Catalytic non-oxidative conversion of methane to ethane, ethylene, aromatics and hydrogen at high temperatures is another direct route for the conversion of methane to value-added chemicals and fuels. Similar to the production of acetylene, the obvious advantage of non-oxidative processes is eliminating the over-oxidations to CO_2 and H_2O. However, the formation of the products from methane in the absence of O_2 is thermodynamically unfavorable at low temperatures because the reactions are highly endothermic (Figure 1.12).[23,27,42] Therefore, the reaction conversion is strongly limited to equilibrium (< 500 ^oC). Several groups proved that selective removal of hydrogen by a membrane could improve the yield of aromatics.[37]
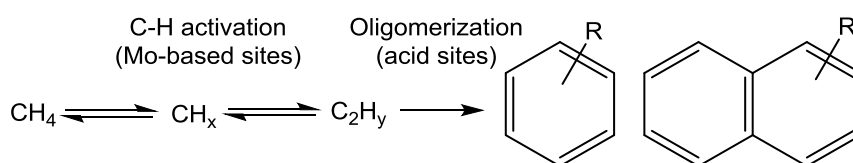
Figure 1.13. Proposed bifunctional mechanism of the conversion of methane to aromatics over Mo/H-ZSM-5 catalysts.[49]

SiO_2-supported Pt and tantalum hydride can catalyze the conversion of methane to ethane and ethylene with high selectivities.[23,48] On the other hand, the mechanism of the formation of aromatics is proposed to involve activation and conversion of CH_4 to C_2H_y fragments on metallic sites and further oligomerization of C_2H_y to aromatic products on acidic sites; therefore, bifunctional catalysts are required to promote the reactions, typically zeolite-based systems.[37,45,49] Mo/H-ZSM-5 first introduced by Wang *et al.* is currently known as the most

promising catalyst (Figure 1.13). Besides the low equilibrium yield and elevated reaction temperature, catalyst deactivation by coke deposition is still a challenge.[27,50] Several methods have been proposed for increasing the catalyst stability including hydrogenation of coke, addition of H_2O, CO, and CO_2 to the feed stream, and post-steam-treatment.[23,42] Recently, the NOCM reaction has been carried out in a pilot plant to demonstrate efficiency of proposed technologies.[37]

1.1.3.3 Partial oxidation of methane to C_1 oxygenates

$$CH_4 \xrightarrow{[O]} CH_3OH, HCHO \xrightarrow{[O]} HCOOH, CO_x \tag{12}$$

Table 1.3. The most promising solid catalysts reported for the gas-phase and high-temperature partial oxidation of CH_4 to formaldehyde.[53,54]

Catalyst	Temperature (^{o}C)	Conversion of methane (%)	Selectivity of CH_3OH (%)	Selectivity of HCHO (%)
SiO_2	620	4.8	0	24
MoO_3/SiO_2	650	5.2	0	32
V_2O_5/SiO_2	650	13.5	0	25.3
$MoSnP/SiO_2$	675	7.2	trace	64.8
SBA-15	625	0.3	0	96
$CuO_x/SBA-15$	625	1.8	0	71

The selective methane oxidation to C_1 oxygenates (methanol and formaldehyde), which is thermodynamically favorable, is regarded as the most challenging route among the studied methane conversion processes due to the much higher reactivity of the desired products for the deeper oxidation to formic acid and carbon oxides compared to methane.[45] Therefore, the main problems in the direct production of methanol and formaldehyde from methane currently consist of difficult activation of methane and poor selectivity with the latter one being more serious. Although a large number of heterogeneous and homogeneous catalytic and non-catalytic systems have been tested under different conditions (i.e., gas phase or liquid phase, RT–500 ^{o}C, 1–200 bar) using various oxidants such as O_2, N_2O, O_3, concentrated H_2SO_4, $K_2S_2O_8$, H_2O_2, and H_2/O_2 mixtures (for *in situ* generation of H_2O_2) since the early 1900s, all so far obtained performances cannot satisfy the requirement for an industrial scale.[13,24,45,51,52] Most of these studies focus on

the methane oxidation to methanol, gaining significant progress and insight into this route, which would be further discussed in the next section, while improving the conversion of methane to formaldehyde seems to be ignored probably due to more desirable methanol production and rigid reaction conditions to produce formaldehyde.
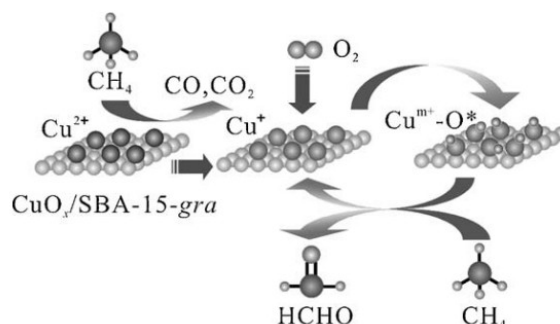
Figure 1.14. Mechanism proposed for the selective oxidation of methane to formaldehyde over CuO_x/SBA-15. Reprinted with permission from ref. [53] (Copyright 2010 Elsevier).

The methane-to-formaldehyde oxidation is typically performed over heterogeneous catalysts at high temperatures (> 500 °C) in presence of a continuous O_2 flow.[45] Under such conditions, a high yield of formaldehyde is extremely difficult to obtain because improving the methane conversion always causes a drop in the selectivity to formaldehyde. This is also a major challenge in the gas-phase methane conversion. It was found that only silica is also active for producing formaldehyde. Parmaliana *et al.* obtained a HCHO yield of about 17% with 50 cycles in a reactor containing SiO_2 at 650 °C.[45,54] Supporting different metal species on silica can lead to an improvement in the activation of methane or/and the selectivity of formaldehyde. Highly dispersed vanadium and molybdenum oxide species-containing catalysts were demonstrated to be the most potential materials for this conversion route.[37,45] Recently, An *et al.* have prepared CuO_x/SBA-15 by a grafting method to obtain Cu^{2+} species highly dispersed on SBA-15. This material exhibited significantly a higher HCHO selectivity (up to 71%) compared to the catalyst prepared via impregnation; nevertheless, the methane conversion was indeed low (1.1–2.4%). In this work, the authors suggested that the isolated Cu^{2+} cations can generate active oxygen species for the selective oxidation of methane to formaldehyde, while the oligomeric CuO_x clusters are responsible for the unwanted oxidation of methane to CO_2 (Figure 1.14).[53] According to analysis of available literature data, unfortunately, no positive developments in the methane oxidation to formaldehyde have been observed since 2010. It was also proposed that a deeper understanding of the relationships between supported species and kinetics of the selective and non-selective

reactions may be keys to develop novel catalysts efficiently operating at lower temperatures for this highly ambitious task.[45]

1.2 Bioinspired, low-temperature conversion of methane to methanol

1.2.1 Present methanol production
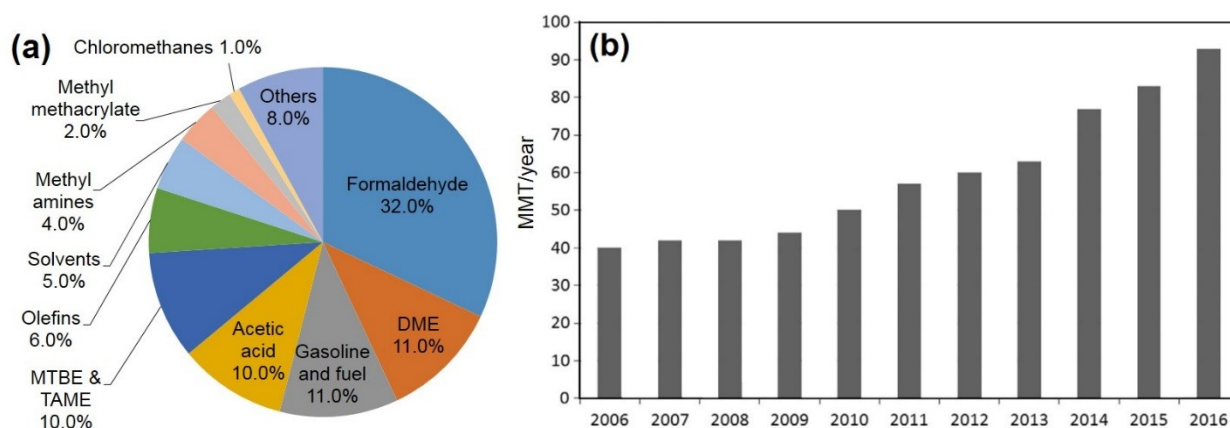
Figure 1.15. (a) Uses of methanol in 2011. (b) Methanol demand in a 10-year period. Reprinted with permissions from ref. 33 (Copyright 2013 Elsevier) and ref. 55 (Copyright 2015 Elsevier), respectively.

Methanol is not only a popular organic solvent for chemical processes but also an important basic chemical widely applied in the chemical and energy industries (Figure 1.15a). Methanol economy has now gained considerable interest as a potential alternative energy resource.[5,55] The energy density of methanol (15.8 MJ l^{-1}) is higher than those of methane and hydrogen (38.1 x 10^{-3} and 13.1 x 10^{-3} MJ l^{-1}, respectively) and the storage and transportation of methanol is evidently easier and safer due to its advantage of being a liquid at normal conditions of pressure and temperature.[12,56,57] Consequently, methanol can be blended with gasoline and also used in fuel cells.[57] In an electrochemical cell, methanol is directly oxidized by air to carbon dioxide and water to produce electricity without the need of initial hydrogen generation, simplifying the fuel cell technology and making it available to a wide scope of applications.[58] There have been some recent developments for transportation vehicles consuming methanol as their energy source. In the chemical industry, methanol is the feedstock for production of formaldehyde, DME, fuel additives (e.g., MTBE, TAME, fatty acid methyl esters), acetic acid, dimethyl carbonate and many other organic chemicals.[33,55,57] The importance of methanol has been emphasized due to the increasing attract of methanol-to-hydrocarbons processes, which directly convert methanol

into gasoline (methanol to gasoline; MTG) and olefin-rich mixtures (methane to olefins; MTO) with high yields over zeolite-based catalysts.[33,34,59] The methanol demand was therefore forecasted to grow rapidly, reaching 92.3 million metric tons (MMT) in 2016 (Figure 1.15b).[33]

$$CO + 2H_2 \rightarrow CH_3OH \qquad\qquad \Delta H_{298} = \text{-90.8 kJ mol}^{-1} \qquad (12)$$

$$CO_2 + 3H_2 \rightarrow CH_3OH + H_2O \qquad\qquad \Delta H_{298} = \text{-49.6 kJ mol}^{-1} \qquad (13)$$

Nowadays, methanol is industrially produced from syngas via hydrogenation of CO_x (Reactions 12 and 13). A high-pressure process was first commercialized by the BASF company (Germany) in 1923, which was operated at 250–350 bar and 320–450 ^{o}C using a ZnO/Cr_2O_3 catalyst resistant to sulphur and chlorine contaminations.[33] In 1960s, the technology to remove sulphur-containing compounds from syngas and the development of a new and more active $Cu/ZnO/Al_2O_3$ catalyst allowed milder operating conditions (50–100 bar, 200–300 ^{o}C). The improved route at the low pressures has been the only process for the global methanol market since 1999.[19,33,60] Interestingly, this catalytic system is also efficiently applied in a promising alternative to the syngas route, using only captured CO_2 as the carbon source for the synthesis of methanol.[55,60]

An industrial-scale plant to produce methanol typically involves three main sections: (i) syngas preparation, (ii) methanol synthesis, and (iii) product separation and purification. Although the efficiency of the syngas route was demonstrated with a methanol selectivity higher than 90% and yield of ~ 70 %, large capital investment and complex industrial infrastructure are its main disadvantages.[19,33] Moreover, a large amount of steam used during the syngas production causes reactor corrosion and difficulty with handling. For these reasons, the price of methanol is currently uncompetitive with petroleum derivative liquid fuels.[32] It was estimated that about 60–70% of the methanol production cost is indeed spent for the syngas generation section. This step also consumes the most energy in the plant. Beside the efforts in optimizing the process and developing new technologies to decrease the investment and operating cost of the present process, the partial oxidation of methane to methanol has become the focus of extensive studies as a promising alternative to the syngas route.[32-34] The direct production of methanol from methane could reduce the number of stages, avoid the large capital investment and the high energy demand, and expand the application of the abundant or renewable resources of methane.[32] Therefore, it is of great economical and environmental interest compared to the traditional methanol production. However, as mentioned in Section 1.1.1.3, to date, these processes are far

from being industrially developed due to the unsolved challenges related to the very low yield of methanol and the low commercial viability.[32] With the aim of revolutionizing the chemical industry, a large number of approaches have been investigated to selectively oxidize methane to methanol during over a century, which can roughly be classified into two main categories including conversion at high temperatures (> 250 ^{o}C) and low temperatures ($\leq$ 250 ^{o}C).[22,37]

In earlier studies, it was pointed out that the high-temperature pathways cannot produce methanol with acceptable yields. The methane oxidation at high temperature occurs via homolytic cleavage of C-H bonds with consecutive reactions (e.g., A $\xrightarrow{k_1}$ B $\xrightarrow{k_2}$ C). Because the C-H bond strength in H-CH$_2$OH is lower than in H-CH$_3$ (Table 1.1), k_2 will be larger than k_1 (typically, $k_2/k_1 > 20$), leading to methanol yields of a few percent at best.[7,61] This conclusion has been demonstrated by numerous unsuccessful efforts devoted to the high-temperature oxidation of methane to methanol. Pressure positively affects the selectivity toward methanol in the homogeneous gas-phase partial oxidation of methane. It was shown that increasing the reaction pressure, the formation of CO decreases and the methanol selectivity is therefore improved. Holmen concluded that the non-catalytic reaction performed at 450–500 °C and under 30–60 bar is able to give a methanol selectivity of 30–40% at a methane conversion of 5–10%.[13,24,37] For the high-pressure reaction, no significant effect of using a solid catalyst was observed. Therefore, at lower pressures, the addition of a catalyst to the gas-phase oxidation process was expected to show the ability to improve the production of methanol. Unfortunately, the methane conversion and the methanol selectivity of the catalytic reaction are less effective than the results reported in the homogeneous process, and formaldehyde was generally the main oxidation product (Table 1.3).[13,37] It is obvious that at the high temperatures needed for the activation of methane, methanol would immediately be decomposed or oxidized into formaldehyde and CO$_x$. Therefore, the low-temperature routes have become the focus of interest in an attempt to improve the methanol selectivity, in which the presence of catalysts is the most important to activate methane.[37] Interestingly, many of these studies are driven by the ability of metalloenzymes to selectively produce methanol under mild reaction conditions.

1.2.2 Enzymatic production of methanol from methanol

While the partial oxidation of methane to methanol is still an unsolved grand challenge in the chemical community, in nature, methanotrophic bacteria (methanotrophs) living at the boundary

of aerobic and anaerobic environments can utilize methane and molecular oxygen to efficiently produce methanol at ambient temperatures (Reaction 14).[62-64]

$$CH_4 + O_2 + 2H^+ + 2e^- \rightarrow CH_3OH + H_2O \qquad\qquad (14)$$

$$CH_4 \xrightarrow[\text{pMMO/sMMO}]{} CH_3OH \xrightarrow[\substack{\text{methanol} \\ \text{dehydrogenase}}]{} HCHO \xrightarrow[\substack{\text{formaldehyde} \\ \text{dehydrogenase}}]{} HCOOH \xrightarrow[\substack{\text{formate} \\ \text{dehydrogenase}}]{} CO_2$$

carbon assimilation
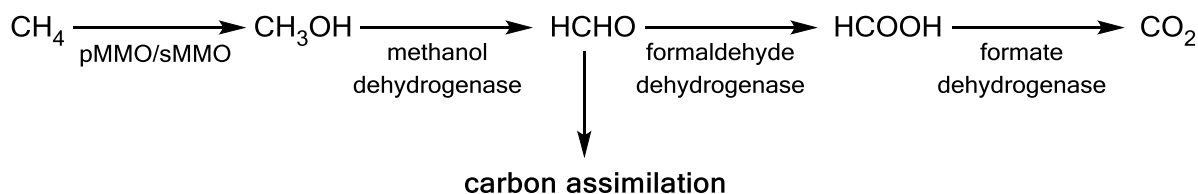
Figure 1.16. Metabolic pathway for the consumption of methane by methanotrophs.[9,63]

In fact, the hydroxylation of methane is the first essential step in the metabolic assimilation process of methanotrophs to consume methane as their sole source of carbon and energy (Figure 1.16). Methanotrophs therefore play a significant role in limiting the methane concentration in the atmosphere and diminishing its global environmental impact.[62,63,65] Enzymes called methane monooxygenases (MMOs) with two different forms are responsible for catalyzing the conversion of methane to methanol in methanotrophs. The membrane-bound or particulate MMO (pMMO) expressed at high concentrations of copper is the more abundant (up to 20 % of the total protein in methanotrophs) but poorly understood form. Most studies on pMMO proposed that the hydroxylation of methane in this form uses copper species as the active site; however, some believe that the catalysis requires further iron species. The cytoplasmic or soluble MMO (sMMO), whose active site contains iron species, is found only in some methanotrophic species under conditions of low copper availability.[12,62,63,65] These two MMO forms also differ from each other in their protein components, reducing power requirements, stability, and activity. In addition, it was found that both MMOs are also able to hydroxylate many other hydrocarbons besides methane. sMMO is active with a wide variety of substrates including saturated and unsaturated, linear, branched, and cyclic hydrocarbons of up to eight carbons, as well as aromatic, heterocyclic, and chlorinated compounds whereas pMMO is more selective toward only linear alkanes and alkenes of up to five and four carbons, respectively.[24,62,63]

sMMO is much more stable and easier to purify and therefore better characterized.[15,62] A multi-component protein system in sMMO includes a hydroxylase (MMOH), a reductase (MMOR), and a regulatory protein (MMOB). Although all components of sMMO are necessary for activity, both O_2 activation and methane oxidation occur at a diiron centre located within MMOH, which is the active site of sMMO (Figure 1.17).[64,66,67] By biologically well-engineered

tunnels or pockets, four substrates, namely methane, O_2, electrons, and protons, are transported selectively and separately to the diiron site coordinated by two histidines, four glutamates, and one or two water molecules.[66,67] Structural features of the iron species in their different oxidation states and in the short-life intermediates generated during the catalytic cycle have been elucidated by many various spectroscopic methods (Figure 1.18).[62,66,68]
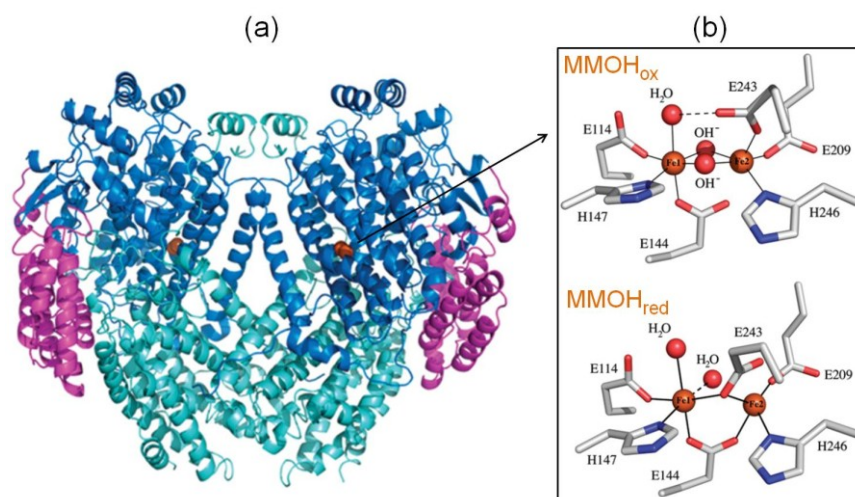
Figure 1.17. (a) Structure of the hydroxylase protein in sMMO with the iron atoms shown as orange spheres. (b) Structure of the active site in diiron(III) ($MMOH_{ox}$) and diiron(II) ($MMOH_{red}$) states. Reprinted with permission from ref. 66 (Copyright 2011 American Chemical Society).
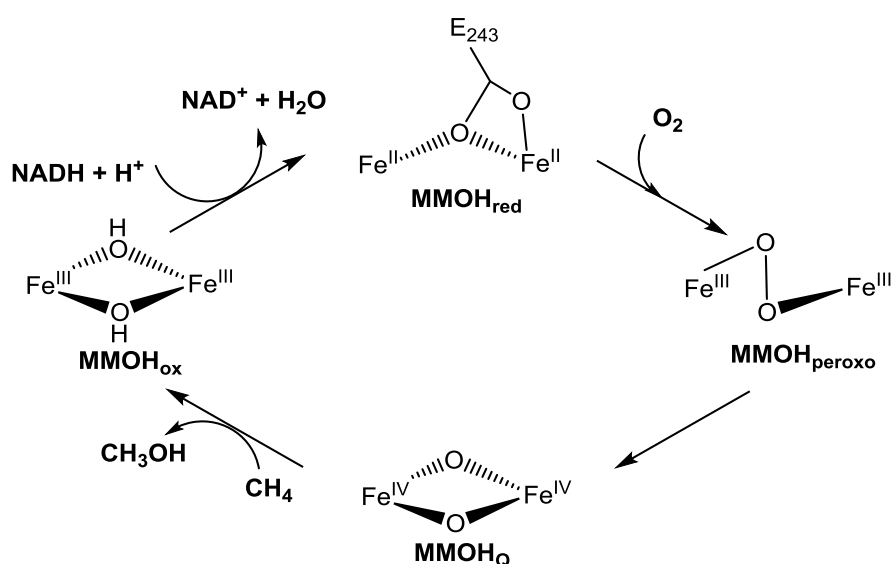
Figure 1.18. Proposed catalytic cycle of the partial oxidation of methane to methanol by atmospheric oxygen in sMMO.[12,67-69]

In detail, the methane-to-methanol conversion is initiated by interaction of O_2 with the diiron(II) center ($MMOH_{red}$), yielding $MMOH_{peroxo}$. Following the O–O bond cleavage, $MMOH_{peroxo}$ is converted to a methane-oxidizing intermediate, $MMOH_Q$, which contains a high-valent dioxodiiron(IV) unit.[67-69] The hydroxylation of methane by $MMOH_Q$ is proposed to be performed via hydrogen-abstraction/oxygen-rebound pathways. After the reaction with methane, the iron atoms in MMOH are reduced to Fe(III) ($MMOH_{ox}$). Finally, a two-electron reduction of $MMOH_{ox}$ with nicotinamide adenine dinucleotide (NADH) via MMOR returns the enzyme to its diiron(II) state, completing the catalytic cycle.[63,67,69] It should be noted that the activity of sMMO is decreased in the absence of MMOB, which is not only responsible for restructuring MMOH to control access of methane to the active site but can also affect the coordination state of the iron species. Therefore, the actual structure and activity of the active site in the native enzyme may differ from the ones clarified from isolated samples.[67]
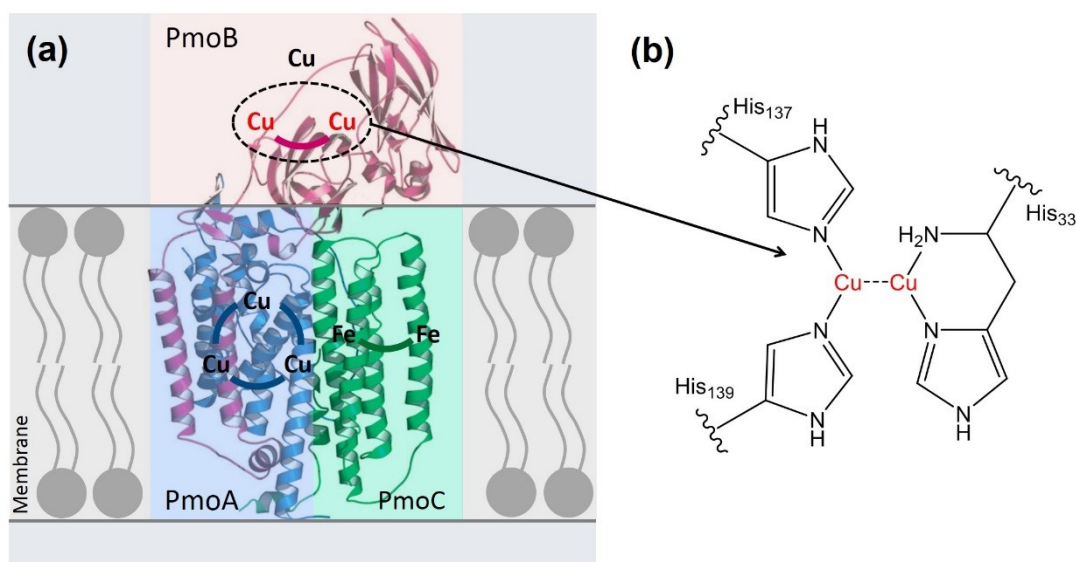
Figure 1.19. (a) Structure of a monomer of the pMMO enzyme with the active sites proposed for the hydroxylation of methane in the subunits.[70,71] Reproduced with permission from ref. 71. (Copyright 2010 Nature Publishing Group). (b) Structure of the dicopper site in the PmoB subunit.[70]

All methanotrophs express the membrane-bound form of MMO, which consists of three subunits (PmoA, PmoB, and PmoC) arranged in a trimeric structure. Due to being located in the membrane, pMMO has a greater access to methane compared to sMMO.[9,15] pMMO is currently known to be the most efficient catalyst for the hydroxylation of methane with a TOF of about 1 s^{-1}. In contrast to the case of sMMO, biochemical and biophysical characterizations of pMMO

are hindered by inherent difficulty in isolation and purification of such a membrane protein system and its instability in solubilizing detergents, explaining why, so far, the nature of the pMMO active site has not been fully determined.[9,15,62,63,70] PmoA and PmoC are transmembrane helical proteins without extensive soluble segments while PmoB contains a soluble domain with Cu ions identified in the crystal structure, which forms a path for substrate and product channeling and plays a key role in catalysis (Figure 1.19a).[64,70]
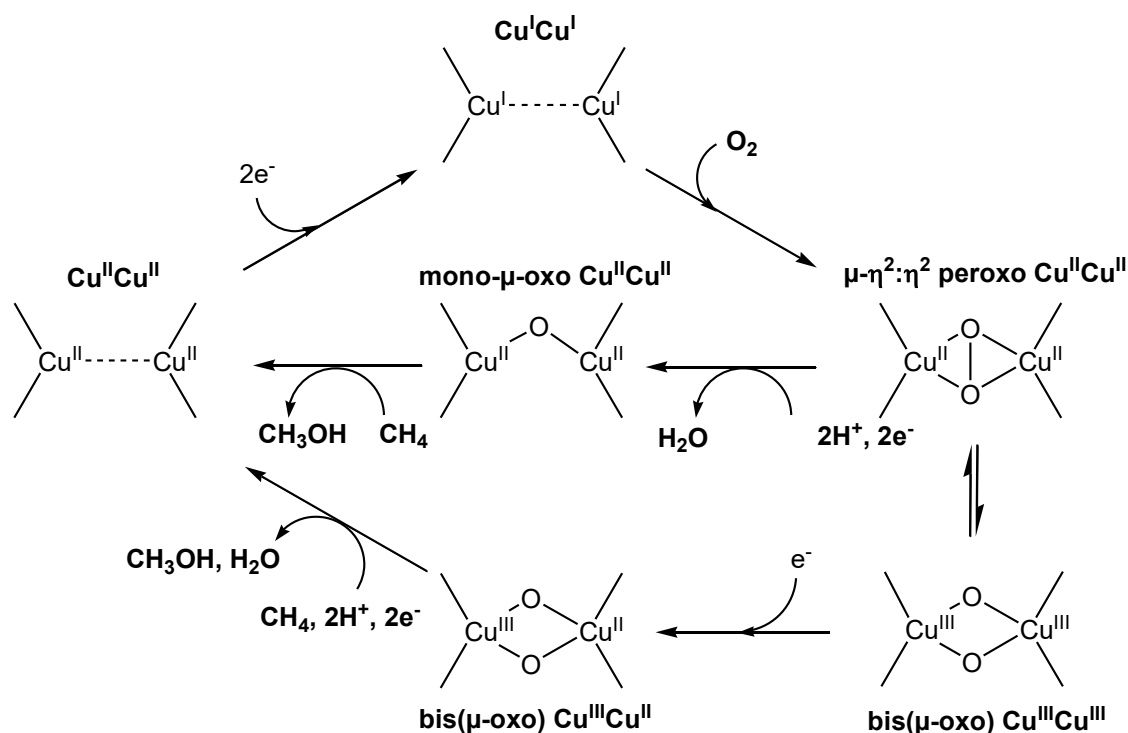
Figure 1.20. Proposed pathways for the activation of O_2 and the oxidation of methane to methanol at the dicopper center of the PmoB subunit.[63,70]

Recent studies provide significant evidences emphasizing that the Cu ions in PmoB are responsible for the high activity of pMMO.[63,72] Two distinct copper sites could be found in the soluble domain of PmoB, namely a dinuclear site coordinated by three histidine ligands (Figure 1.19b) and a mononuclear site coordinated by two other histidines. The case for the dicopper center as an active site is stronger than that for a monocopper center as all of the ligands to the former are highly conserved and the appearance of the dicopper cluster is clear from obtained spectroscopic data. Also, the ability of a dinuclear copper center to catalyze the hydroxylation was previously known in other enzyme systems.[70,73] By analogy to these well-studied enzymes and model complexes, either a μ-η^2:η^2 peroxo dicopper(II) or a bis(μ-oxo)dicopper(III) species could be formed upon the initial reaction of the dicopper(I) center with O_2 (Figure 1.20). The

subsequent conversion produces either a mixed valent bis(μ-oxo)Cu(II)Cu(III) species or a bent mono-μ-oxo dicopper(II). Such complexes were found to be more reactive toward methane.[63,70,74,75]
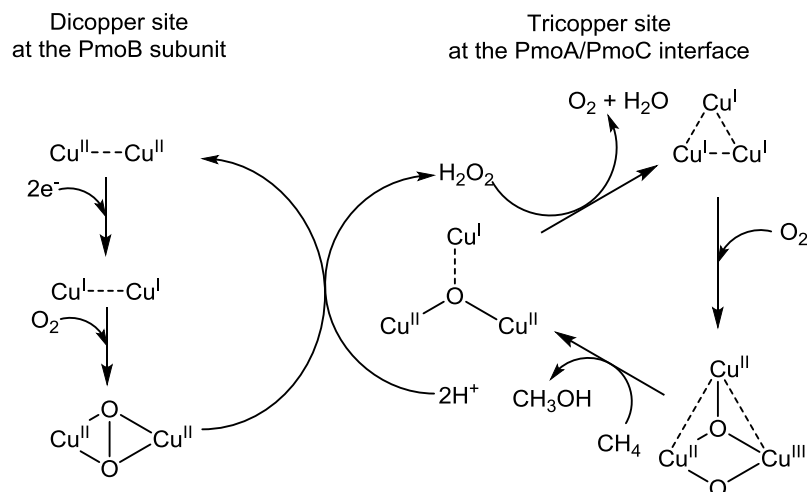
Figure 1.21. Proposed catalytic cycle in pMMO linking the tricopper catalytic site and the dicopper center. Reproduced with permission from ref. 15 (Copyright 2017 American Chemical Society).

On the other hand, the earlier study of Chan *et al.* showed EPR spectroscopic evidences to indicate the existence of a further tricopper cluster, which is located at the interface of PmoA and PmoC, as the site of the methane oxidation.[70,76,77] Upon this hypothesis, a full catalytic cycle in pMMO was proposed consisting of both dicopper and tricopper clusters. Accordingly, the trinuclear complex is the main active site to activate O_2 and subsequently oxidize methane to methanol while the dinuclear site is responsible for production of H_2O_2 to regenerate the spent catalyst (Figure 1.21).[15]

Also, it is believed that pMMO is an iron-copper enzyme as higher iron content in pMMO seemed to lead to a better catalytic performance.[63,78-80] Given similarities of the analytic results of the purified pMMO with those obtained with sMMO, Martinho *et al.* concluded that pMMO possesses an active site containing a diiron cluster in the PmoC subunit.[81] Like the issue with the active site, the source of electrons for the pMMO performance is not yet determined. Membrane-bound quinols related to the electron transport chain may be the pMMO reductants whereas the necessity of either NADH or a soluble cytochrome was noted in several studies.[9,63,79,80] In general, most scientists in this field agree on the fact that pMMO is a Cu-containing enzyme but disagree on the metal content, metal type, active site location, and electron donor. Despite many

efforts devoted to the characterization of pMMO, numerous questions related to the nature of the active site and the mechanism of the methane hydroxylation have not been fully resolved.[79,80,82]

MMOs have received significant attention because they are successful in one of the most difficult chemical challenges, the cleavage of the first C-H bond of methane at ambient temperatures. Other enzymes can readily hydroxylate more reactive hydrocarbons but are inactive to methane, indicating the uniqueness of MMOs.[63] Although the MMOs-based biocatalyses show the ideal activity for the methane-to-methanol conversion, microorganisms are limited for the industrial application. The isolation of considerable amounts of such multicomponent systems to produce methanol on a large scale is extremely difficult while these enzymes are found to be unstable, leading to a poor productivity. Moreover, the requirement of expensive reducing power equivalents for their activity is unfavorable for the commercial manufacture of methanol.[9,13,83] Obviously, the investigation of the pMMO and sMMO systems have significantly improved our understanding of aspects of the biological hydroxylation including the metalloenzyme structures and the detailed O_2 and C-H activation processes, which are inspiration sources for designing novel and improved synthetic catalysts. In the last two decades, numerous attempts have been made to develop biomimetic catalysts capable of the selective oxidation of methane to methanol under milder conditions.[15,63] Just a few of them have indeed been investigated for activity in the "dream reaction", which are introduced in the next section.

1.2.3 Bioinspired catalysts

1.2.3.1 Homogeneous system

Considering that the catalytic site in pMMO might be a trinuclear copper cluster, Chan *et al.* have synthesized a homogeneous catalyst with a similar structure for the hydroxylation of methane.[84] The bioinspired complex containing three copper atoms coordinated by the ligand 3,3'-(1,4-diazepane-1,4-diyl)bis[1-(4-ethylpiperazine-1-yl)propan-2-ol] could efficiently convert methane to methanol without the over-oxidation in the presence of both O_2 and H_2O_2 at room temperature. To initiate the catalytic cycle, the fully reduced form $[Cu^{I}Cu^{I}Cu^{I}(L)]^{+}$ (L = the organic ligand) is activated by O_2, yielding a highly reactive intermediate $[Cu^{II}Cu^{II}(\mu\text{-}O)_2Cu^{III}(L)]^{+}$. Methanol is subsequently produced via transferring one of the O-atoms in this intermediate to methane (Figures 1.22a and -b). The reaction was almost complete within ten minutes, indicating that the oxidation of methane readily occured (Figure 1.22c). Interestingly,

the catalytic cycle could be maintained by adding an appropriate amount of H_2O_2 to the reaction mixture to regenerate the $[Cu^ICu^{II}(\mu\text{-}O)Cu^{II}(L)]^+$ species, thereby remarkably improving the TON (Figure 1.22d).[84] It was noted that H_2O_2 acts as a reductant in the productive cycle similar to the enzymatic catalysis, not as an oxidant, which is O_2 in this case. Furthermore, no additional consumption of O_2 is required as O_2 for the next cycles can be recovered during the reduction of the spent catalyst with H_2O_2. However, the strong oxidizing $[Cu^{II}Cu^{II}(\mu\text{-}O)_2Cu^{III}(L)]^+$ species can facilely react with H_2O_2 under homogeneous conditions instead of methane and furthermore the solubility of methane in the used solvent is low, both limiting the yield of methanol.[85] This tricopper complex also showed the ability to catalyze the oxidation of linear C_2–C_6 alkanes to corresponding alcohol and ketones with high efficiencies at ambient temperature.[84]
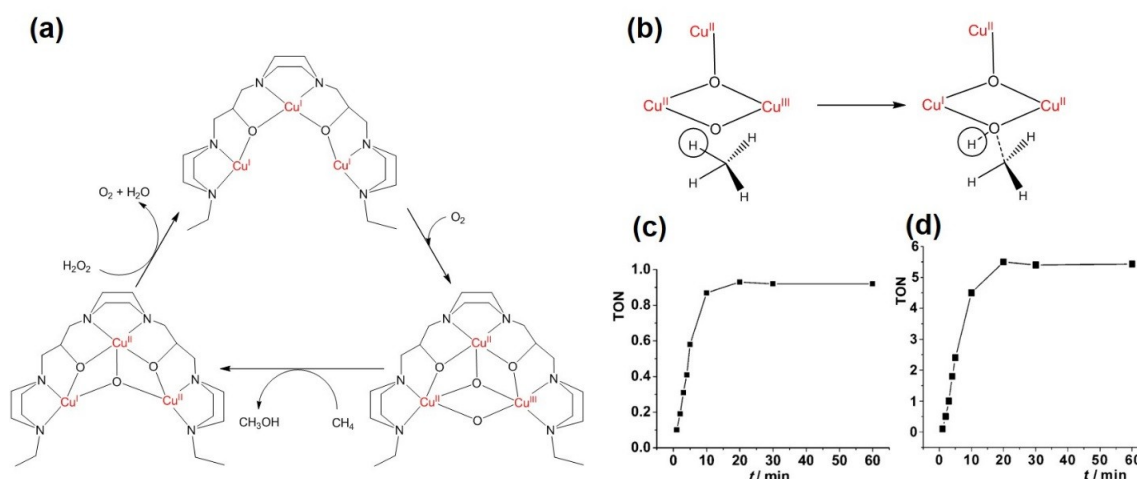
Figure 1.22. (a) Proposed catalytic cycle for the oxidation of methane to methanol mediated by the tricopper complex. (b) Facile transfer of an O-atom from the activated site to methane. (c) Methanol production over time in the absence of H_2O_2 (d) Methanol production over time in the presence of 20 equivalents of H_2O_2. Reprinted with permission from ref. 84 (Copyright 2013 Wiley-VCH).

Irritatingly, since this work, no further reports on the successful methane-to-methanol conversion mediated by homogeneous complexes have been seen although a large number of diiron, dicopper, and tricopper models were synthesized to mimic the possible active sites of MMOs. In fact, their reactivity toward activation of more reactive C-H bonds was found to be surprisingly low, showing that the catalytic pathways in MMOs are much more complex than the artificial systems. Sophisticated preparation and often observed sensitivity to air and moisture are grand challenges for the application of such bioinspired complexes and the development of heterogeneous catalytic systems is therefore an attractive alternative.[15,86]

1.2.3.2 Heterogeneous systems

Both H_2O_2 and O_2-requiring reaction

As a continuation of the work described above, the $[Cu^ICu^ICu^I(L)]^+$ tricopper cluster complex was immobilized onto mesoporous silica nanoparticles (MSNs) to take advantage of heterogeneous catalysis.[85] Before Cu loading, the surface negative-charge density of MSNs was improved by functionalizing with the anionic 3-(trihydroxysilyl)propyl methylphosphonate or doping with Al species. Similar to the earlier study, during the room-temperature hydroxylation of methane in CH_3CN, the immobilized tricopper clusters were activated by O_2, and after the hydroxylation of methane, H_2O_2 is needed to regenerate the initial state. Importantly, no further methanol production was detected in the reaction phase after removal of the catalyst; it was therefore concluded that the catalytic activity is based on the immobilized copper sites and the catalysis is indeed heterogeneous.[85]

H_2O_2-mediated reaction
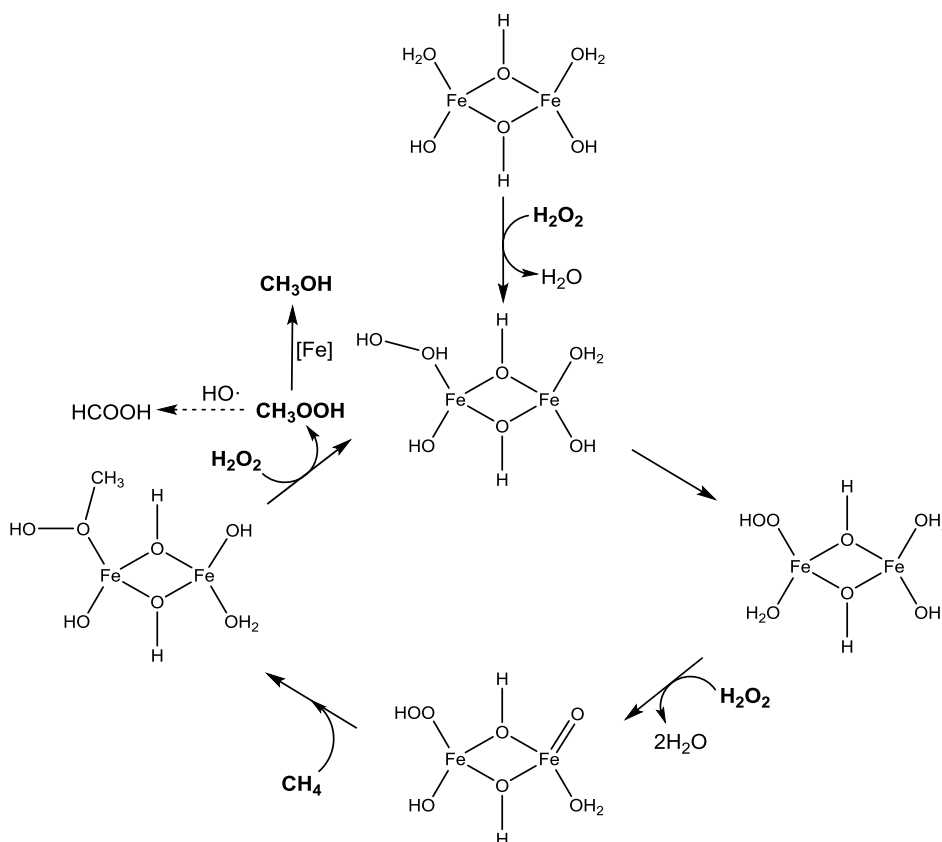
Figure 1.23. Proposed cycle for the conversion of methane to the oxygenates catalyzed by Fe/ZSM-5 using H_2O_2 as the oxidant.[88]

Although homogeneous Fe^{3+} salts can catalyze the partial oxidation of methane by H_2O_2, which is proposed to occur via the Fenton-type radical mechanism, poor selectivities to oxygenated products (25–50%, including methanol, formaldehyde, methyl hydroperoxide, and formic acid) were observed.[28,87,88] Hammond *et al.* found that the oxygenates can be also produced in the H_2O_2-mediated oxidation of methane using Fe-containing zeolites, namely ZSM-5 and silicalite-1, as solid catalysts with much higher selectivities (83–94 %).[88] Importantly, addition of a radical scavenger (Na_2SO_3) into the Fe/ZSM-5-catalyzed reaction did not lead to a loss in activity while the yield of oxygenates in a Fenton's system using $Fe(NO_3)_3$ as a homogeneous catalyst was significantly reduced in the presence of Na_2SO_3, suggesting that the performance of Fe-ZSM-5 is not based on a free-radical chain reaction.[28,89] By UV-vis and X-ray absorption near edge structure (XANES) spectroscopic studies, extra-framework Fe species were confirmed to be the active sites for the oxidation of methane with H_2O_2. Combining the understanding obtained from the Fe-dependent sMMO enzyme and further DFT calculations, the authors proposed a catalytic cycle for the Fe-ZSM-5-based system, in which a binuclear iron cluster is responsible for the initial reaction with H_2O_2 and the following activation of methane (Figure 1.23).[28,88,90,91]

The time-course study showed that methyl hydroperoxide was formed as the primary product and can subsequently decompose to give methanol. However, over Fe/ZSM-5 alone, formic acid was the major product probably due to the over-oxidation of methyl hydroperoxide and methanol with highly active OH· radicals.[28,88,92] Interestingly, the presence of Cu either as a soluble additive (*i.e.,* $Cu(NO_3)_2$) or as a supported component (i.e., Cu/silicalite-1) in the Fe/zeolites-catalyzed reaction can considerably enhance the selectivity toward methanol up to 93%. It should be noted that such additional Cu species did not affect the methane conversion. On the other hand, no oxygenated products were detected in the experiment using a Cu-containing catalyst only.[28,88] The role of Cu species was therefore proposed to control the formation of OH· radicals, most likely radical scavengers, preventing the over-oxidation to formic acid and CO_2. The results reported by Hutchings *et al.* indeed demonstrated that Cu-promoted Fe/zeolite is an excellent catalytic system for the selective oxidation of methane and, promisingly, higher hydrocarbons using H_2O_2 as the oxidant.[28,93-95] However, the insignificant difference in activity of the zeolite-based catalysts with various Fe loadings, namely commercial ZSM-5 (0.014 wt.%), Fe/ZSM-5 (2.5 wt.%) and Fe-silicalite-1 (0.5 wt.%) was not elucidated in these studies, suggesting that the oxidation of methane to methanol in H_2O_2 possibly occurs via different mechanistic pathways.

O_2 or N_2O-mediated reaction

Although Fe/zeolite is able to catalyze the aqueous oxidation of methane into methanol by H_2O_2 with a very high selectivity (90%) and at 10% conversion under appropriate conditions, the fact that H_2O_2 is more expensive than methanol prevents this discovery from the industrial application. The use of abundant oxidants, typically molecular oxygen, is therefore the preferred route.[92] Inspired by the activity of MMOs, Fe- and Cu-containing zeolites have been the subject of intensive studies on the gas-phase hydroxylation of methane. It was found that the Fe and Cu sites in zeolites activated by O_2 or N_2O at high temperatures (over 150 ^{o}C) indeed are reactive to methane.[24]

In the case of Fe/ZSM-5, after the treatment at temperatures above 500 ^{o}C under vacuum or in a steam flow, an Fe(II) active form, called α-site, is formed via auto-reduction of extra-framework Fe(III) species. Such Fe(II) sites are strongly stabilized within the zeolite matrix, making their reoxidation to Fe(III) by O_2 unfavorable, but have a special affinity to N_2O.[96-98] Decomposition of N_2O at 150–250 ^{o}C on the α-site produces a reactive intermediate (α-oxygen). The structure of α-oxygen is assigned to a mononuclear high-spin Fe(IV)=O species, which is also the key active species in biological oxidations. Similar to the active oxygen of sMMO, the α-oxygen species can readily oxidize methane to methoxy groups bound on the α-sites at room temperature. The subsequent conversion of methoxy groups to methanol requires hydrolysis by water while heating the catalyst led to formation of CO_x (Reactions 15–17).[28,96,99-101] In addition to methanol, significant amounts of DME as a result of the reaction either of α-oxygen with methane or of the methane dehydration, and non-extractable products, most likely a carbonaceous form, were produced (Table 1.4).[96] Panov *et al.* demonstrated that the methanol yield could be improved by increasing the reaction temperature up to 200 ^{o}C.[102] It was also noted that performing the reaction at above 300 ^{o}C would lead to combustion of methane.[101] Interestingly, TONs higher than 1 were obtained in reactions using a mixture of N_2O and CH_4, suggesting that the products could migrate from α-sites to other surface centers, thus facilitating the regeneration of the α-sites for further catalytic cycles.[24,97] Furthermore, an underestimation of the amount of active sites and other mechanisms for the methane hydroxylation cannot be ruled out.

$$(Fe^{II})_\alpha + N_2O \rightarrow (Fe^{IV}=O)_\alpha + N_2 \tag{15}$$

$$CH_4 + 2(Fe^{IV}=O)_\alpha \rightarrow (Fe^{III}\text{-}OH)_\alpha + (Fe^{III}\text{-}OCH_3)_\alpha \tag{16}$$

$$(Fe^{III}\text{-}OCH_3)_\alpha + H_2O \rightarrow (Fe^{III}\text{-}OH)_\alpha + CH_3OH \tag{17}$$
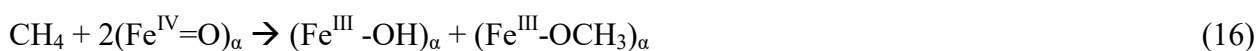
Table 1.4. Yield of the products in the low-temperature oxidation of methane by N_2O over Fe/ZSM-5.[96,102]

Reaction temperature ($^{\circ}$C)	Reaction time (h)	Extraction solvent	Extracted products		Non-extractable products ($\mu mol\ g_{cat}^{-1}$)
			MeOH ($\mu mol\ g_{cat}^{-1}$)	DME ($\mu mol\ g_{cat}^{-1}$)	
RT	Not given	THF	1	1.5	48.5
RT	Not given	Acetonitrile	0.5	1.5	49.0
RT	Not given	Water	30.1	0.8	20.1
RT	Not given	90 vol.% acetonitrile + 10 vol.% water	35.7	1.5	13.8
160	4	90 vol.% acetonitrile + 10 vol.% water	213.2	31.8	175
175	4	90 vol.% acetonitrile + 10 vol.% water	238.7	71.3	180
200	4	90 vol.% acetonitrile + 10 vol.% water	265.2	124.8	260
200	16	90 vol.% acetonitrile + 10 vol.% water	145.0	139.2	580

Fe-containing catalysts showed poor activity when O_2 was used as an oxidant instead of H_2O_2 or N_2O whereas the use of O_2 is apparently the most desired route.[28] Fortunately, recent notable discoveries on Cu/zeolites-based systems have convinced the scientific community that the opportunity to obtain efficient catalysts for the partial oxidation of methane by O_2 is still available. In 2005, Groothaert *et al.* reported a seminal work, in which a multistep procedure to convert methane to methanol over Cu/zeolite was introduced for the first time.[103] The catalytic performance requires a high-temperature (450 $^{\circ}$C) pretreatment of Cu/zeolites in O_2, which is followed by their reaction with methane at lower temperatures (175–200 $^{\circ}$C). Similar to the hydroxylation of methane with N_2O over Fe/ZSM-5, CH_3OH could only be obtained via the extraction with a mixture of acetonitrile and water. None of any other products than methanol was detected during the reaction, implying a selectivity of at least 98% toward methanol. This system was not considered as a catalytic process until Alayon *et al.* obtained a closed catalytic cycle via steam-assisted desorption of methanol.[104] After the online methanol extraction, the catalyst bed was heated in O_2 to dehydrate and reactivate Cu sites for the next use, demonstrating

a practical feasibility of operating the system in a catalytic cycle. Based on this stepwise manner, latter studies with focus on many Cu-containing zeolites have been carried out, indicating the activity of Cu/zeolites in the methane conversion.[24,28,105] However, varied amounts of methanol were reported to be produced over similar catalysts by different laboratories (Table 1.5), suggesting that the catalytic results are not only dependent on the reaction conditions, but possibly also on the techniques used to collect the products (e.g., extraction in water, desorption by steam followed by condensation of liquid products in a cold trap, and online analysis of the outlet stream) and to quantify them (e.g., off-line GC, online GC, online MS, and ^{1}H-NMR).
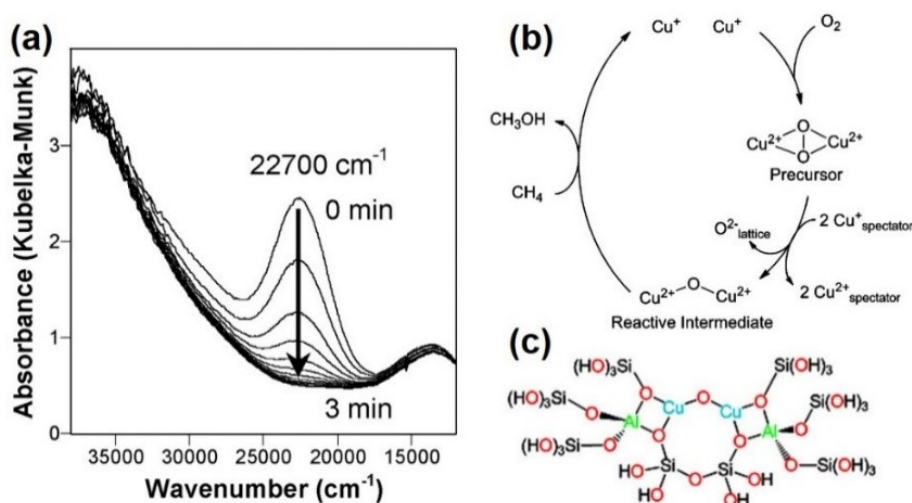
Figure 1.24. (a) UV-vis spectroscopy of Cu/ZSM-5 showing disappearance of an intense band at 22 700 cm^{-1} upon the contact with methane. (b) Proposed formation of the $[Cu_2(\mu\text{-O})]^{2+}$ active site. (c) DFT-predicted structure of $[Cu_2(\mu\text{-O})]^{2+}$ located at the 10-MR of ZSM-5. Reprinted with permissions from ref. 103 (Copyright 2005 American Chemical Society), ref. 75 (Copyright 2010 American Chemical Society), and ref. [108] (Copyright 2009 National Academy of Sciences), respectively.

In spite of being intensively studied for a long time, identification of the active sites in Cu/zeolites is still a controversial topic.[24] The activity of Cu species in ZSM-5 and mordenite was found to be related to an absorption at ~ 22 500 cm^{-1} in their UV-vis spectra since this feature was observed after the high-temperature treatment in O_2 and disappeared after the contact with methane. In combination with further EXAFS and EPR measurements, the active site was originally believed to be a bis(μ-oxo)dicopper(II) core, $[Cu_2\text{-}(\mu\text{-O})_2]^{2+}$.[103,106,107] Afterwards Woertink *et al.* argued against this structure and instead suggested the active site to be a bent mono-μ-oxo dicopper(II) site, $[Cu_2(\mu\text{-O})]^{2+}$, based on resonance-enhanced Raman spectroscopy and DFT calculations. [24,108] When pre-reduced Cu/ZSM-5 (in He at 450 ^{o}C) was exposed to O_2 at

room temperature, UV-vis measurements revealed a rapid formation of an absorption band at ∼ 29 000 cm^{-1}, which was assignable to a μ-(η^2:η^2) peroxo dicopper(II) species, $[Cu_2(\mu$-η^2:η^2-$O_2)]^{2+}$ (Figure 1.24). From 175 ^{o}C, the 22 700 cm^{-1} band was observed along with a parallel disappearance of the 29 000 cm^{-1} band, proposing that the $[Cu_2(\mu$-η^2:η^2-$O_2)]^{2+}$ species transformed into the highly reactive $[Cu_2(\mu$-$O)]^{2+}$ site.[75] The subsequent reaction of the active site with methane led to a reduction of Cu(II) to Cu(I), which was further indicated by *in situ* XAS spectroscopy.[109-111] Furthermore, it was proposed that the copper dinuclear cluster could be accommodated within 10-membered rings (MR) of the ZSM-5 lattice.[75] For the case of Cu/mordenite, which has always shown significantly better catalytic performance, 8-MR windows of side pockets in the mordenite framework are the most appropriate candidates to house the Cu-O-Cu cores. The discovery of the $[Cu_2(\mu$-$O)]^{2+}$ site has had a broad impact on the fields of heterogeneous catalysis and bioinorganic chemistry.[112] To date, it is the most used cupric model to characterize and design Cu-containing catalysts for the activation of C-H bonds and even to elucidate the activity of pMMO.
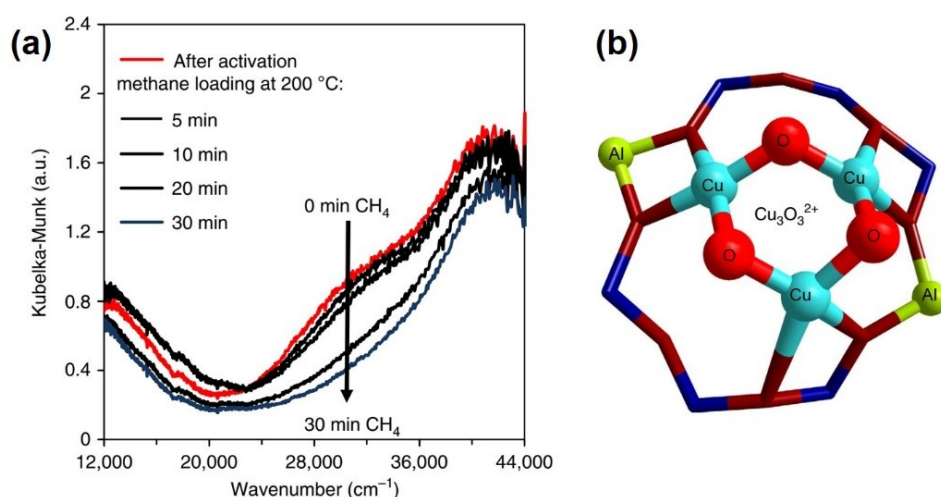
Figure 1.25. (a) UV-vis spectroscopy of Cu/Mor in the study of Grundner *et al.* showing a broad band at ∼ 31 000 cm^{-1}, which disappeared upon the contact with methane. (b) DFT-predicted structure of the $[Cu_3(\mu$-$O)_3]^{2+}$ cluster cluster located at the pore mouth of the side pocket in mordenite. Reprinted with permission from ref. [109] (Copyright 2015 Nature Publishing Group).

However, in several recent studies, a development of another band centered at ∼ 31 000 cm^{-1} was observed in the UV-vis spectra of O_2-activated Cu/mordenite while the 22 500 cm^{-1} feature was absent (Figure 1.25).[109,113] As expected, the intensity of the new band rapidly decreased due to the interaction of the material with methane, indicating the presence of other active sites than $[Cu_2(\mu$-$O)]^{2+}$ in mordenite. According to the overall TON of ∼ 0.33 obtained for the methane-to-

methanol conversion on Cu/modernite and DFT calculations, Lercher *et al.* proposed a trinuclear Cu-oxo cluster, namely $[Cu_3(\mu\text{-}O)_3]^{2+}$, as the active site in Cu/mordenite and Cu/ZSM-5 as well.[109,114,115] Inspired by this discovery, Palagin *et al.* proposed that different active $[Cu_nO_n]^{2+}$ and $[Cu_nO_{n-1}]^{2+}$ clusters (n = 2–5) can be formed and stabilized within the 8-MR pores of mordenite. Stability and activity of the system generally increases with the cluster size due to an additional stabilizing effect of Cu–O bonds on the overall cluster.[116] In addition to larger Cu-oxo clusters, monocopper species ($[CuOH]^+$) and even well-dispersed small/ultrasmall CuO clusters were suggested to be responsible for catalytic activity under specific reaction conditions.[26,117-119] Furthermore, small-pore Cu-exchanged zeolites including Cu/SSZ-16, Cu/SSZ-13, and Cu/SSZ-39 were reported to produce more methanol compared to Cu/ZSM-5, confirming that the 8-MRs are more favorable for the formation and stabilization of the active Cu sites.[120,121]

Performing the steps in a cycle at very different temperature ranges, namely 450–550 ^{o}C for the activation of catalyst, 200 ^{o}C for the reaction with methane, and RT–200 ^{o}C for the extraction of formed methanol (Figure 1.26a), wastes energy and operation time in cooling and heating the setup. In order to overcome this challenge, an isothermal cyclic process at 200 ^{o}C has recently been developed.[26,118] It was found that methanol yield increased with methane pressure while pressure of oxygen in the activation step seemed to have a negligible influence on the reaction performance (Figures 1.26b and -c).[26] Notably, in the UV-vis spectra of both Cu/mordenite and Cu/ZSM-5 activated in O_2 at 200 ^{o}C, there were no bands in the region of 20 000 cm^{-1}, confirming the absence of the mono-μ-oxo dicopper site. The authors therefore concluded that other copper sites such as small clusters of CuO are responsible for activity under the isothermal conditions. Such CuO species are apparently less active than the dicopper core and require higher methane pressures to enable the reaction with methane.[118] Although these results strongly demonstrated the possibility of simplifying the methane-to-methanol conversion procedure, the isothermal conditions should be critically studied to avoid operating the system at elevated pressure. In addition, Narsimhan *et al.* designed a catalytic process in replacement of the complex chemical looping system and showed a steady-state methanol production over Cu/ZSM-5 at 210 ^{o}C by using a feed gas mixture of water, O_2, and methane. A methanol selectivity of only ~ 70% was obtained while data on the amount of converted methane were not reported for this continuous system.[119] Besides Fe- and Cu-based catalysts, Co-containing ZSM-5 also showed the ability to oxidize methane to methanol and formaldehyde in a similar multistep route with O_2. Unfortunately, this material seems to be unattractive for deeper investigations probably due to its very low activity.[124]

Table 1.5. An overview on the stepped oxidation of methane to methanol by O_2 over Cu/zeolites.

Entry	Catalyst[a]	Cu content (wt. %)	Cu/Al ratio	Activation in O_2 at 1 bar	Reaction with CH_4 at 200 °C	MeOH extraction (extr.)	MeOH analysis	MeOH yield (µmol g⁻¹)	Other products detected	TON[b]	Selectivity[c] (%)	Ref.
1	Cu/ZSM-5	2.4	0.31					8.9		0.023		
2	Cu/Mor	Not given (NG)	0.43	450 °C, overnight	15 min, 50 mbar	Off-line extr. in a H_2O/CH_3CN mixture	Off-line GC	11.3	None	NG	> 98	103
3	Cu/zeoY	NG	0.29					<1		NG		
4	Cu/Mor	4.3	0.38	450 °C, 4 h	20 min, 50 mbar	Off-line extr. in water	Off-line GC	13	None	0.019	> 98	88
5	Cu/Mor	4.9	0.34					31		0.04		
6	Cu/ZSM-5	3.4	0.34					16		0.03		
7	Cu/SSZ-39	2.6	0.26	450 °C, 10 h	20 min, 50 mbar	Online extr. by steam	Online GC	36	CO_2, DME	0.09	NG[d]	120
8	Cu/SSZ-16	5.0	0.35					39		0.05		
9	Cu/SSZ-13	3.3	0.35					31		0.06		
10	Cu/Mor	NG	0.36	550 °C, 5 h	30 min, 50 mbar	Off-line extr. in D_2O	^{1}H-NMR	12.3	NG	NG	NG	122
11	Cu/Mor	3.07	0.32	450 °C, 1 h	240 min, 50 mbar	Online extr. by steam	Online MS	~ 70	CO_x, DME	0.145	~ 85	109, 123
12	Cu/Mor	2.90	0.28					~ 97		~ 0.33	~ 82	
13	Cu/Mor	4.7		450 °C, 4 h	30 min, 50 mbar			14.4		0.019		
14	Cu/Mor	4.7	NG	200 °C, 18 h	30 min, 37 bar	Off-line extr. in water	Off-line GC	56.2	NG	0.074	NG	118
15	Cu/zeoY	7.6			30 min, 32 bar			10.5		0.009		
16	Cu/ZSM-5	2.8			30 min, 32 bar			17.7		0.040		
17	Cu/SSZ-13	3.9	0.49	500 °C, 8 h	360 min, 1 bar	Online extr. by steam	Online GC	125	CO_x, DME	0.2	~ 86	121

[a]All Cu/zeolites were prepared via aqueous ion exchange between Na-form zeolites and $(CH_3COO)_2Cu$, except Entry 12, for which an NH_4-form mordenite was used. [b]TON = $moles_{products}$/$moles_{Cu}$. [c]Selectivity to MeOH and DME.
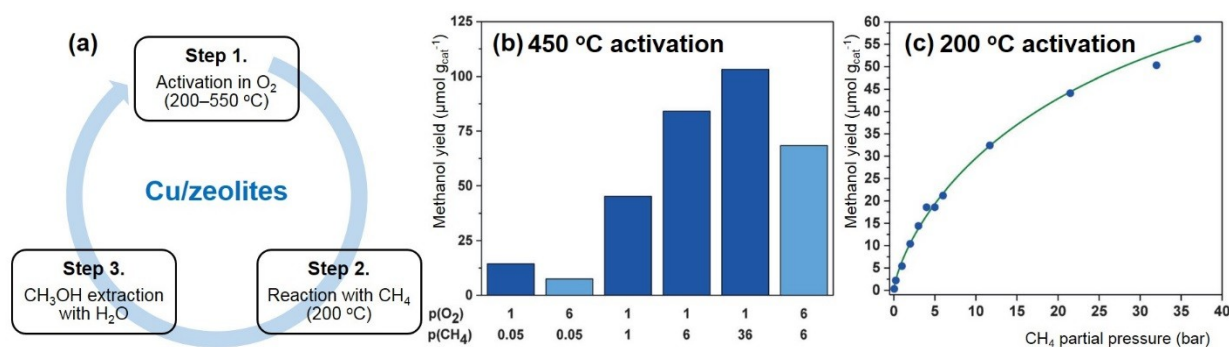
Figure 1.26. (a) Stepped conversion of methane to methanol over Cu/zeolites. (b) Methanol yields on Cu/mordenite after activation at 450 $^{\circ}$C and off-line extraction at different pressures of O_2 and methane. (b) Methanol yields on Cu/mordenite after activation at 200 $^{\circ}$C at 1 bar of O_2 and off-line extraction. Reprinted with permission from ref. 26 (Copyright 2016 Wiley-VCH).

1.3 Scope of the thesis

The above-described achievements have evidenced the great potential of MMOs-inspired protocols in developing environmentally friendly and highly selective catalysts for the low-temperature hydroxylation of methane. Although many designs of Fe- and Cu-based catalytic systems have recently been reported with improved activity and methanol selectivity, there is still a requirement for further investigations of bioinspired solid catalysts to gain more insight into possible active sites and catalytic mechanisms, and to provide further opportunities for catalyst synthesis and optimization, which are goals of this study. Both the reactions using either H_2O_2 or O_2 as the oxidant were carried out due to their fundamental significance. Initially, Cu- and Fe-containing zeolites, which were previously reported to be active for the methanol production from methane, were reproduced, characterized and tested to confirm their ability to hydroxylate methane under corresponding conditions. The next step was focused on development of improved or new catalytic systems.

Chapter 2 presents the results on comparison and optimization of aqueous-phase methanol production in the presence of various Cu/zeolites and Fe/zeolites. From these results in combination with XPS analysis, catalytic performances of Fe/zeolites were explained based on different mechanistic pathways for the activation of methane with H_2O_2.

In Chapter 3, the stepwise conversion of methane to methanol were performed over zeolitic catalysts prepared by solid-state ion exchange. Cu/zeolite showed a greatly better activity for this O_2-mediated oxidation compared to the Fe-based material. *In situ* UV-vis, IR and H_2-TPR

measurements were utilized with the aim of identifying the correlation between catalytic performance and location of metal species in the zeolite.

The preparation of novel silica-supported Cu catalysts was described in Chapter 4. Besides common Cu-containing compounds, a variety of molecular complexes resembling the proposed active center of pMMO, which were synthesized within the UniCat Cluster, were transferred into mesoporous silica via an immobilization strategy. The resulting materials were subsequently tested for their activity in the partial oxidation of methane by O_2 using a typical stepwise manner.

Chapter 2

Aqueous-Phase
Hydroxylation of Methane
Catalyzed by Fe- and Cu-
Containing Zeolites

2.1 Introduction

In the last decades, methane, the main component of natural gas and biogas, has emerged as a major energy source and an alternative chemical feedstock in the world. With a low C/H ratio in methane, the combustion of methane produces a much lower amount of CO_2 compared to crude oil and coal. Unfortunately, methane is still underutilized because of its costly transportation and storage.[15,21,22,105] The conversion of methane to liquid methanol is an ideal solution to retain mostly the energy content of methane and raise its value.[15,21] In addition, methanol would be also used as an important feedstock for chemical industry to either directly or indirectly produce value-added organic compounds. The current industrial route for the transformation of methane to methanol involves multiple steps via high-temperature and high-pressure manufacture of syngas (a mixture of H_2 and CO), which can be subsequently catalytically converted to methanol.[24,25,59,105] An attractive but challenging alternative to the energy-intensive syngas process is the direct production of methanol from methane.[26] However, methane is the most stable and unreactive hydrocarbon ($\Delta H_{C-H} = 439$ kJ mol^{-1}). The selective oxidation of methane to methanol is therefore extremely difficult to control under harsh conditions.[15,26] To date, the development of a commercially viable process with a high yield of methanol still remains unsolved.[105]

Inspired by the enzymatic structures containing active diiron and tri-/dicopper sites, which can efficiently catalyze the partial oxidation of methane to methanol in methanotrophic bacteria at room temperature, numerous novel catalysts have been introduced under both homogeneous and heterogeneous conditions.[15,24,125] Recently, the aqueous-phase conversion of methane to oxygenated products at low temperatures (50–70 ^{o}C) using hydrogen peroxide (H_2O_2) as an oxidant was performed in the presence of Fe/zeolite catalysts. Notably, Cu^{2+} species added to the reaction under either a heterogeneous (Cu/silicalite-1) or homogeneous (Cu(II) nitrate) form were able to reduce the deeper oxidation, yielding an improved selectivity toward methanol.[88] However, no comparative results on activity of the zeolite-based catalysts prepared by various methods in the H_2O_2-mediated hydroxylation of methane were reported. To gain a deeper understanding of this biomimetic catalytic system, in this chapter, the effect of the reaction conditions and the role of Cu on the activity of different Fe-containing MFI-type zeolites in the direct production of methanol from methane was critically investigated. The catalytic performances showed conflicting tendencies, proposing that the mechanism of activation and conversion of methane to methanol depends on the used catalyst type.

2.2 Synthesis of materials

2.2.1 Hydrothermal synthesis (HT)

Table 2.1. An overview on preparation of the materials used in this chapter.

Entry	Material	Preparation method	Metal and silica sources	Metal content[a] (wt.%)	Surface area$_{BET}$ (m²/g)
1	Silicalite-1	HT	TEOS	-	321.3
2	H-ZSM-5[b]	Calcination	-	Fe: 0.022	336.9
3	H-mordenite[b]	Calcination	-	Fe: 0.029	352.1
4	Fe-Si-1	HT	$Fe(NO_3)_3.9H_2O$, TEOS	Fe: 0.43	352.9
5	H-Fe-Si-1			Fe: 0.45	367.0
6	Fe-Si-2	HT	$Fe(NO_3)_3.9H_2O$, TEOS	Fe: 0.82	376.5
7	H-Fe-Si-2			Fe: 0.81	373.5
8	H-Cu-Si	HT	$Cu(NO_3)_2.6H_2O$, TEOS	Cu: 0.47	340.7
8	H-FeCu-Si	HT	$Fe(NO_3)_3.9H_2O$, $Cu(NO_3)_2.6H_2O$, TEOS	Fe: 0.54 Cu: 0.52	344.9
10	Fe/ZSM-5	SSIE	$Fe(acac)_3$, NH₄-ZSM-5	Fe: 2.28	287.1
11	Cu/ZSM-5	SSIE	$Cu(acac)_2$, NH₄-ZSM-5	Cu: 2.62	307.5
12	Cu/mordenite	SSIE	$Cu(acac)_2$, NH₄-mordenite	Cu: 2.58	307.0
13	FeCu/ZSM-5	SSIE	$Fe(acac)_3$, $Cu(acac)_2$, NH₄-ZSM-5	Fe: 2.39 Cu: 2.68	260.1
14	Fe/mordenite	SSIE	$Fe(acac)_3$, NH₄-mordenite	Fe: 2.30	308.1
15	Fe/Si	Dry impregnation[c]	$Fe(acac)_3$, silicalite-1	Fe:2.32	260.6
16	Fe/SBA-15	Dry impregnation[c]	$Fe(acac)_3$, SBA-15	Fe: 2.36	660.3
17	Cu/Si	Dry impregnation[c]	$Cu(acac)_2$, silicalite-1	Cu: 2.51	274.7

[a]ICP analysis.

[b]H-form zeolites were obtained via calcination of their NH₄-form at 550 °C in static air for 4 h.

[c]Dry impregnation of non-ion-exchangeable materials with $Fe(acac)_3$ was performed similarly to solid-state ion exchange.

Fe- and Cu-containing silicalites-1 prepared by hydrothermal treatment were denoted as M-Si (M: Fe, Cu). According to the procedure reported,[88] in a typical batch for the synthesis of Fe-Si-1 (0.43 wt.% of Fe), tetraethyl orthosilicate (TEOS, 10.24 g, 49.4 mmol) was stirred vigorously at room temperature for 1 h. An aqueous solution of tetrapropylammonium hydroxide (15.0 g, 1 M) was then added drop-wise under vigorous stirring. The mixture was then stirred at 60 ^{o}C for 2 h. A prepared solution of iron(III) nitrate nonahydrate (0.154 g, 0.38 mmol) in water (10 ml) was added drop-wise to the mixture. Subsequently, the resulting gel was homogenized at 60 ^{o}C for 5 h and crystallized in a Teflon-lined stainless steel autoclave in oven at 175 °C for 120 h. The white solid was then isolated by filtration, washed with water, and dried at 110 ^{o}C for 16 h. Calcination of the material was performed at 550 ^{o}C (1 ^{o}C min^{-1}) under a N_2 flow for 5 h and then under a O_2 flow for another 3 h. With the aim of removing undesired extra-framework cations,[126] the as-synthesized sample was protonated in a 1.0 M solution of ammonium nitrate at 85 ^{o}C for 48 h and finally calcined at 550 ^{o}C (2 ^{o}C min^{-1}) for 3 h under static air, yielding H-Fe-Si-1 (0.45 wt.% of Fe).

2.2.2 Solid-state ion exchange (SSIE)

In a second approach, metal cations were supported on NH_4-ZSM-5 (Si/Al = 15) and NH_4-mordenite (Si/Al = 10), which were commercially obtained from Alfa Aesar, by solid-state ion exchange.[88] Post-synthesized catalysts were denoted as M/zeolite (M: Fe, Cu). For example, to prepare Fe/ZSM-5 (2.28 wt.% of Fe), a mixture of iron(III) acetylacetonate (Fe(acac)$_3$, 0.158 g, 0.45 mmol) and NH_4-ZSM-5 (0.975 g) was intensively ground in a mortar for 30 min. The resulting powder was then calcined at 550 ^{o}C (2 ^{o}C min^{-1}) for 3 h under static air before use.

2.3 Catalytic studies
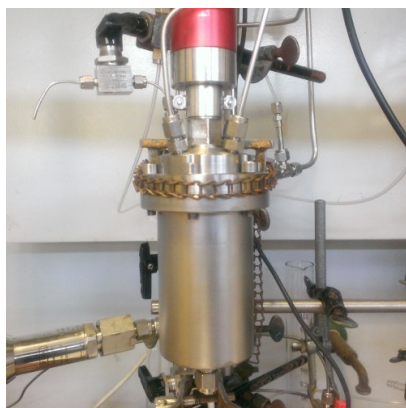
Figure 2.1. High-pressure autoclave reactor (up to 50 bar) equipped with a thermocouple and a pressure sensor for the partial oxidation of methane to methanol by H_2O_2.

In a typical test, the selective oxidation of methane using H_2O_2 as an oxidant in the presence of a metal-loaded zeolite catalyst was carried out in a stainless-steel autoclave containing a glass vessel with a total volume of 100 mL. A predetermined amount of the catalyst was added to an aqueous solution of H_2O_2 (10 mL, 0.5 M) in the vessel. After the batch reactor was sealed, the contaminant gasses were removed by a series of purges (5 times with CH_4 at 30 bar). The reactor was recharged with CH_4 to a pressure of 30 bar and then heated to 50 °C. The reaction was maintained for 30 min under vigorous stirring (1500 rpm). The autoclave was subsequently cooled in an ice bath to 10 °C. The reaction solution was filtrated, dosed with a predetermined volume of acetonitrile and analyzed by gas chromatography (GC).
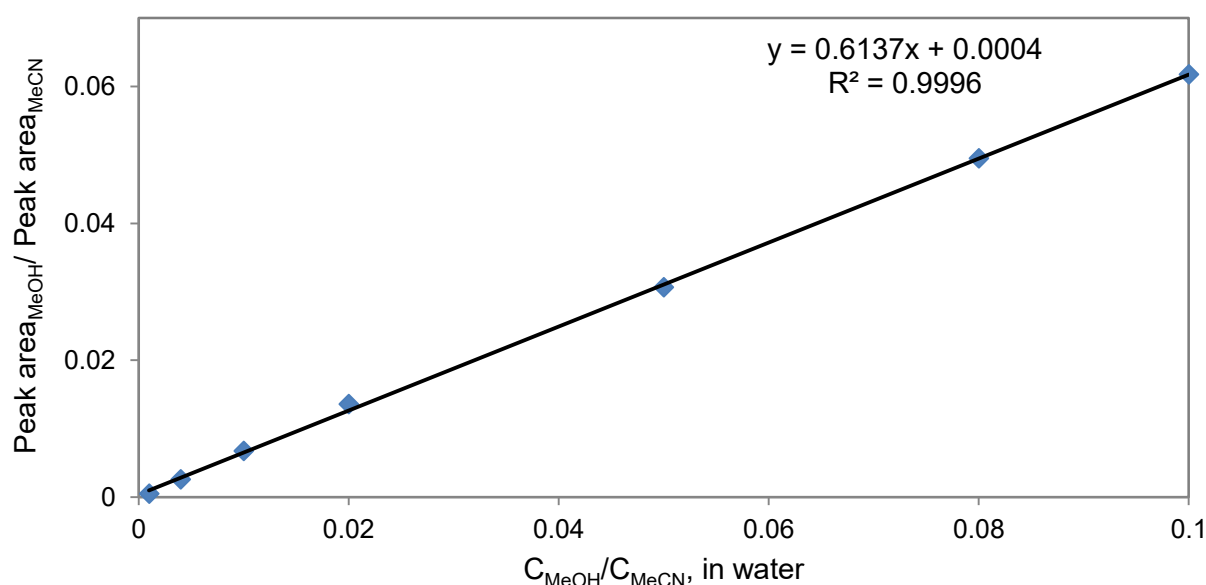
Figure 2.2. Calibration curve for methanol in the concentration range of 0.01 – 1 μl/ml using acetonitrile as an internal standard.

Gas chromatographic analysis was performed using a Shimadzu GC 17-A equipped with flame ionization detector (FID) and a SUPELCOWAX® 10 column (length = 30 m, inner diameter = 0.53 mm, and film thickness = 1.00 μm). The oven was held at 60 °C for 8 min; then heated to 120 °C at a rate of 30 °C min^{-1}. Inlet and detector temperatures were set constant at 180 °C. Methanol concentration in the aqueous samples was determined using the calibration curve with acetonitrile as an internal standard.

TONs were calculated based on the ratio of methanol amount produced (mol) per Fe loading (mol).

2.4 Results and discussion
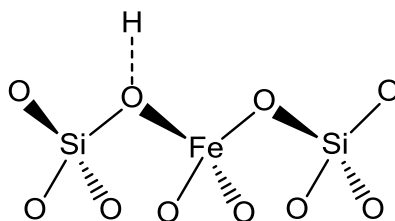
Figure 2.3. Proposed structure of an Fe site at the framework position in silicalite-1 after calcination.[101,127-129]
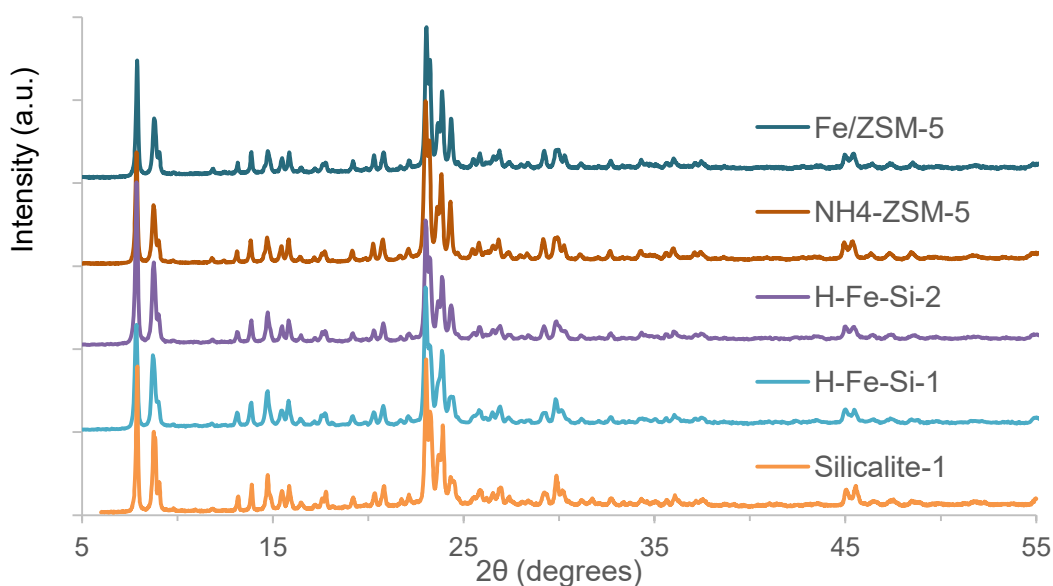
Figure 2.4. PXRD patterns of MFI framework-type materials.

Fe and Cu species were loaded into zeolites by either one-pot hydrothermal synthesis or solid-state ion exchange. The direct route yields isomorphously substituted Fe^{3+} sites in tetrahedral positions of silicalite-1 (Figure 2.3) while Fe species are preferentially located at exchangeable sites via solid-state ion exchange.[127,130,131] PXRD patterns of all calcined samples confirmed that the MFI-type framework of sililicalite-1 and ZSM-5 was maintained (Figure 2.4). No peaks of Fe and Cu-containing crystalline phases were observed and TEM images showed no detectable nanoparticles (Figure 2.5), indicating that a high dispersion of metallic species in the zeolites could be obtained upon both synthetic approaches. Furthermore, in the TEM image of H-Fe-Si-1 (0.45 wt.% of Fe), it can be observed that morphology and size of Fe-containing zeolitic crystals generally remained unchanged in comparison with those of control silicalite-1. However, increasing the Fe content to 0.81 wt.% led to an observation of a flower-like form of large

particles consisting of agglomerated smaller nanocrystals, i.e. 50–100 nm in diameter. This change proves that the isomorphous substitution of Fe at a high loading into the MFI-type zeolite could significantly affect the formation and development of zeolitic crystals prepared via the hydrothermal treatment.
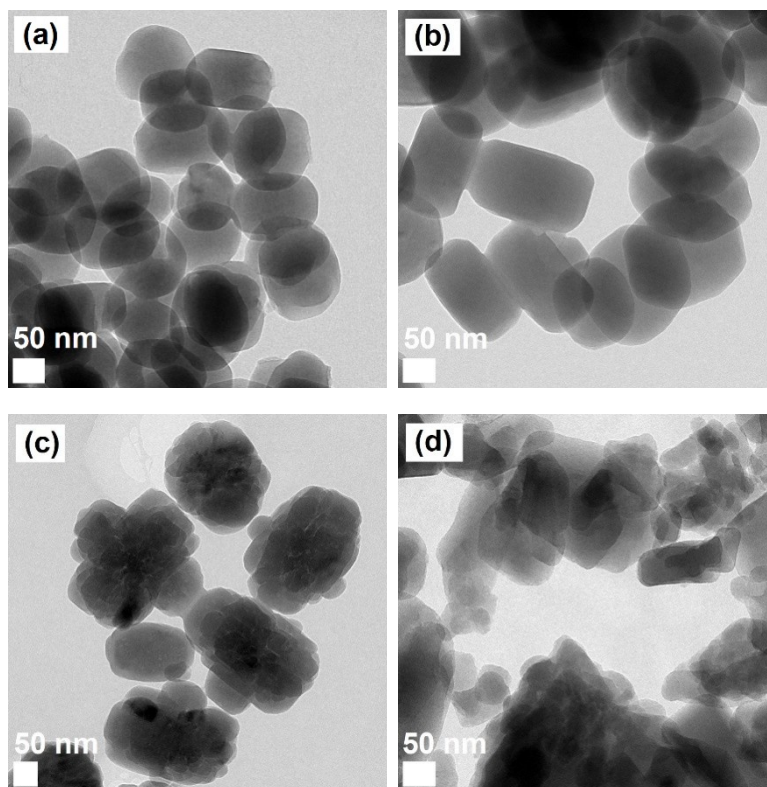
Figure 2.5. TEM images of (a) as-synthesized silicalite-1, (b) H-Fe-Si-1, (c) H-Fe-Si-2, (d) Fe/ZSM-5.

N_2 sorption isotherms confirmed the typical microporous structure for all Fe- and Cu-containing zeolites. Loading Fe and Cu species in ZSM-5 via the post-synthesis modification resulted in a significant decrease in the surface area of the materials, demonstrating that other species than exchanged cationic sites, e.g. oligonulear oxo-metal complexes and small M_xO_y clusters, were also present, occupying the zeolite pores.[127] In contrast, the surface area of metal-containing silicalites-1, which were hydrothermally synthesized, was found to be higher than that of pure silicalite-1. Among them, Fe-Si-2 possesses the most improved surface area probably due to its smaller particle size.

No noticeable differences between the FT-IR spectra of silicalite-1 and metal-containing ones were detected (Figure 2.6). Accordingly, the spectra exhibited a band centered at 550 cm^{-1}, which is assigned to the vibration of double 5-membered rings in MFI-type lattices.[132,133] In earlier studies, a small band appearing at ~ 650 cm^{-1} was attributed to the stretching vibration of

the $\equiv$Fe-O-Si$\equiv$ bond.[133,134] On the other hand, Hammond *et al.* assigned this band to extra-framework Fe species in the zeolite.[90] Interestingly, such a band was also observed in the spectra of the Cu-based sample and even of metal-free silicalite-1. We can therefore conclude that the band centred at ~ 650 cm^{-1} should not be considered as a spectroscopic evidence for the successful incorporation of Fe species into the MFI framework. In addition, a further observation of a band at 710 cm^{-1} based on the isomorphous substitution of Fe in silicalite-1 was reported. In this study, the low Fe concentrations and poor sensitivity of the IR measurement probably led to the absence of this band for Fe-silicalite-1 samples.[90]
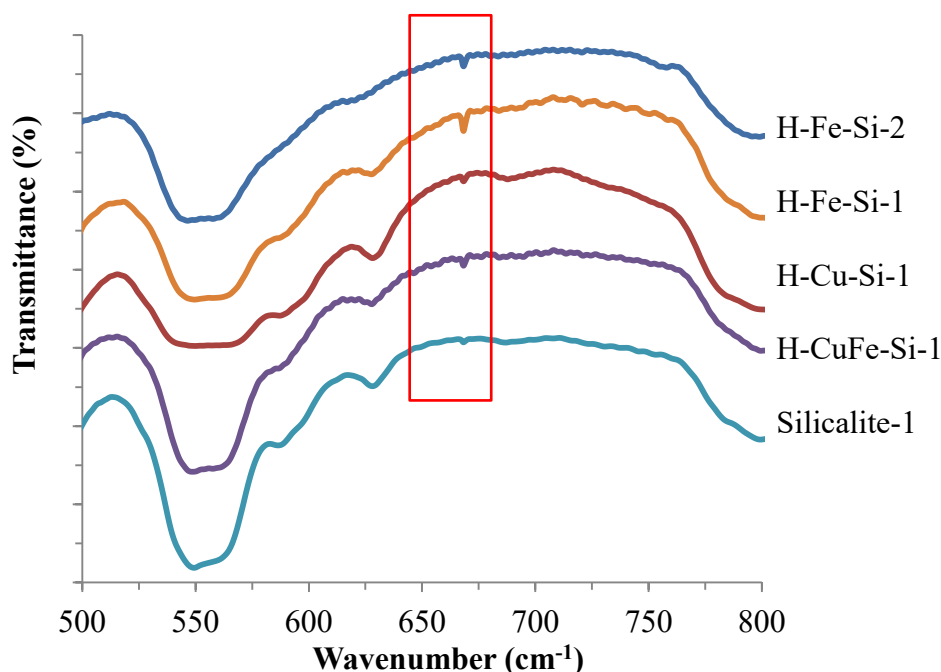
Figure 2.6. FT-IR spectra of silicalite-1-based materials.

The metal-loaded zeolites were then used as solid catalysts for the partial oxidation of methane to produce methanol as the target product under liquid-phase conditions. Typically, the reaction was performed in a batch reactor at an initial CH$_4$ pressure of 30 bar using an aqueous solution of H$_2$O$_2$ as the oxidant. As-synthesized silicalite-1 was found to be inactive for this reaction while the commercial zeolites always containing trace Fe impurities were able to produce small amounts of methanol (Table 2.2, Entries 1, 2 and 4). As expected, following addition of Fe^{3+} species to silicalite-1 by hydrothermal synthesis and to ZSM-5 via solid-state ion exchange led to a significant enhancement in activity (Table 2.2, Entries 7, 9, 10, and 11), emphasizing that Fe species are active sites for the liquid-phase conversion of methane to methanol in the presence of H$_2$O$_2$. However, not all types of Fe species are able to catalyze the methane-to-methanol conversion. No methanol was indeed obtained in the reactions using Fe-impregnated silica

materials, i.e. Fe/Si and Fe/SBA-15 (Table 2.2, Entries 12 and 13), ruling out the catalytic role of supported Fe_xO_y clusters.

Table 2.2. Initial investigations of activity of the solid catalysts in the H_2O_2-mediated hydroxylation of methane.

Entry	Catalyst	Fe content (wt. %)	MeOH yield (μmol)	TON
1	Silicalite-1	0	0	-
2	H-ZSM-5	0.022	9.1	858
3	Cu/ZSM-5	0.022	6.5	613
4	H-mordenite	0.029	10.0	715
5	Cu/mordenite	0.029	6.4	458
6	Fe-Si-1	0.43	0	0
7	H-Fe-Si-1	0.45	16.4	76
8	Fe-Si-2	0.82	0	0
9	H-Fe-Si-2	0.81	24.2	62
10	Fe/ZSM-5	2.28	20.0	18
11	Fe/mordenite	2.30	21.0	19
12	Fe/Si	2.32	0	0
13	Fe/SBA-15	2.36	0	0
14	Cu/Si	0	0	-
15	H-Cu-Si	0	0	-

Reaction conditions: catalyst 27 mg, 50 ^{o}C, 30 min, 1500 rpm, P(CH$_4$) 30 bar, V$_{solution}$ 10 ml, [H$_2$O$_2$] 0.5 M.

For the case of Fe-silicalite-1 catalysts, it was observed that as-synthesized Fe-silicalite-1 was inactive independent on the Fe loading. Surprisingly, a great activity enhancement was obtained after the materials were further protonated in a solution of NH_4NO_3 and subsequently calcined in static air (Table 2.2, Entries 6-9). The increase of extra-framework Fe species was previously reported to elucidate the improved catalytic performance of Fe-silicalite-1 for the H_2O_2-based oxidation of methane to methanol. It was proposed that the Fe sites isomorphously substituted are ineffective in the activation of methane while active sites can be generated from the extra-framework Fe species.[89,126,135,136] Powder XRD, TEM and N$_2$ sorption results showed no

recognizable changes in structure, morphology, and porosity of the materials before and after the post-synthetic treatment. Also, it should be noted that the Fe content in Fe-silicalites-1 was maintained during the treatment, proving that no Fe species were leached from the solid to the solution and therefore most, if not all, of the Fe species in Fe-silicalite-1 were indeed stably located in the zeolitic framework. However, after the second calcination, the resulting H-Fe-Si-2 (0.81 wt.% of Fe) turned ivory-white while the former one was colorless, indicating the migration of Fe species from the framework sites to the extra-framework positions as cationic sites.[127,131] It seems to be difficult to detect such a color change for H-Fe-Si-1 because of its low Fe loading (0.45 wt.%).

Further XPS analysis was performed to gain more insight into the relocation of Fe species on the MFI surface. The XPS spectra of all Fe-containing samples at the Fe 2p region showed peaks characteristic of oxidized Fe species (Figure 2.7). Only a peak centered at ~ 711 eV corresponding to Fe^{3+} $2p_{3/2}$ was detected in the deconvoluted spectra of as-synthesized Fe-silicalites-1 (Fe-Si-1 and Fe-Si-2). This result indicates that Fe ions in Fe-silicalites-1 are in the trivalent oxidation state consistent with the location of Fe in the framework tetrahedral sites. After the further treatment, the corresponding samples (H-Fe-Si-1 and H-Fe-Si-2) revealed an additional peak centered at ~ 709 eV attributed to Fe^{2+} $2p_{3/2}$.[137-143] A similar result is also observed for the Fe/ZSM-5 sample, which mainly contains exchanged Fe sites at the extra-framework positions. Extra-framework Fe^{3+} can be partially autoreduced to Fe^{2+} upon dehydration of the sample at high temperatures.[98,101,135,136,144,145] The presence of Fe^{2+} species detected by the XPS measurements therefore demonstrated that a fraction of the isomorphously substituted Fe^{3+} sites indeed migrated to the extra-framework positions, at which Fe species are highly reactive, leading the enhanced activity of Fe-silicalite-1.

Copper species showed no activity in the methane-to-methanol oxidation by H_2O_2 as no traces of CH_3OH could be detected in the reactions using the Cu-only materials (Table 2.2, Entries 13 and 14). Nevertheless, the presence of Cu^{2+} species in commercial zeolites led to a slight decrease in methanol production, showing that the catalytic performance of the Fe-containing zeolites can be influenced by Cu^{2+} species (Table 2.2, Entries 2–5). The role of supported Cu^{2+} species on the Fe-catalyzed methanol synthesis from methane was therefore investigated. This study was first performed on the Fe-silicalite-1-containing system (Table 2.3). Further adding Cu-loaded silicalites-1 resulted in a decrease of the methanol amount compared to the reactions using Fe-silicalite-1 catalyst alone. Slight improvements in the production of methanol were observed as different amounts of Cu/ZSM-5 were added to this catalytic system. However, it should be noted

that Cu/ZSM-5 itself could produce a small amount of methanol due to impurity Fe species, therefore contributing such additional yields. In general, no significant enhancements in the methane-to-methanol conversion were obtained based on the combination of Fe-silicalite-1 and Cu-containing zeolites.
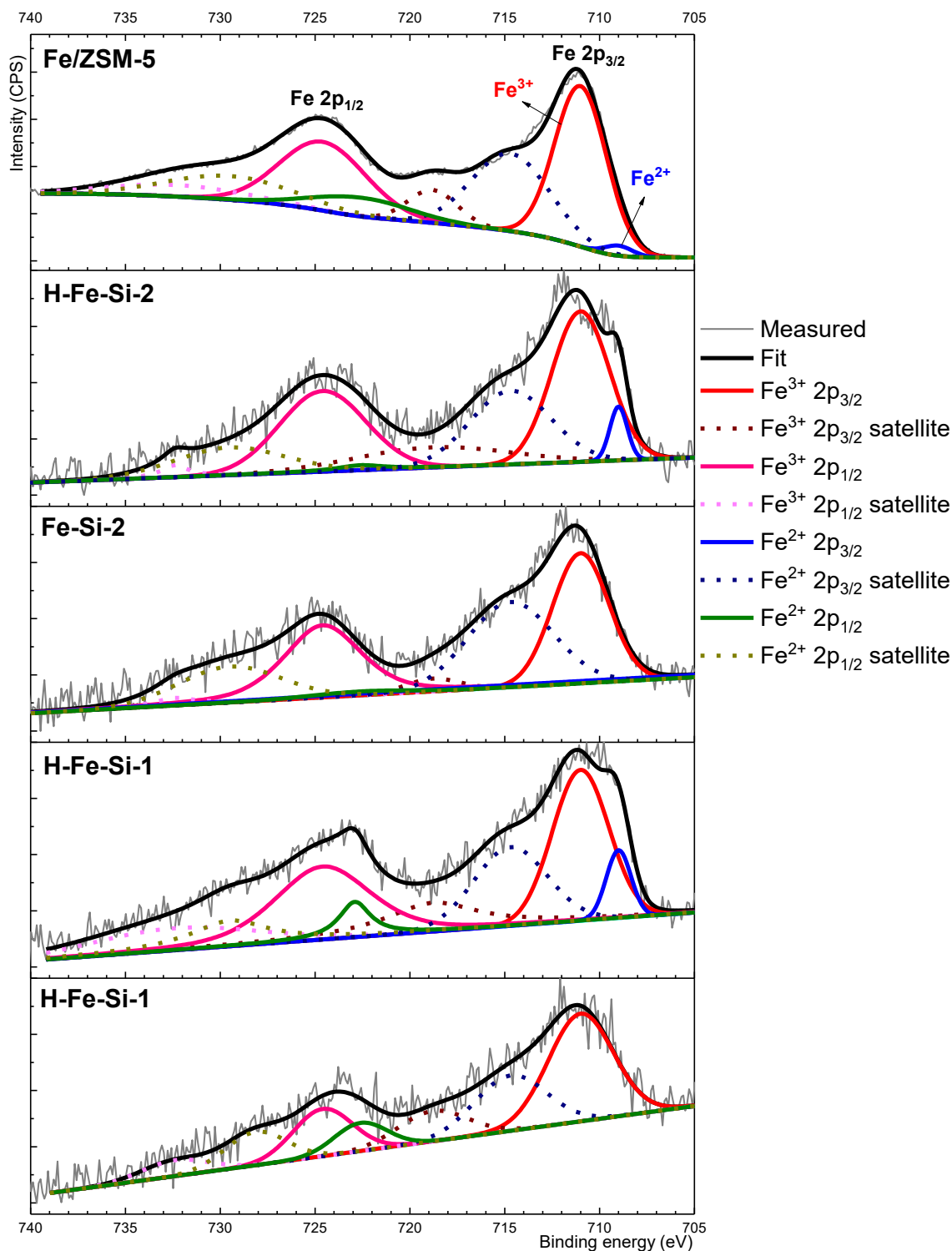

Figure 2.7. Fe 2p XPS spectra of the Fe-containing zeolites.

Table 2.3. Methanol production catalyzed by Fe-silicalites-1 in the presence of Cu species.

Entry	Main catalyst	Fe content (wt. %)	Co-catalyst	MeOH yield (μmol)	TON
1	H-Fe-Si-1	0.45	-	16.4	76
2			H-Cu-Si	16.2	75
3			Cu/Si	16.9	78
4			Cu/ZSM-5	22.7	105
5			Cu/ZSM-5 (13.5 mg)	19.2	89
6			Cu/ZSM-5 (54 mg)	21.0	97
7	H-FeCu-Si-1	0.54	-	14.3	55
8	H-Fe-Si-2	0.81	-	24.2	62
9			H-Cu-Si	20.3	52
10			Cu/Si	18.8	48
11			Cu/ZSM-5	24.8	63

Reaction conditions: Fe-silicalite-1 catalyst 27 mg, co-catalyst (if used) 27 mg, 50 $^{\circ}$C, 30 min, 1500 rpm, P(CH$_4$) 30 bar, V$_{solution}$ 10 ml, [H$_2$O$_2$] 0.5 M.

In contrast, the addition of Cu-containing zeolites to the Fe/ZSM-5-mediated reaction yielded notable positive results. Indeed, the methanol amount significantly increased upon the presence of Cu species (Figure 2.8). Compared to the Fe/ZSM-5-only system, the Cu-assisted yield increased ranged from 3 to nearly 6 times, depending on the added Cu-loaded zeolite. Similar yields of methanol observed for Cu/silicalite-1 and Cu/ZSM-5, which contain similar Cu loadings, indicated that the presence of Al sites and the form of supported Cu species have no considerable effect on the improved methanol production. CuFe/ZSM-5 prepared via simultaneous deposition of Fe and Cu onto ZSM-5 was less efficient than a physical mixture of Fe/ZSM-5 and Cu/ZSM-5 since active Fe sites were probably hindered from interacting with other reactants by the appearance of Cu species. Decreasing the amount of Cu/ZSM-5 to 13.5 mg and 6.75 mg led to just minor losses in the production of methanol, strongly confirming the promoting role of Cu in the methane-to-methanol conversion catalyzed by Fe/ZSM-5 (Figure 2.9). However, in the reaction using 54 mg of Cu/ZSM-5, the methanol yield dropped to about half of the value obtained with 27 mg of Cu/ZSM-5. This yield decrease can be attributed to accelerated H$_2$O$_2$ decomposition by a large amount of metallic cation species added to the reaction.
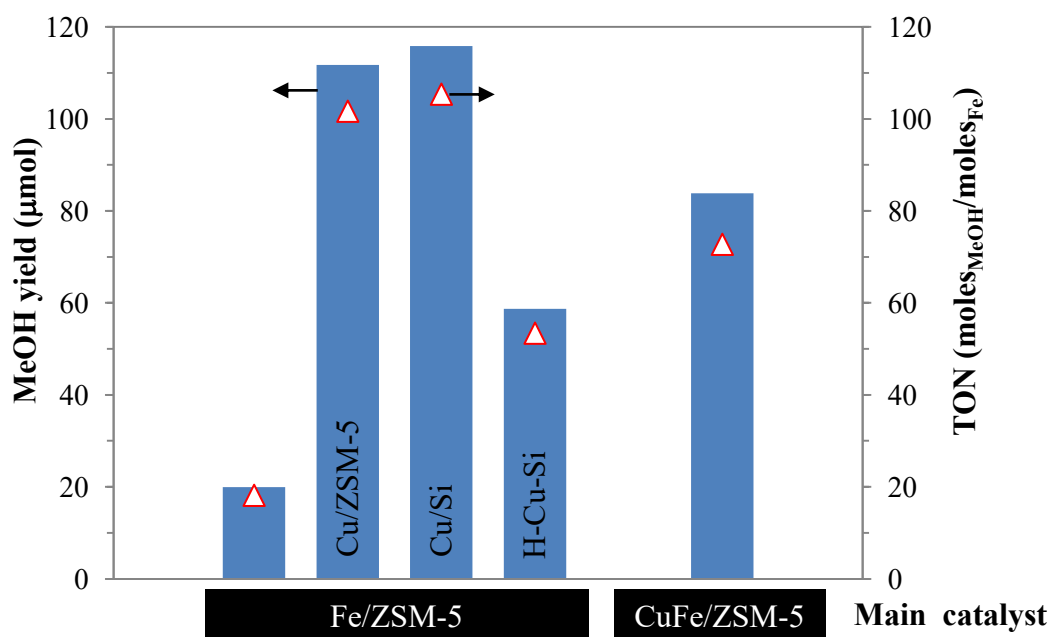
Figure 2.8. Methanol production catalyzed by Fe/ZSM-5 in the presence of Cu. Reaction conditions: Fe/ZSM-5 27 mg, co-catalyst (if used) 27 mg, 50 $^{\circ}$C, 30 min, 1500 rpm, P(CH$_4$) 30 bar, V$_{solution}$ 10 ml, [H$_2$O$_2$] 0.5 M.

Figure 2.9. Effect of Cu/ZSM-5 amount on the Fe/ZSM-5-catalysed conversion of methane to methanol. Reaction conditions: Fe/ZSM-5 27 mg, 50 $^{\circ}$C, 30 min, 1500 rpm, P(CH$_4$) 30 bar, V$_{solution}$ 10 ml, [H$_2$O$_2$] 0.5 M.

Based on the different reaction performances in the presence of additional Cu species, it was proposed that the catalytic mechanism of the selective oxidation of methane by H_2O_2 as the oxidant using the Fe-silicalite-1 catalyst is different from that of the Fe/ZSM-5 system. To further elucidate this conclusion, the effect of reaction conditions on the methanol production was investigated.
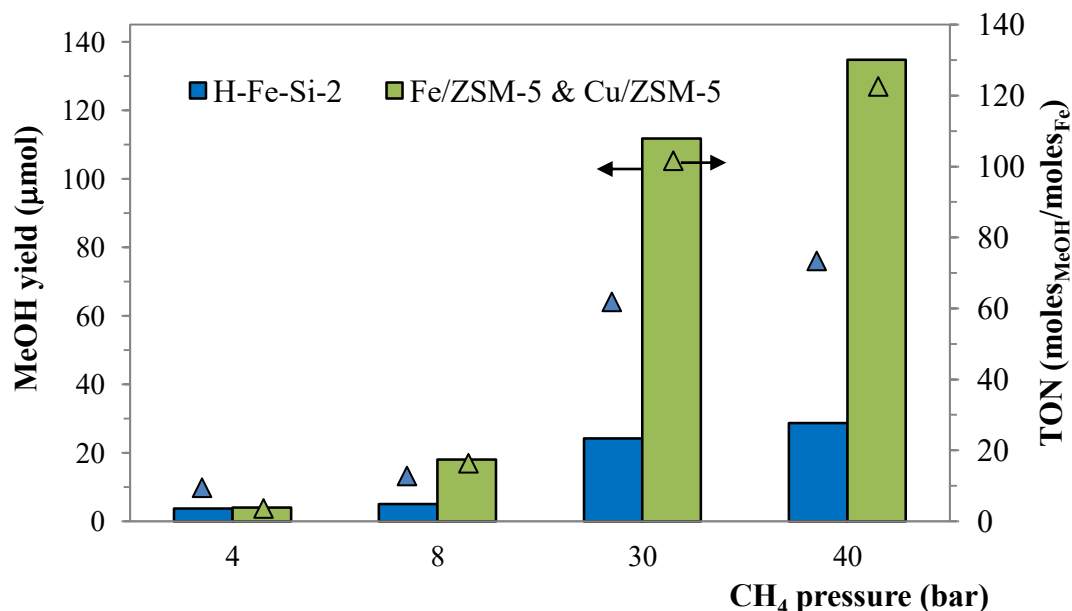
Figure 2.10. Effect of CH_4 pressure amount on the methanol production. Reaction conditions: main catalyst 27 mg, Cu/ZSM-5 (if used) 27 mg, 50 ^{o}C, 30 min, 1500 rpm, $V_{solution}$ 10 ml, $[H_2O_2]$ 0.5 M.

Poor yields of methanol were obtained in the reactions performed at a methane pressure below 10 bar (Figure 2.10). Under heterogeneous catalytic conditions, the gas-reactant pressure always plays an important role in reaction kinetics. In particular, a high pressure of methane should be applied to obtain an efficient interaction of methane with the solid catalyst and the aqueous oxidant phase. As can be expected, the reaction was able to produce greater amounts of methanol as conducted at elevated pressure, namely 30 and 40 bar.

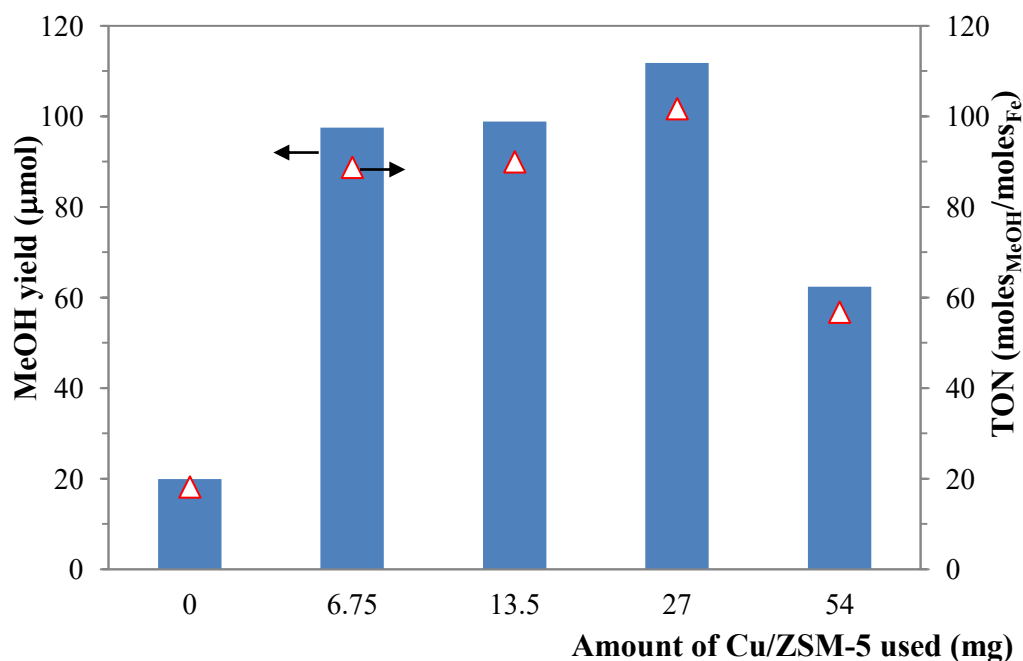In the Fe/ZSM-5 and Cu/ZSM-5-catalyzed reaction, raising the H_2O_2 concentration caused a moderate decrease in the methanol production. Namely, 111.8, 106.9 and 94.0 µmol of the desired product were produced in 0.5, 1.0 and 2.0 M solutions of H_2O_2, respectively (Figure 2.11). A high concentration of H_2O_2 is unfavorable for the selective oxidation of methane toward methanol in the presence of Fe/ZSM-5 and Cu/ZSM-5. Surprisingly, an opposite tendency was observed for the Fe-Si-2-based system, in which using more H_2O_2 was found to be necessary to increase the methanol yield. A clear improvement in the production of methanol by increasing

the H_2O_2 amount was observed, giving maximum 70.5 μmol of CH_3OH with 20 mmol of H_2O_2 used. Also, the inhibiting role of Cu species on the catalytic performance of Fe-silicalite-1 was further confirmed as the product amount was just slightly improved and always greatly lower than the case of the pure catalyst independent on the H_2O_2 concentration.
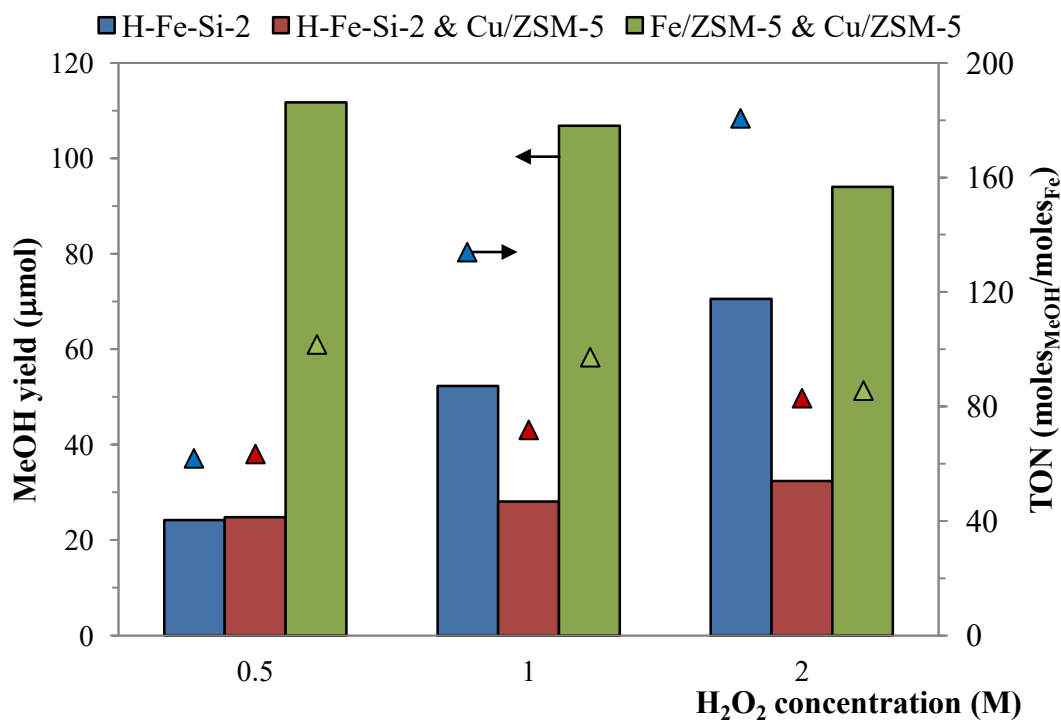
Figure 2.11. Effect of H_2O_2 concentration on the methanol production in different catalytic systems. Reaction conditions: main catalyst 27 mg, Cu/ZSM-5 if used 27 mg, $P(CH_4)$ 30 bar, 50 ^{o}C, 30 min, 1500 rpm, $V_{solution}$ 10 ml.

In oxidation reactions, the study on temperature is important to obtain an optimal balance between the reaction rate and the selectivity to a major product. Indeed, efficient activation of methane requires high temperatures and strong oxidants while milder conditions can avoid the over-oxidation of methanol. Again, the influence of reaction temperature on the production of methanol was found to be dependent on the used catalyst type (Figure 2.12). In the tested range from room temperature to 70 ^{o}C, the reaction using Fe/ZSM-5 and Cu/ZSM-5 catalysts performed at room temperature could yield the greatest amount of methanol. Remarkable losses of methanol were observed as a result of the promoted over-oxidation at elevated temperature. On the other hand, the methanol production catalyzed by H-Fe-Si-2 reached the highest yield at an intermediate temperature of 50 ^{o}C. The conversion of methane toward methanol proceeded much more slowly as carried out at room temperature. Unlike the Fe/ZSM-5 and Cu/ZSM-5-based system, increasing the reaction temperature from 50 to 70 ^{o}C led to just a minor decrease

in the methanol amount in the presence of the H-Fe-Si-2 catalyst although a high H_2O_2 concentration of 2 M was used.
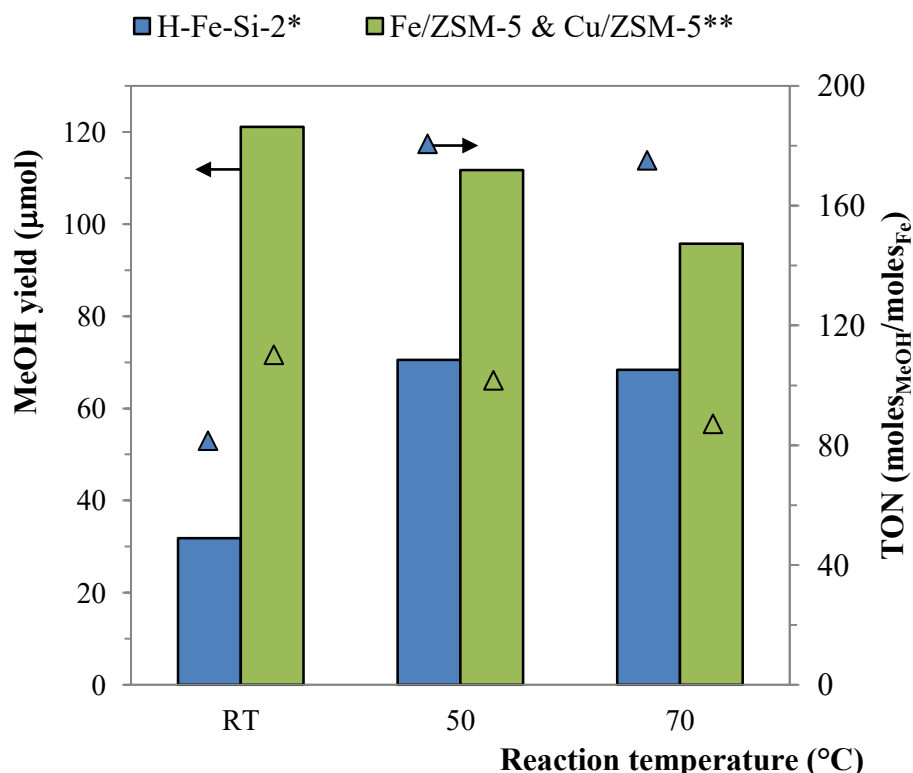
Figure 2.12. Effect of reaction temperature on the methanol production. General reaction conditions: main catalyst 27 mg, Cu/ZSM-5 if used 27 mg, P(CH$_4$) 30 bar, 30 min, 1500 rpm, V$_{solution}$ 10 ml; (*) [H_2O_2] 2.0 M, (**) [H_2O_2] 0.5 M.

It can be concluded that the selective oxidation of methane to methanol catalyzed by Fe/ZSM-5 is greatly enhanced by the addition of Cu species and this catalytic system can produce more methanol under milder conditions, i.e. low H_2O_2 amount and low temperature. In contrast, Fe-silicalite-1 shows a negative response to the appearance of Cu species and should be performed with a high H_2O_2 concentration at a moderate temperature to obtain high methanol yields. As mentioned above, in recent reports, Fe species at the extra-framework positions within the MFI matrix are assigned to be the active sites for methane oxidation. However, the different catalytic performances of Fe/ZSM-5 and Fe-silicalite-1 suggest that methanol could be produced in following different pathways.

By a combination of EXAFS measurements and periodic DFT calculations, Hammond *et al.* previously proposed a mechanism for the conversion of methane to methanol in H_2O_2 based on an extra-framework diiron complex [Fe$_2$(μ_2-OH)$_2$(OH)$_2$(H$_2$O)$_2$]$^{2+}$ in ZSM-5 (Figure 2.13).[88] Accordingly, this diiron site successively reacts with two H_2O_2 molecules to produce an

$[Fe^{4+}=O]$ site and an adjacent $[Fe^{4+}\text{-OOH}]$ site. The resulting bifunctional oxidation center is able to activate methane, forming methyl hydroperoxide (MeOOH) as a primary product. The target product is subsequently produced by Fe-mediated decomposition of MeOOH.[146] However, MeOOH and methanol can further react with highly reactive hydroxyl radicals produced via a homolytic cleavage of the O-O bond of H_2O_2, forming formic acid and CO_2.[146] Cu^{2+} species was added to the reaction to inhibit the over-oxidation by hydroxyl radicals; therefore the selectivity toward methanol could be significantly improved. It was demonstrated that the crucial role of Cu is to act as a hydroxyl radical scavenger, leading to a drastic decrease in concentration of hydroxyl radicals in the reaction solution.[88,146] Also, it was suggested that the Cu ion can catalyze the heterolytic cleavage of the O-O bond of MeOOH, promoting the subsequent formation of methanol.[147] The catalytic results on the Fe/ZSM-5 and Cu/ZSM-5-catalyzed production of methanol in this study are in good agreement with the proposed hypothesis. Increasing reaction temperature and H_2O_2 concentration can accelerate the formation of hydroxyl radical which is obviously favorable for the deeper oxidation to the unwanted products.

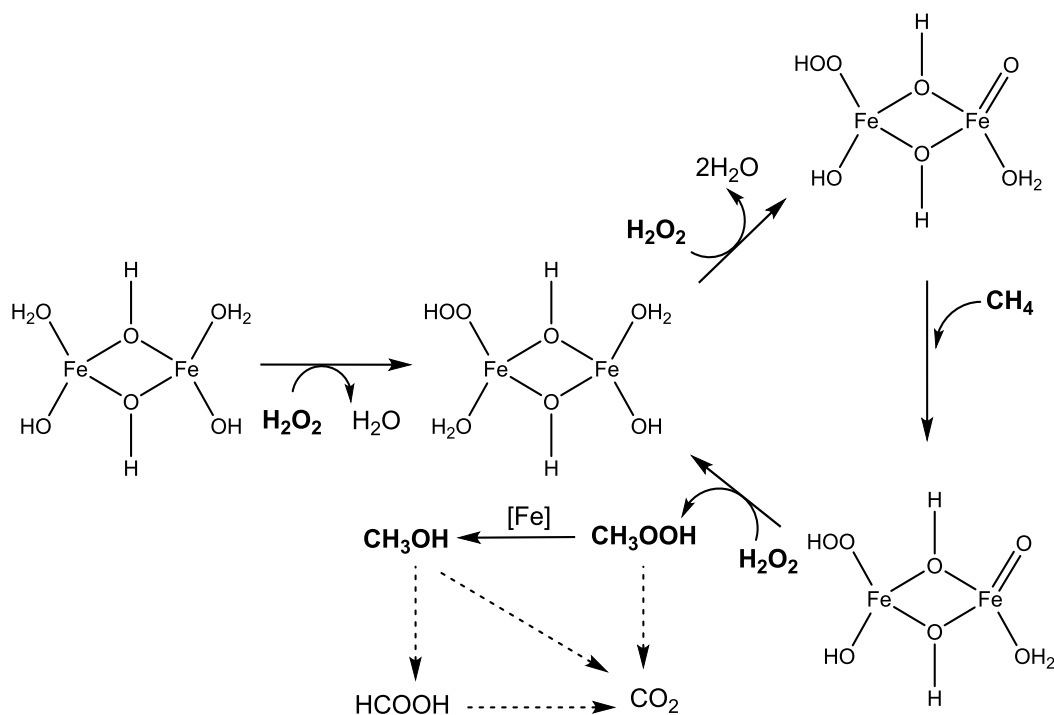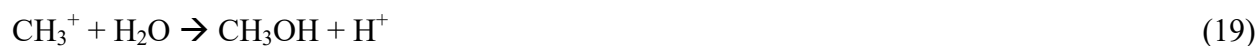**Figure 2.13.** Mechanism proposed by Hammond *et al.* for the oxidation of methane to methanol by H_2O_2 catalyzed by a diiron site in ZSM-5.[88]

The effect of varying the reaction conditions on the Fe-silicalite-1-based system is basically opposite to Fe/ZSM-5. Applying the above described mechanism to this catalytic system therefore seems to be irrational. In addition, only a fraction of Fe sites is extracted from the

framework positions to the active cation sites while the Fe content in silicalite-1 is much lower than in the Fe-exchanged sample. Therefore, extra-framework dimeric Fe species are probably uncommon in Fe-silicalites-1. It was indeed previously demonstrated that the extra-framework iron ions are mainly present as isolated species in the MFI matrix with a low Fe concentration.[148,149] The hydroxylation of methane is proposed to be preferably upon the free radical mechanism. Extra-framework isolated Fe^{2+} sites are capable of reacting with H_2O_2 to generate hydroxyl radicals (Reaction 15) that are responsible for activation and conversion of methane into oxygenated products like the Fenton reaction (Reactions 17–19).[89,101,133,150-152] Based on the area of the deconvoluted Fe $2p_{3/2}$ peaks in the XPS spectra, a higher ratio of Fe^{2+}/Fe^{3+} was observed for the activated Fe-silitcalites-1 in comparison to Fe/ZSM-5, which might be of advantage for the formation of hydroxyl radicals. Performing the reaction with a high concentration of H_2O_2 and at an elevated temperature can increase the hydroxyl radical amount, therefore leading to the great improvements in the methanol yield. This catalytic pathway is also consistent with the result that the appearance of Cu^{2+} species scavenging the hydroxyl radicals in the reaction resulted in a notable decrease in the methanol amount compared to the performance of only Fe-silicalite-1.

$$Fe^{2+} + H_2O_2 \rightarrow Fe^{3+} + \cdot OH + OH^- \tag{15}$$

$$Fe^{3+} + H_2O_2 \rightarrow Fe^{2+} + \cdot OOH + H^+ \tag{16}$$

$$\cdot OH + CH_4 \rightarrow \cdot CH_3 + H_2O \tag{17}$$

$$\cdot CH_3 + Fe^{3+} \rightarrow Fe^{2+} + CH_3^+ \tag{18}$$

$$CH_3^+ + H_2O \rightarrow CH_3OH + H^+ \tag{19}$$

Furthermore, with aim to produce more methanol, the reaction was prolonged up to 2 h using the described catalysts (Figure 2.14). It should be noted that formed methanol is much more active than methane; keeping methanol in the oxidative phase for a long time can therefore cause a considerable loss of methanol. It was shown that the hydroxylation of methane proceeded readily in the first 15 min for all catalytic systems, yielding major amounts of methanol. With longer reaction times, further production of methanol with a moderate rate was observed for all systems. The over-oxidation of methanol in the reaction catalyzed by Fe/ZSM-5 and Cu/ZSM-5 can be better controlled at ambient temperature, at which the highest methanol yield of 157.6 μmol was obtained after 2 h. In the reaction performed at 50 ^{o}C, the over-oxidation of methanol became more significantly after the first hour, leading to a slight methanol loss in the next hour. Using

Fe-silicalite-1 only in a solution containing 20 mmol of H_2O_2 (initial amount), about half of the methanol amount produced within the first hour was indeed consumed within the second hour as a consequence of the dominating over-oxidation process. The reaction time should therefore be considered with care to optimize the yield of desired product in the presence of highly reactive free radicals.
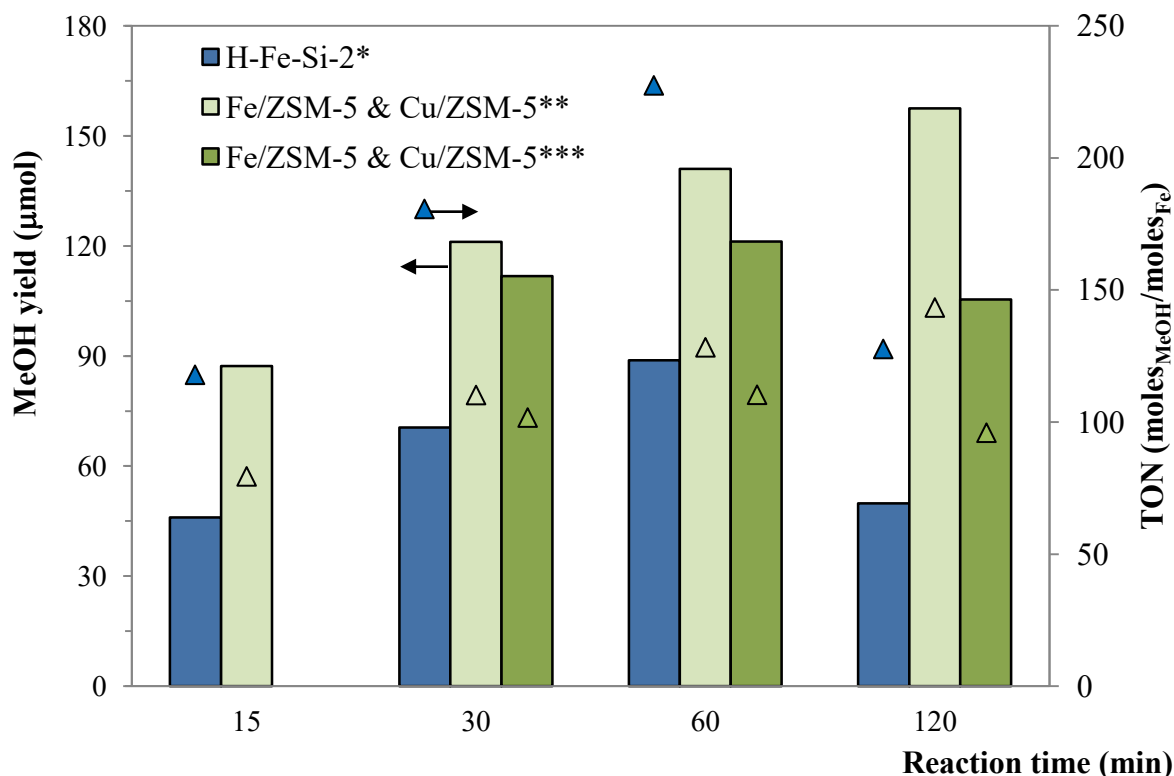
Figure 2.14. Effect of reaction time on the methanol production. General reaction conditions: main catalyst 27 mg, Cu/ZSM-5 if used 27 mg, P(CH$_4$) 30 bar, 1500 rpm, V$_{solution}$ 10 ml; (*) [H$_2$O$_2$] 2.0 M, 50 °C, (**) [H$_2$O$_2$] 0.5 M, 30 °C, (***) [H$_2$O$_2$] 0.5 M, 50 °C.

2.5 Conclusions

Various Fe- and Cu-containing zeolites have been applied as solid catalysts for the partial oxidation of methane to methanol by H_2O_2 at low temperatures (RT–70 $^{\circ}$C). Combining the results from the catalytic tests and XPS analysis, it was confirmed that the extra-framework Fe sites are the active centers while the supported Cu species can act as either a promoter or an inhibitor for the methane-to-methanol conversion, depending on the applied Fe-based zeolite catalyst. Investigating the influence of reaction conditions on the methanol yield revealed the opposite tendencies between the catalytic systems containing Fe/ZSM-5 and Fe/silicalite-1, suggesting that the conversion toward methanol is based on two different mechanisms.

The results for Fe/ZSM-5 are in good agreement with the previously proposed mechanism based on a bioinspired oxo-diiron site. The binuclear Fe species located at the extra-framework positions are responsible for activation and following transformation of methane into CH_3OOH as a primary product, which can yield methanol via further catalytic decomposition. Adding Cu species to the reaction led to a great improvement in the methanol production due to the ability of Cu to reduce the amount of hydroxyl radicals generated from H_2O_2, which strongly promote the over-oxidation of CH_3OOH and methanol to formic acid and CO_2. An increase in methanol yield was therefore observed by employing milder reaction conditions such as low H_2O_2 concentration or temperature, under which the formation of hydroxyl radical could be efficiently controlled.

Table 2.4. Optimized methanol production using the different Fe-containing MPI-type zeolites.

Catalyst	Co-catalyst	Reaction conditions	MeOH yield (μmol)	TON
H-Fe-silicalite-1 (0.81 wt.%, 27 mg)	-	[H_2O_2] 2.0 M, 50 °C, 60 min, P(CH_4) 30 bar, 1500 rpm, $V_{solution}$ 10 ml	88.8	227
Fe/ZSM-5 (2.28 wt.%, 27 mg)	Cu/ZSM-5 (2.51 wt.%, 27 mg)	[H_2O_2] 0.5 M, RT, 120 min, P(CH_4) 30 bar, 1500 rpm, $V_{solution}$ 10 ml	157.6	143

In silicalite-1, the extra-framework Fe sites are mainly present as isolated species and in much lower concentration. Unlike the case of Fe/ZSM-5, the appearance of Cu in the reaction mixture significantly diminished the methanol yield. A hydroxyl radicals-based pathway is suggested for the Fe-silicalite-1-catalysed hydroxylation of methane. As expected, the reaction with a high concentration of H_2O_2 or carried out at a relatively elevated temperature yielded more methanol due to the improved production of hydroxyl radical under such conditions. Based on the calculated TONs, the well-dispersed isolated Fe species show a remarkable higher activity for the methane-to-methanol conversion than the pure Fe/ZSM-5 catalyst and even the system consisting of Fe/ZSM-5 and Cu/ZSM-5 under identical conditions (Table 2.4).

The H_2O_2-mediated conversion of methane to methanol was proved to be strongly dependent on the type of Fe species accommodated in the zeolite framework. Further studies on varying Fe concentration and evaluating the production of other oxygenated products are needed to gain more insight into structure, role and fraction of different active Fe sites and to improve the selectivity to the target product.

2.6 Appendix

(a) (b) (c)

(d) (e) (f)

Figure 2.15. Photographs of (a) silicalite-1, (b) Fe-Si-1, (c) H-Fe-Si-1, (d) Fe-Si-2, (e) H-Fe-Si-2, and (f) Fe/ZSM-5.
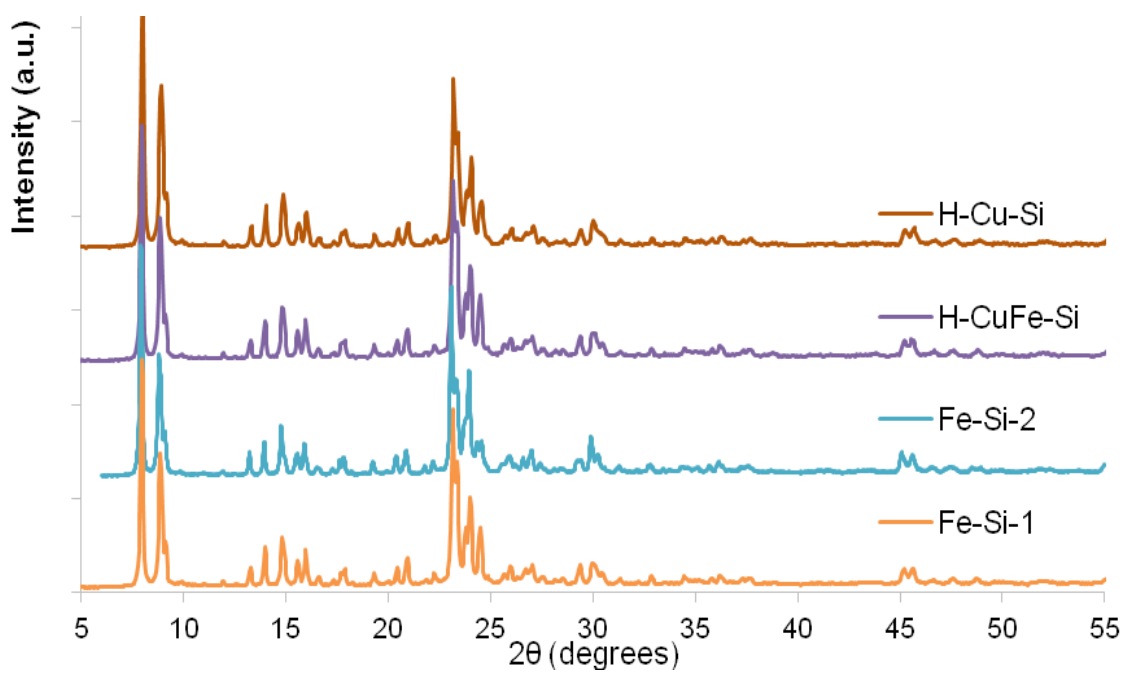

Figure 2.16. PXRD patterns of other Fe- and Cu-containing silicalites-1.
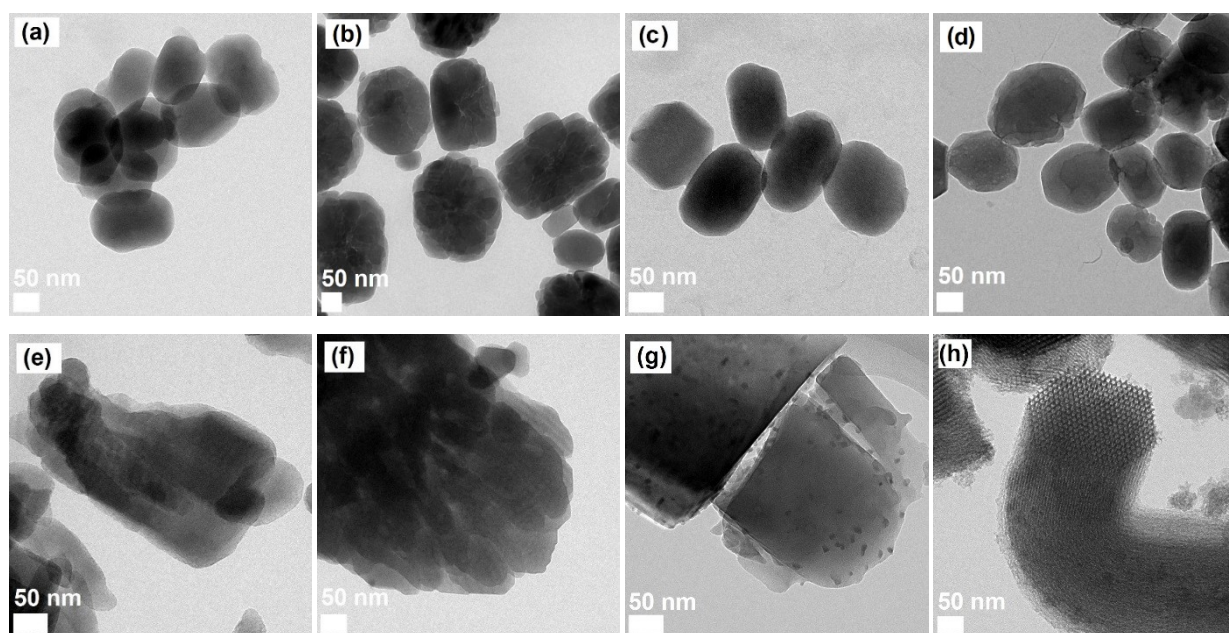
Figure 2.17. TEM images of (a) Fe-Si-1, (b) Fe-Si-2, (c) H-Cu-Si, (d) H-FeCu-Si, (e) FeCu/ZSM-5, (f) Cu/ZSM-5, (g) Fe/Si, and (h) Fe/SBA-15.

Chapter 3

Improved Cu/Mordenite Catalysts for the Direct Conversion of Methane to Methanol

3.1 Introduction

The selective oxidation of methane to methanol is of considerable interest for obtaining valuable chemicals directly from abundant natural gas resources without the need of syngas production.[22,29,37,153] To reach this challenging target, harsh reaction conditions are required as activation of methane is hampered due to its strong C-H bonds. Moreover, the desired product, methanol, is more reactive than methane, which easily results in over-oxidations into formic acid or carbon oxides.[28,97,120,154,155] Interestingly, methanotrophic bacteria in nature can selectively perform this "dream reaction" under ambient condition using methane monooxygenase enzymes, which contain di-iron or di/tri-copper active clusters.[68,73,83,84] These enzymatic structures provide intriguing structural motifs for the development of biomimetic catalytic systems toward the activation of methane.[83,156,157]

To date, many different bioinspired catalysts for the direct methanol formation from methane have been synthesized and intensively studied with the aim of improving the methanol yield under milder reaction conditions. In the previous chapter, H_2O_2 was used to partially oxidize methane into methanol in the presence of different Fe- and Cu-containing zeolites. However, as H_2O_2 is more expensive than methanol, the direct use of O_2 as the oxidant is inevitable for industrial applications.[29] Several research groups have demonstrated that iron-, cobalt-, and copper-exchanged zeolites activated in O_2 or N_2O can react with methane at low temperatures ($\leq$ 200 ^{o}C) and subsequently release methanol upon treatment with water or organic solvents (acetonitrile, ethanol, tetrahydrofuran).[97,101-103,109,118,124,158] Among them, Cu/zeolites have currently been emerged as the most efficient catalyst.[109,111,118,120]

Cu^{2+} cations are typically loaded into zeolites *via* liquid-phase ion exchange in most of the reports. Bozbag *et al.* have recently performed a solid-state ion exchange between H-mordenite with copper(I) chloride to achieve a Cu/mordenite catalyst. It was observed that residual chlorine hindered the production of methanol from methane in the first runs.[159] In this study, the activity of solid-state ion-exchanged Cu/mordenite prepared from NH_4-mordenite and copper(II) acetylacetonate was investigated for the catalytic conversion of methane to methanol for the first time. The methanol yield was found to be considerably higher than the results achieved from conventional Cu/mordenites, which were prepared in liquid phase.

3.2 Synthesis of materials

Zeolites in different forms and types were obtained from Alfa Aesar. NH_4-mordenite (Si/Al = 10) is denoted as NH_4-Mor-1 while Na-mordenite (Si/Al = 6.5) is denoted as Na-Mor-2. Silicalite-1 was hydrothermally synthesized as described in Section 2.2.1 of Chapter 2.

3.2.1 Conversion of commercial mordenites to the Na- or NH_4-form

Ammonium exchange of Na-Mor-2 was performed as previously described.[120] In detail, a mixture of Na-Mor-2 (2 g) and a NH_4NO_3 solution (80 ml, 1 M) was stirred vigorously for 2 h at 80 °C. Ion exchange was repeated 3 times. The sample was then filtrated, washed with water, and dried at 105 °C for 12 h. Mor-2 in the NH_4 form is denoted as NH_4-Mor-2.

A similar procedure was applied for the preparation of the Na-form of Mor-1 using an aqueous solution of CH_3COONa. The dried solid was further calcined at 550 °C (2 °C min^{-1}) under static air for 4 h, yielding Na-exchanged Mor-1 denoted as Na-Mor-1.

3.2.2 Solid-state ion exchange (SSIE)

Cu^{2+} exchange of NH_4-zeolites was performed in solid state using copper(II) acetylacetonate ($Cu(acac)_2$) as a Cu source.[88] In a typical procedure to prepare CuMorS-1 (Table 1, entry 1), $Cu(acac)_2$ (0.120 g) and NH_4-Mor-1 (0.975 g) were intensively ground for 30 min. The resulting powder was pressed into pellets at 100 bar for 60 s, lightly ground, and sieved to a 200–400 μm diameter fraction. Ion exchange was performed *in situ* with the activation step of the catalytic testing. The Cu loading in the samples was determined by inductively coupled plasma-optical emission spectrometry (ICP-OES).

Another Cu-containing mordenite sample, CuMorS-Cl (Table 1, entry 1), was prepared via the solid-state ion exchange of NH_4-Mor-1 with copper(I) chloride based on the modified procedure of Wulfers *et al.*[120] Firstly, CuCl (0.043 g) was mixed with NH_4-Mor-1 (0.975 g) as described above. The well-ground mixture was pressed and sieved to a 200–400 μm diameter fraction. A U-shaped quartz reactor containing the sample (0.7 g) was placed in an oven. Before the catalytic test, the reactor was heated to (2 °C min^{-1}) in a 50 Nml min^{-1} flow of N_2. The temperature was kept constant at 650 °C for 10 h, and then decreased to 550 °C under the same flow. The next activation step in O_2 was carried out as described in Section 3.3 in this chapter.

3.2.3 Liquid-phase ion exchange (LIE)

Cu-exchanged mordenites could be prepared by a traditional procedure in aqueous phase.[120] To obtain CuMorL-1 (Table 1, Entry 7), Na-Mor-2 (2 g) was added to an aqueous solution of

copper(II) acetate ($Cu(OAc)_2$, 0.476 g). The resulting mixture was stirred for 18 h at room temperature. The sample was subsequently filtrated, washed with water, dried at 105 °C for 12 h, and calcined at 550 °C (2 °C min^{-1}) for 4 h under static air.

Table 3.1. An overview on the synthesis of catalysts used in Chapter 3.

Entry	Catalyst	Preparation method	Substrates[a]	Si/Al ratio	Cu content[b] (wt.%)
1	CuMorS-1	SSIE	$Cu(acac)_2$ (0.120 g) and NH_4-Mor-1	10	2.58
2	CuMorS-2	SSIE	$Cu(acac)_2$ (0.045 g) and NH_4-Mor-1	10	1.01
3	CuMorS-3	SSIE	$Cu(acac)_2$ (0.084 g) and NH_4-Mor-1	10	1.84
4	CuMorS-4	SSIE	$Cu(acac)_2$ (0.180 g) and NH_4-Mor-1	10	3.74
5	CuMorS-5	SSIE	$Cu(acac)_2$ (0.120 g) and NH_4-Mor-2	6.5	2.66
6	CuMorS-Cl	SSIE	CuCl (0.043 g) and NH_4-Mor-1	10	2.84
7	CuMorS-OA	SSIE	$Cu(OAc)_2$ (0.084) and NH_4-Mor-1	10	2.55
8	FeMorS	SSIE	$Fe(acac)_3$ (0.150 g) and NH_4-Mor-1	10	2.27
9	CuMorL-1	LIE	$Cu(OAc)_2$ (0.476 g) and Na-Mor-2	6.5	3.21
10	CuMorL-2	LIE	$Cu(OAc)_2$ (0.476 g) and Na-Mor-1	10	3.10
11	CuMorL-3	LIE	$Cu(OAc)_2$ (0.476 g) and NH_4-Mor-1	6.5	2.07
12	CuZSM-S	SSIE	$Cu(acac)_2$ (0.120 g) and NH_4-ZSM-5	15	2.57
13	CuBeta-S	SSIE	$Cu(acac)_2$ (0.120 g) and NH_4-zeolite β	12.5	2.66
14	CuY-S	SSIE	$Cu(acac)_2$ (0.120 g) and NH_4-zeolite Y	6	2.46
15	CuFer-S	SSIE	$Cu(acac)_2$ (0.120 g) and NH_4- ferrierite	10	2.61
16	CuSil-S	Dry impregnation[c]	$Cu(acac)_2$ (0.120 g) and silicalite-1	-	2.51

[a]Amounts of zeolite used for each batch of SSIE and LIE are 0.975 g and 2.0 g, respectively.
[b]ICP analysis.
[c]Dry impregnation of Cu species into silicalite-1 was performed similarly to the Cu exchange in solid phase.

3.3 Catalytic studies

The sample in 200–400 μm particles (0.6–0.7 g) was loaded in a U-shaped quartz reactor (ID = 6 mm). The reactor was then placed in an oven and connected to a gases-supplying system

equipped with independent mass flow controllers. The sample was heated to 550 $^{\circ}$C (2 $^{\circ}$C min^{-1}) in a 50 Nml min^{-1} flow of O_2. Activation of the sample in O_2 was performed at this temperature for 8 h. After cooled to 60 $^{\circ}$C, the sample was purged with a 50 Nml min^{-1} flow of N_2 for 5 min for removal of the gas-phase O_2. A mixture of 5 Nml min^{-1} CH_4 and 30 Nml min^{-1} N_2 was then introduced to the reactor. The temperature of 60 $^{\circ}$C was kept unchanged for 20 min before the catalyst was heated to 200 $^{\circ}$C (5 $^{\circ}$C min^{-1}) under the same flow. After 60-min interaction of the catalyst with methane, the gas stream was switched off and the catalyst bed was cooled to room temperature.
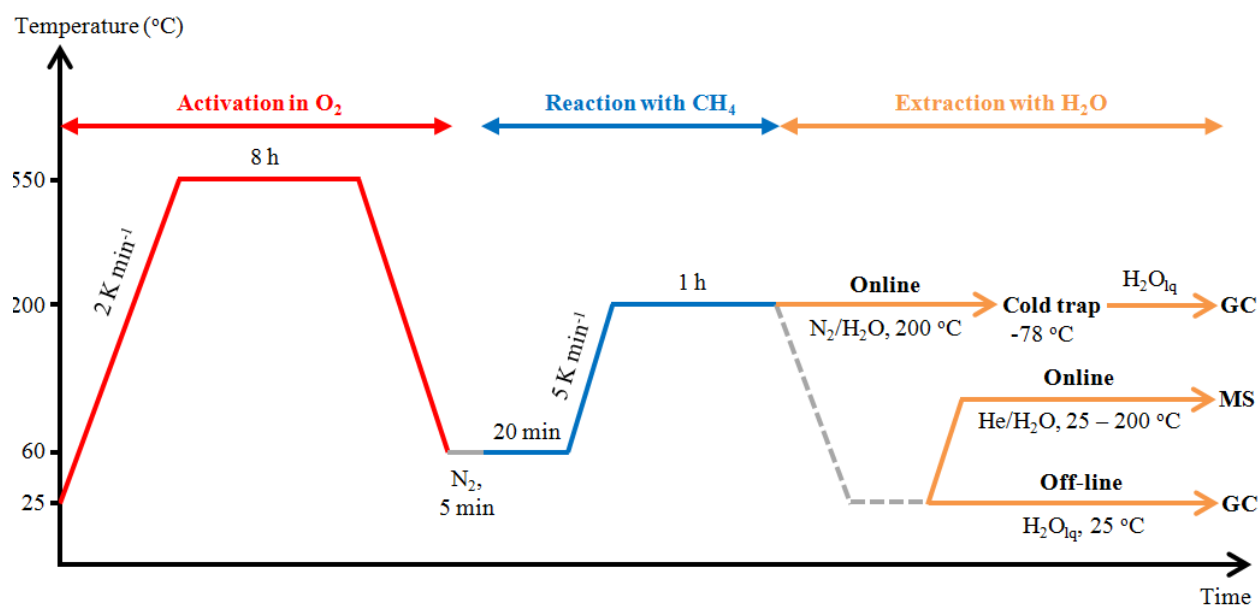
Figure 3.1. Schematic diagram of a catalytic cycle over Cu/zeolite.

For extraction of methanol by liquid water (off-line extraction), the cooled catalyst was afterward dispersed in 10 ml of water under vigorous stirring for 2 h. After centrifuging and filtration, the liquid phase was transferred to a volumetric flask, mixed with a predetermined volume of acetonitrile, which was used as an internal standard, and analyzed with a GC for quantification of methanol produced. The conditions of GC analysis were described in Section 2.3.

In an experiment using the online extraction method, after the contact of the catalyst with methane for 60 min at 200 $^{\circ}$C, a water-saturated N_2 flow (50 Nml min^{-1}) was introduced to the reactor. The reactor temperature was kept at 200 $^{\circ}$C while the temperature of the gas-washing bottle was set to 25 $^{\circ}$C during the whole experiment. The outlet stream was directed to a cold trap at -78 $^{\circ}$C placed in an isopropanol/dry ice bath for condensing liquids. After 8-h extraction, the cold trap was warmed to room temperature, diluted with water, mixed with acetonitrile, and

analyzed by GC. To collect methanol remaining on the catalyst after this experiment, the off-line extraction was further applied as described above after the catalyst bed was cooled to room temperature.

Also, the online extraction was performed on the setup connected with a quadruple mass spectrometer (InProcess Instruments GAM 200) for detection of products in the outlet stream. After reacting with methane at 200 ^{o}C, the catalyst was cooled to room temperature. The reaction products were extracted from the catalyst by a water-saturated He flow (50 Nml min^{-1}) at room temperature for 3 h. The reactor temperature was then raised to 200 ^{o}C (1 ^{o}C min^{-1}) and kept constant for another 3 h. The products were identified based on the revolution of the signal $m/z =$ 31, 44, and 45 characteristic for methanol, CO_2, and DME, respectively. The He signal ($m/z = 4$) was used as an internal standard to quantify DME and CO_2.

To investigate catalyst recyclability, after the extraction of methanol with water, the catalyst was dried at 105 ^{o}C, re-compressed and sieved to 200–400 μm particles, and loaded in the reactor for the next cycle under identical conditions.

TONs were calculated based on the ratio of methanol amount produced (mol) per metal loading (mol).

3.4 Results and discussion

Cu/zeolites are known as the most efficient catalyst for the partial oxidation of methane to methanol by molecular oxygen using a stepwise procedure. In earlier studies on this catalysis, Cu exchange of the zeolites was commonly carried out with an aqueous solution of a Cu(II) salt, producing much toxic waste water. Solid-state ion exchange is a promising alternative with notable advantages such as a more facile and simple protocol, less contaminants, and ease in adjusting the Cu loading. Therefore it is of interest to study the catalytic performance of Cu/mordenite prepared in the solid phase for the methane-to-methanol conversion in comparison with traditional catalysts (Table 1). Cu^{2+} exchange of mordenite was typically performed by calcination of a solid mixture of the NH$_4$-form mordenite and Cu(acac)$_2$ in O$_2$. The Cu loading was varied by changing the ratio of mordenite to Cu(acac)$_2$. In fact, to prepare metal-exchanged zeolites in solid phase, both the H- and NH$_4$-forms can be used.[160] An additional calcination step is required for the conversion of the NH$_4$-form to the H-form; however, this can be as well carried out during solid-state ion exchange at high temperature between Cu(II) acetylacetonate and NH$_4$-mordenite. Furthermore, it was reported that the degree of Cu exchange using the NH$_4$-

zeolite is considerably higher than for using the H-zeolite under the same calcination condition.[161]
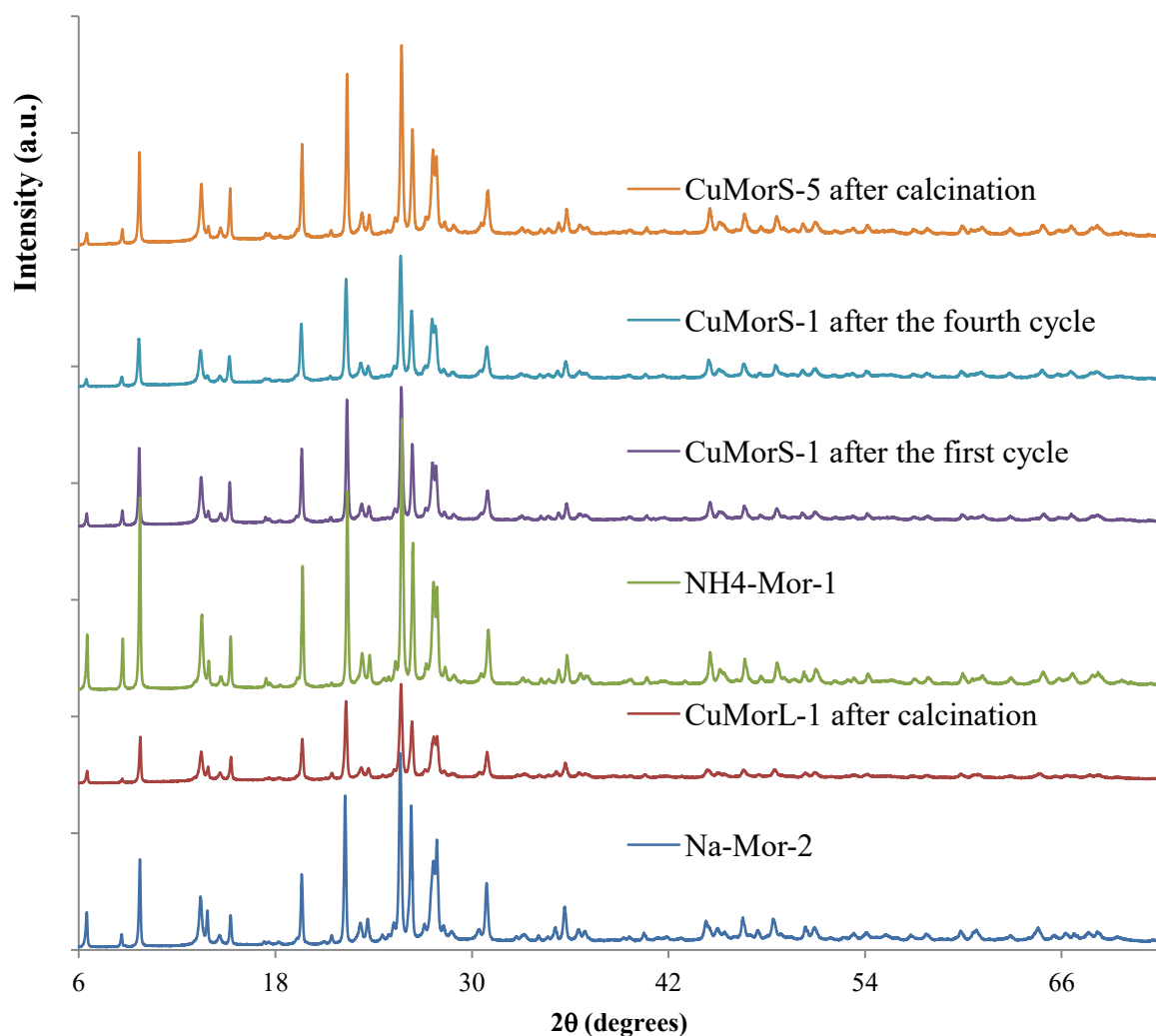
Figure 3.2. Powder XRD patterns of mordenite-based materials.

N_2 sorption measurements of Cu-exchanged mordenites showed a decrease in both surface area and total volume of the material in comparison to the pristine NH_4-form because of the presence of Cu species in the mordenite framework. Powder XRD measurements indicated that the crystalline structure of mordenite was maintained after Cu exchange at 550 ^{o}C (Figure 3.2). No additional peaks for Cu-containing crystalline phases were observed in the XRD patterns of Cu/mordenites, proving that the Cu species were highly dispersed throughout the zeolite framework and Cu-based nanoparticles. Conversely, TEM measurements show the formation of small nanoparticles. Interestingly, it was found that the number and size of nanoparticles observed in the TEM images significantly increased by prolonging irradiation time, consistent with the previous reports that Cu-based nanoparticles were not formed during synthesis but

during the TEM analysis because of irradiation within the high-energy electron beam.[159,162] The presence of regular nanoparticles for all Cu/zeolite samples however confirmed that the high dispersion of Cu species can be obtained by both ion exchange methods (Figure 3.3).

(a)   (b)   (c)

(d)   (e)   (f)
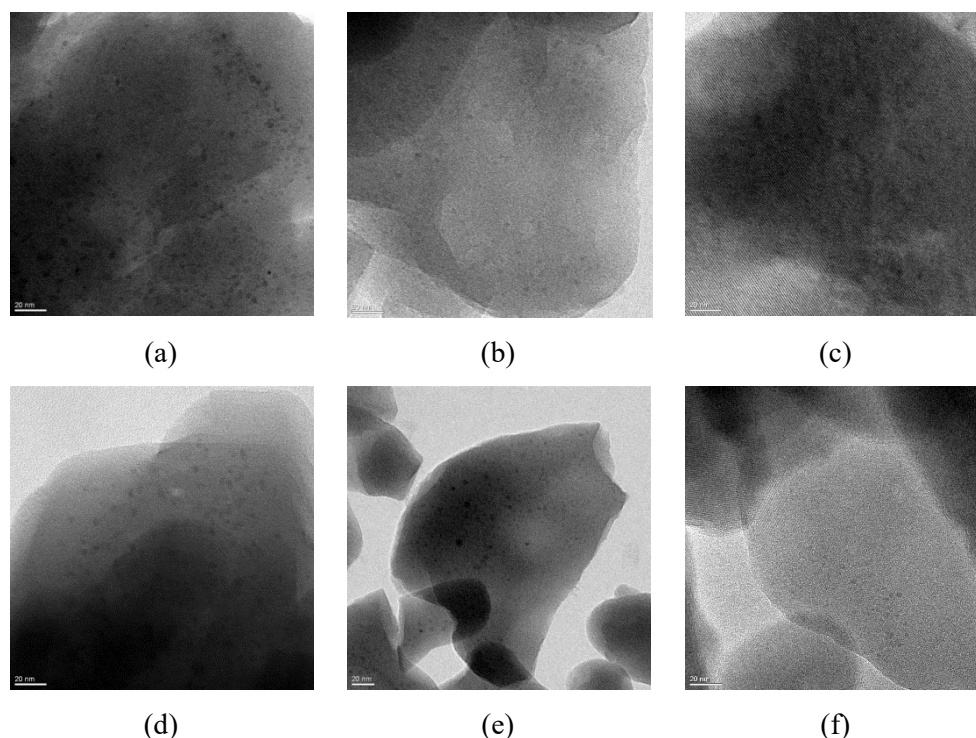
Figure 3.3. TEM images of Cu/mordenites (a) CuMorS-1, (b) CuMorS-1 after the 4th cycle, (c) CuMorS-3, (d) CuMorS-4, (e) CuMorL-1, (f) CuMorS-OA, scale bar: 20 nm.

Since the first report on the stepwise conversion of methane to methanol over Cu/zeolites,[103] several modifications of the catalytic procedure have been developed but still require further investigation.[105,109,112,114,116,118,119,125] In this study, the catalyst testing was performed in a well-described typical manner, namely *i)* activation of the material at 550 $^{\circ}$C in O_2 for 8 h, *ii)* treatment of the material with methane at 200 $^{\circ}$C, and *iii)* extraction of formed methanol with water (Figure 3.1).

Cu-exchanged mordenites prepared in solid state from different precursors including Cu(acac)$_2$, Cu(OAc)$_2$, and CuCl were tested. It was observed that the catalytic activity of CuMorS is strongly dependent on the Cu source used for the catalyst synthesis. The reaction yielded 39.3 μmol g$_{cat}^{-1}$ of methanol over the Cu(acac)$_2$-based catalyst (CuMorS-1) while Cu/mordenites prepared from Cu(OAc)$_2$ and CuCl showed significantly lower performances (Figure 3.4). It should be noted that the Cu loading and reaction conditions were identical to enable comparison of the catalytic performances. The Cu exchange using Cu(OAc)$_2$ produced a grey material while

other Cu/mordenites showed a light blue color after the high-temperature calcination in O_2. $Cu(OAc)_2$ was probably decomposed into CuO species before exchanged at the cation positions of mordenite, where highly active sites may be generated. The low methanol yield over the CuCl-based catalyst was consistent with the one recently reported,[159] in which Bozbag *et al.* showed the negative influence of chlorine remaining in mordenite on the first catalytic cycles. Furthermore, it was demonstrated in this study that inactive Cu^+ species could be still detected in mordenite after the first O_2 activation, which also led to the poor performance of CuMorS-Cl. Using $Cu(acac)_2$ as a precursor is therefore clearly preferable for Cu exchange in solid state.
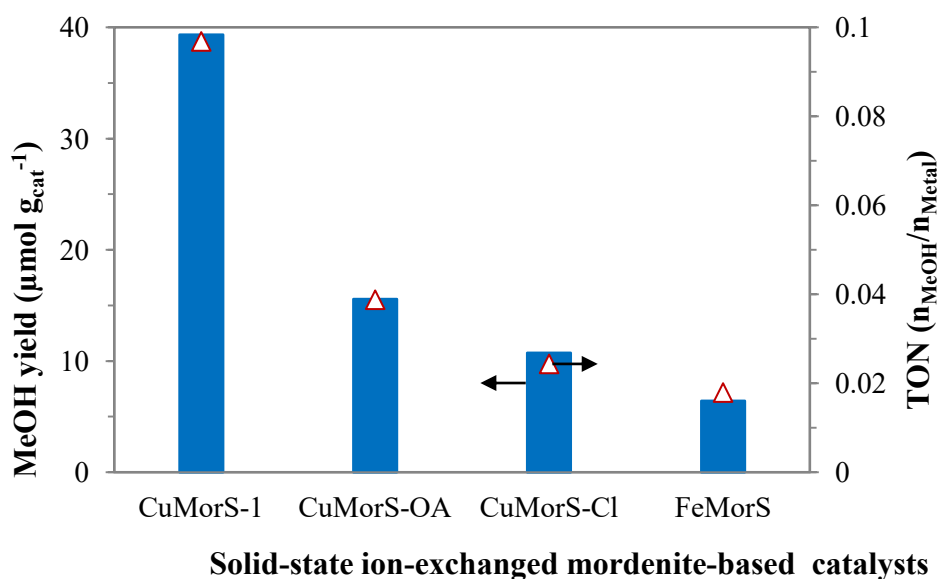
Figure 3.4. Methanol production over different metal/mordenite catalysts prepared in solid state. Reaction conditions: activation in O_2 at 550 ^{o}C for 8 h, reaction with CH_4 at 200 ^{o}C for 30 min, collection of MeOH with 5 ml of liquid water at RT.

As reported in the previous chapter, Fe-containing zeolites are highly active for the liquid-phase oxidation of methane to methanol by H_2O_2. In the here described O_2-assisted oxidation route, also a small amount of methanol was produced over the FeMorS catalyst (Figure 3.4). It can thus be concluded that Fe species activated in O_2 at 550 ^{o}C can as well react with methane although with a much lower catalytic activity compared to CuMorS-1. In contrast, in a study reported by Starokon *et al.*, the Fe-based zeolite catalyst was found to be able to yield significantly more methanol using N_2O as the oxidant (up to 160 µmol of methanol per gram of 2.0 wt.% Fe/ZSM-5).[97] Obviously, N_2O is more active than molecular oxygen; the activation of Fe sites by N_2O could be therefore performed under much milder conditions (from 130 to 200 ^{o}C), yielding a

better methanol production.[96,97] When O_2 as an inexpensive oxidizing agent should be used, Cu-based zeolites is evidently the more attractive catalysts.
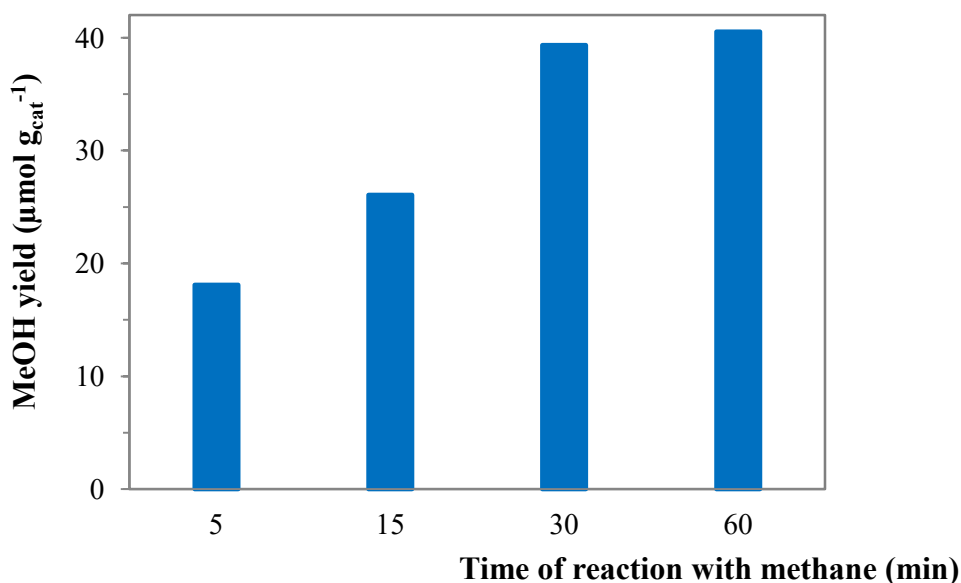

Figure 3.5. Methanol production at different reaction times. Reaction conditions: activation in O_2 at 550 $^{\circ}$C for 8 h, reaction with CH_4 at 200 $^{\circ}$C, collection of MeOH with 5 ml of liquid water at RT.

No methanol was produced when the O_2-activated catalyst interacted with pure N_2 only, proving that methanol was indeed generated from methane. The heterogeneous reaction between CuMorS-1 and methane at 200 $^{\circ}$C was further studied applying different reaction times (Figure 3.6). As expected, methanol production over CuMorS-1 could be enhanced by prolonging the reaction time. Only 18.1 μmol g_{cat}^{-1} of methanol were achieved after a 5-min contact with methane but the methanol yield was about doubled (39.3 μmol g_{cat}^{-1}) as the reaction was carried out for 30 min. Further extending the reaction time to 1 h just led to just a negligible yield improvement. In total, a methanol amount of 40.5 μmol g_{cat}^{-1} was produced after 1 h. These results are consistent with the previous studies, in which Cu/zeolite catalysts had to be treated for at least 20 min with methane to obtain considerable methanol yields.[109,118,120] Also, it can be expected that Cu loading and methane concentration in the gas flow may have an important role on the time required for completion of the reaction.

In earlier studies, only low amounts of methanol were obtained by the off-line extraction with dry solvents, e.g. acetonitrile, tetrahydrofuran and *n*-hexane. Increasing the water content in a mixture with acetonitrile gave significant enhancements in the methanol yield.[96,162] It was therefore proposed that water do not only act as a methanol-desorption agent but also as a proton

source for hydrolysis of intermediates stabilized on the catalyst surface, most likely methoxy species.[96,104,162,163] In addition, the last step can be performed using either liquid water (off-line extraction) or a vapor stream (online extraction), yielding similar amounts of methanol.[118,159]
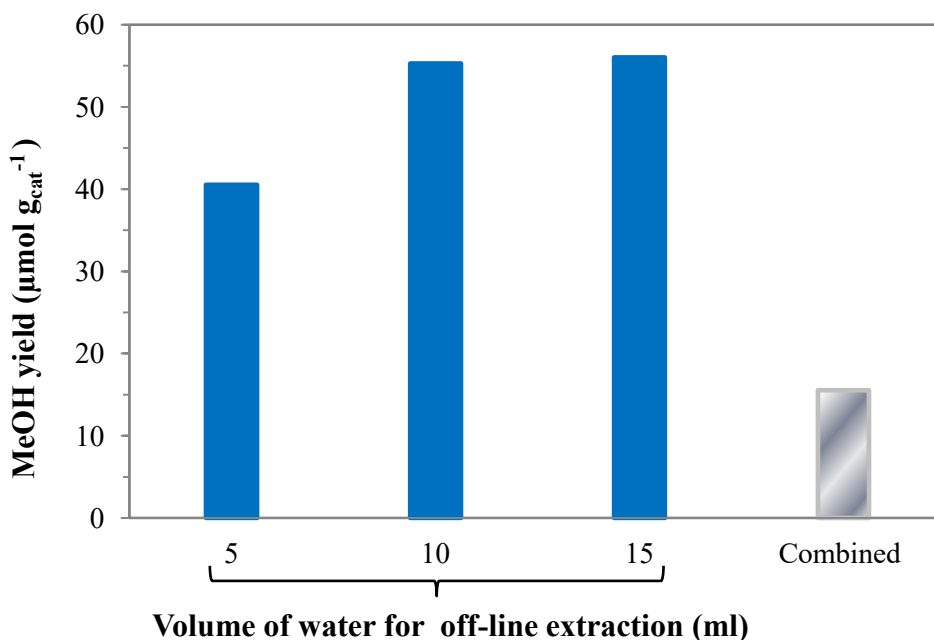

Figure 3.6. Effect of water amount and extraction method on methanol yield. Reaction conditions: activation in O_2 at 550 ^{o}C for 8 h, reaction with CH_4 at 200 ^{o}C for 1 h, collection of MeOH with water at RT. The bar named "Combined" exceptionally shows the total methanol amount obtained by online extraction and subsequent off-line extraction.

In the off-line protocol, a high concentration of the catalyst in water can hinder the extraction process because of difficult stirring and strong methanol adsorption on the zeolite surface.[164,165] Starokon *et al.* observed that methanol could be still collected after the first extraction with a ratio of 0.5 g of the catalyst/1.5 ml of water.[96] In this study, the effect of water amount used for extraction on the methanol production showed a similar trend (Figure 3.6). More methanol was extracted by increasing the water volume from 5 ml to 10 ml per reaction batch using ~ 0.6 g of calcined catalyst. However, further addition of water yielded no further improvement in the extraction of methanol. Besides, an online extraction protocol at 200 ^{o}C using a water-saturated N_2 flow was performed for 8 h. Only 8 μmol g_{cat}^{-1} of methanol was collected in the cold trap compared to a methanol yield of 55.3 μmol g_{cat}^{-1} obtained from the off-line extraction in 10 ml of liquid water. After the high-temperature extraction, the wet N_2 flow was switched off and the catalyst bed was cooled to room temperature. Another extraction stage by liquid water was performed with the catalyst at room temperature. Surprisingly, an additional methanol amount of 7.6 μmol g_{cat}^{-1} was further found, confirming that activated methane species are indeed strongly

bound at the catalyst surface. The overall methanol yield obtained after two successive extractions was still extremely lower than the results in the off-line process. A significant amount of formed methanol was possibly dehydrated into DME within the acidic zeolite matrix at such a high temperature. The conditions of the extraction step should therefore be seriously considered to obtain the maximum methanol amount that a catalytic cycle was able to produce.
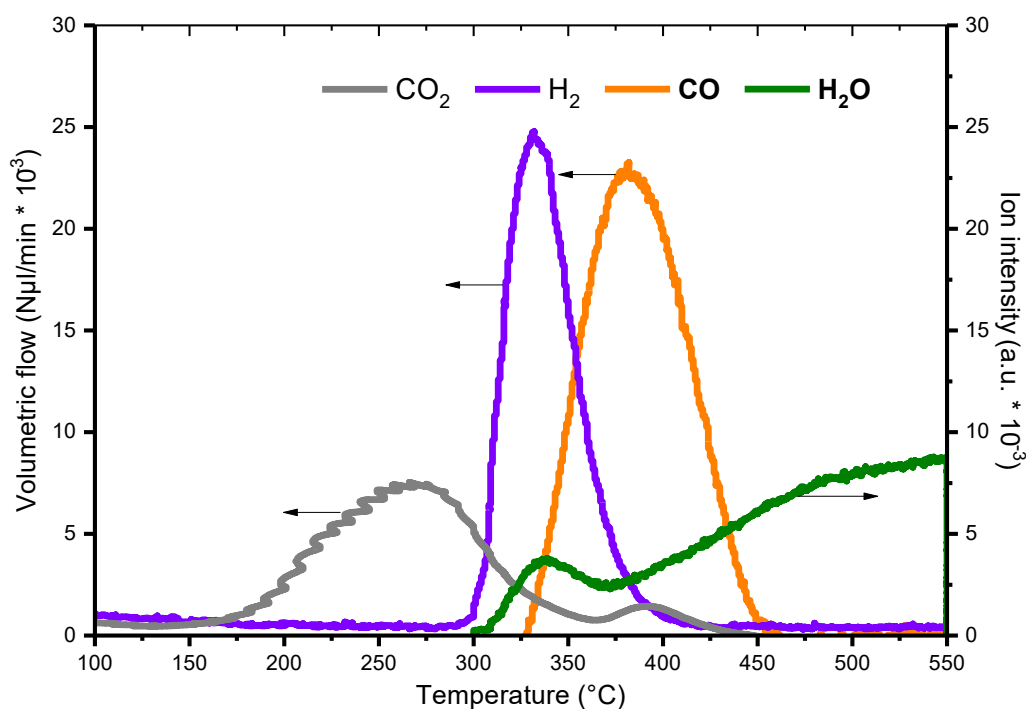
Figure 3.7. Volumetric flows of CO_2, H_2, CO, and H_2O during heating CuMorS-1 after interaction with CH_4 in a dry He flow.

To further investigate the role of water in producing methanol, a high-temperature treatment of the catalyst in dry inert gas was performed instead of addition of water to the catalyst. In detail, after the contact with CuMorS-1, the methane-containing flow was stopped and the reactor was cooled to room temperature. The material was then slowly heated to 550 ^{o}C (1 K min^{-1}) in a He flow. Products in the outlet stream were detected by a quadruple mass spectrometer as described in the experimental section (Figure 3.7). Neither methanol nor DME was detected during the reaction with methane and the subsequent treatment in helium, indicating that only intermediate(s) are formed after the reaction and water is indeed necessary for converting intermediate species. The presence of such intermediates on the catalyst surface is confirmed as CO_2, which is considered as a product of thermal-oxidative decomposition of oxygenated species, was detected starting from approx. 200 ^{o}C. Based on the proposed formation of methoxy species bound to a dicopper-oxo site,[104,163] the remaining hydrogen atom abstracted from

methane reacts with the next site, yielding a corresponding hydroxyl species, confirmed by detecting water starting at around 300°C. Beside CO_2 and H_2O, other species, namely H_2 and CO, were detected as well, which could also be the result of decomposition of stabilized methoxy species. The release of CO at a higher temperature compared to CO_2 demonstrates that the reaction of CuMorS-1 with methane results in the formation of at least two intermediates with different stabilities.
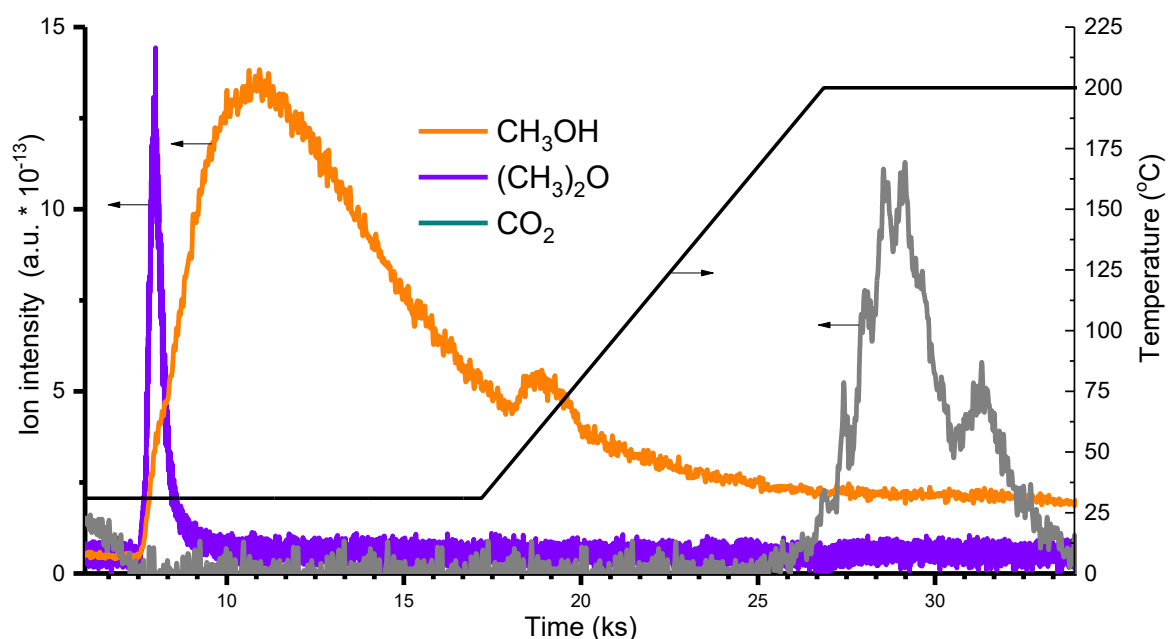
Figure 3.8. Mass spectroscopy-based signal of products during the treatment of CuMorS-1 in a wet He flow.

Notably, the CO amount was 58 $\mu mol\ g_{cat}^{-1}$ from overall 84 $\mu mol\ g_{cat}^{-1}$ of carbon oxides, which is close to the methanol yield obtained after addition of liquid water, suggesting that the intermediate, which is thermally decomposed to H_2 and CO in the dry He flow, is responsible for the methanol production by reaction with water. This conclusion was further confirmed by another experiment, in which a water-saturated He flow was introduced to the catalyst CuMorS-1 after its contact with methane. As expected, methanol and DME were produced already at room temperature, and CO_2 was formed again at 200°C but no H_2 and CO were observed afterwards when the catalytic bed was heated to higher temperatures (Figure 3.8). A similar result was also achieved over a reference Cu/mordenite (CuMorL-1, 3.21 wt.% Cu) prepared by liquid-phase ion exchange between Na-mordenite and copper(II) acetate. DME was previously observed in a wet He flow at 135 °C and therefore considered as a product of acid sites-catalyzed dehydration of methanol.[109] However, the early appearance of DME at even room temperature

in the present study suggested that DME is with high probably not formed from dehydrated methanol and another intermediate is responsible for the production of DME. The mechanism of the formation of these products would be further investigated and discussed in the next chapter.
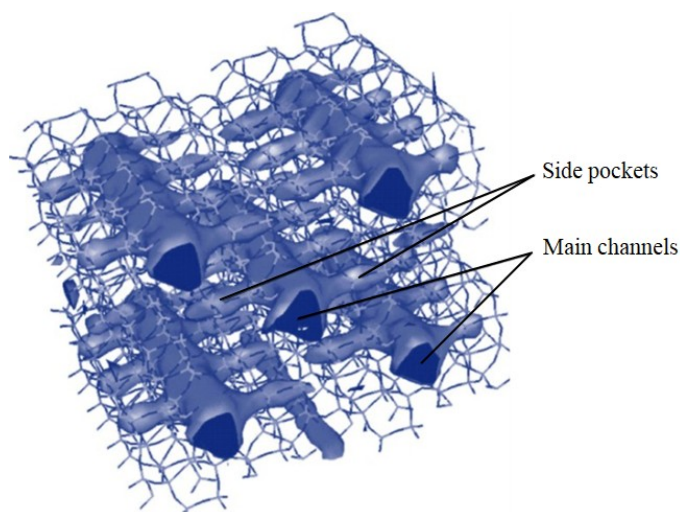

Figure 3.9. Mordenite topology. Reprinted with permission from ref. [123] (Copyright 2016 The Royal Society of Chemistry).

An MOR-type structure consists of non-intersecting large 12 membered-ring (MR) channels (6.5 Å x 7.0 Å) with parallel small 8 MR channels (5.7 Å x 2.6 Å). The 12 MR and 8 MR pores are connected by small side pockets (3.4 Å x 4.8 Å) (Figure 3.9).[112,166,167] Recent studies demonstrated that the Cu species located at 8 MR windows of such side pockets are able to produce oxygen-bridged di-/trinuclear Cu sites by the high-temperature treatment in O_2. These Cu-oxo sites were found to be highly reactive to methane.[109,112,117,168] In the work of Tomkins *et al.*, it was however reported that the O_2-activation step insignificantly influence the methane-to-methanol transformation. Activation of Cu/mordenite at 450 ^{o}C under 6 bar of O_2 even led to a decrease in methanol yield compared to the result obtained at lower pressures of O_2. The study focused on changing O_2 pressure while the effect of activation temperature was not further investigated.[118]

The O_2-activation of CuMorS-1 was therefore performed at different temperatures in the range from 450 to 750 ^{o}C. The catalytic activity of CuMorS-1 was remarkably enhanced by raising the activation temperature up to 650 ^{o}C (Figure 3.10). The reaction of CuMorS-1 activated at 450, 550, and 650 ^{o}C with methane at 200 ^{o}C produced 37.3, 55.3, and 65.2 μmol g_{cat}^{-1} of methanol, respectively. The improved methanol production indicated that elevated temperature could promote the activation of Cu species by O_2. However, no significant further increase in the conversion performance was observed with a final methanol yield of 65.8 μmol g_{cat}^{-1} as the

activation was performed at 750 ^{o}C. It should be noted that Cu exchange in this study was carried out *in situ* during the activation step. An elevated activation temperature might therefore also accelerate the ion exchange at the 8-MR side pockets, which is more difficult to access than exchangeable positions at larger pores, besides facilitating the formation of active Cu-oxo clusters.
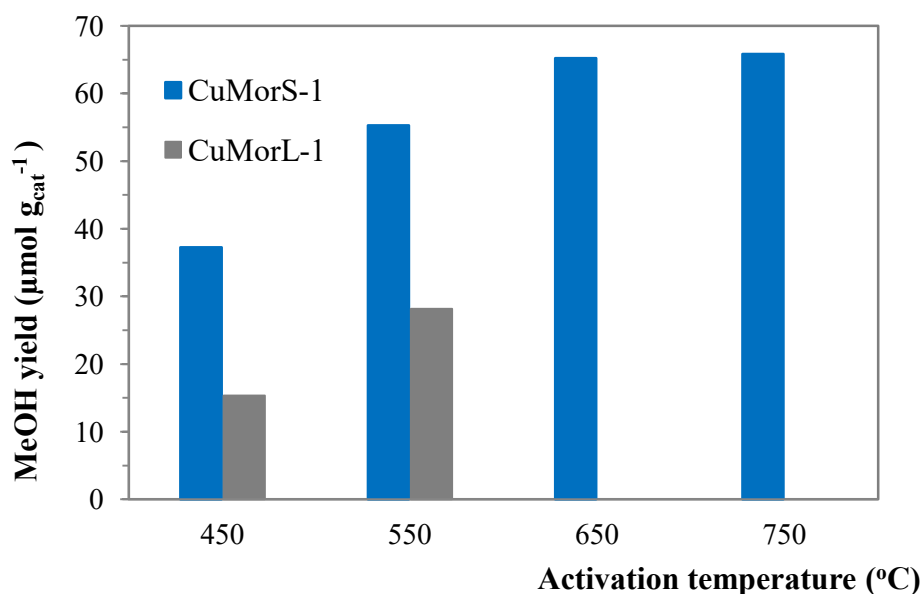
Figure 3.10. Methanol production at different activation temperatures. Reaction conditions: activation in O_2 for 8 h, reaction with CH_4 at 200 ^{o}C for 1 h, collection of MeOH with 10 ml of liquid water at RT.

Previous studies showed that the different abilities of acid cites in mordenite in ion exchange and selective sorption can be recognized via IR measurement.[109,123,169,170] Indeed, an intensive band at ~ 3600 cm^{-1} in the IR spectrum of modernite is assigned to strongly acidic hydroxyl group. The Brønsted acid sites (BAS) in the side pocket and the main channel show only a slight asymmetry of the SiO(H)Al band, leading to overlaid peaks at 3600 cm^{-1}. It was confirmed that this hydroxyl band consists of a low frequency peak at ~ 3590 cm^{-1} due to the stretching vibrations of BAS in the side pockets (BAS-SP) and a high frequency peak at ~ 3612 cm^{-1} due to the stretching vibrations of BAS in the main channels (BAS-MC).[123,169,170] Before the measurements, the samples were activated at a high vacuum level (< 10^{-6} mbar) to minimize disturbance by adsorbed contaminants. The IR spectra in the region of 3300–3700 cm^{-1} were deconvoluted into the bands attributed to BAS-MC (3612 cm^{-1}), BAS-SP (3590 cm^{-1}) and perturbed O-H vibrations (3500 cm^{-1}). The distribution of BAS in the main channels and in the side pockets was determined by measuring the area of the corresponding peaks.
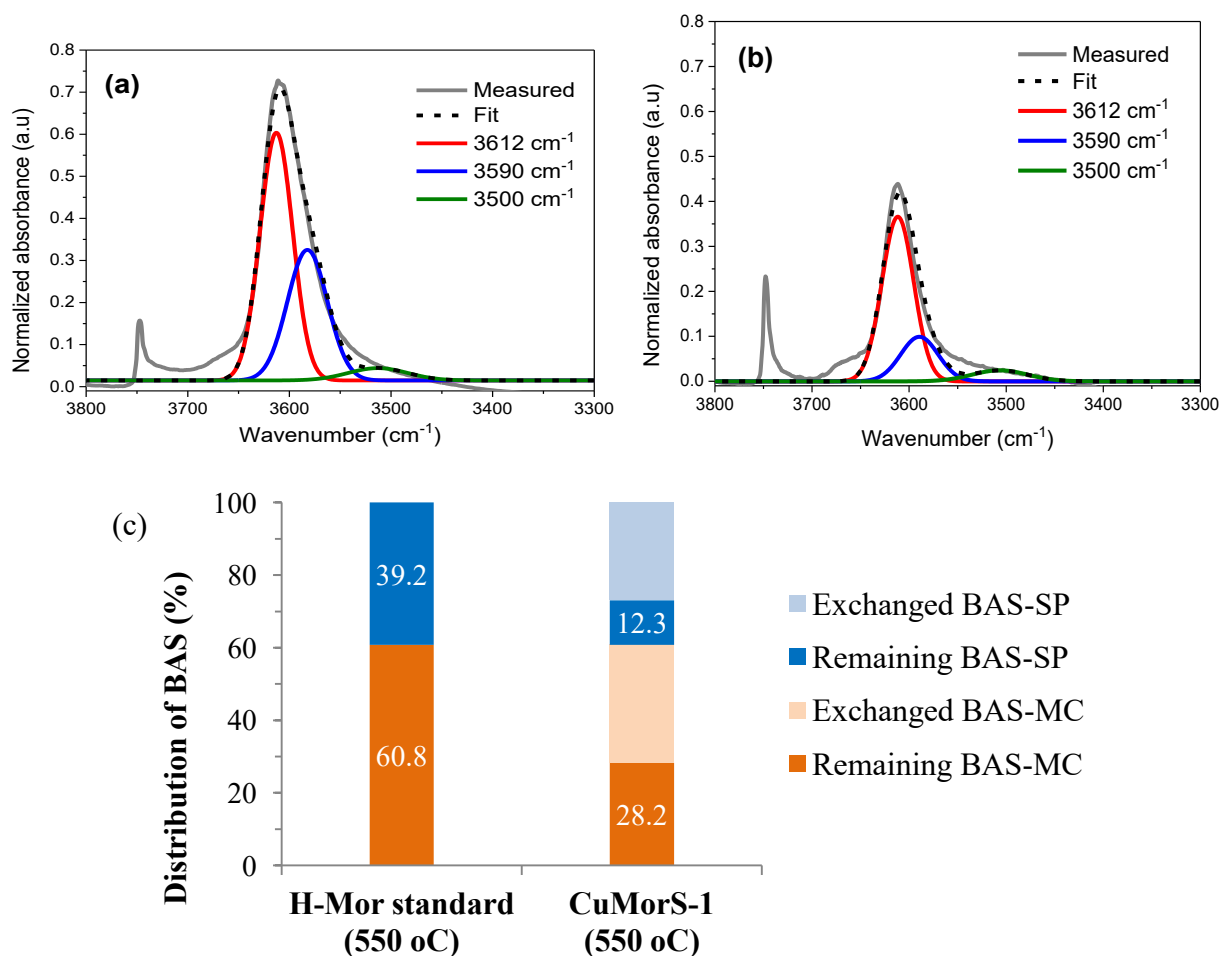
Figure 3.11. (a, b) Deconvoluted IR spectra of the O-H stretching vibrations of BAS of NH_4-Mor-1 calcined at 550 °C, producing corresponding H-Mor-1 and CuMorS-1 ion-exchanged at 550 °C, respectively. (c) Distribution of BAS on the samples based on the deconvoluted bands.

H-Mor-1 used in this study was directly produced from NH_4-Mor via calcination at 550 °C. The IR spectra of H-Mor-1 revealed a BAS-MC/BAS-SP proton distribution of ~ 61%:39%, close to the values previously reported.[169,170] The first comparison was made between H-Mor-1 and CuMorS-1, which were prepared at the same temperature of 550 °C (Figure 3.11). A clear decrease in intensity and area of the BAS bands in the IR spectrum of CuMorS-1 compared to those for H-Mor-1 indicated that the acid sites in mordenite were successfully exchanged with Cu^{2+}. Although BAS-SP have apparently a lower accessibility and BAS-MC are much more abundant, comparable Cu exchanges were observed at these sites, i.e. ~ 69% of BAS-SP were occupied by Cu^{2+} while this value for BAS-MC was ~ 54%, proving that solid-state Cu exchange in flowing O_2 preferentially occurred at sites in the side pockets.
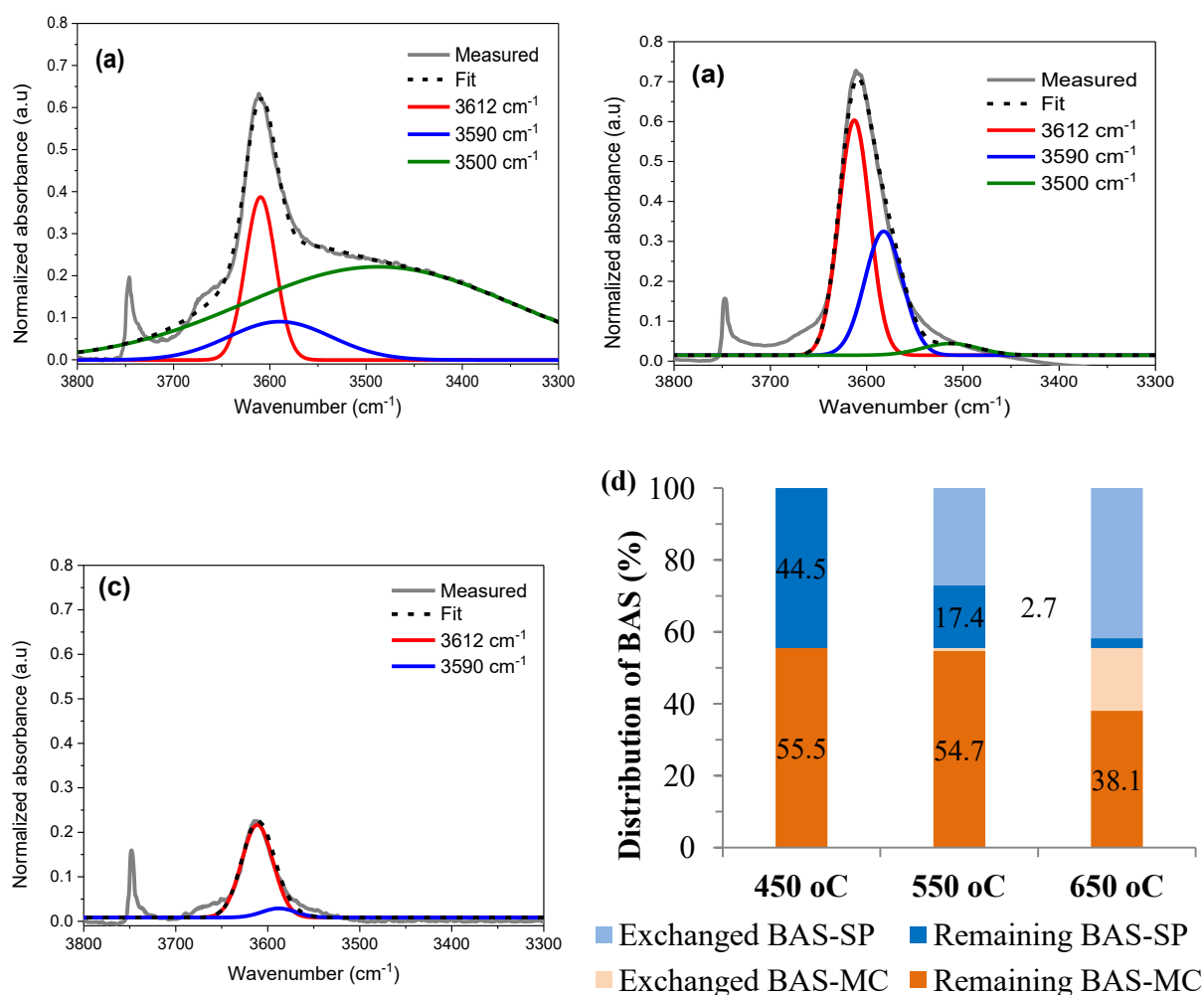
Figure 3.12. (a, b, c) Deconvoluted IR spectra of the O-H stretching vibrations of BAS of CuMorS-1 ion-exchanged at 450, 550, and 650 ^{o}C, respectively. (d) Distribution of BAS based on the deconvoluted bands.

To elucidate the beneficial impact of increasing the calcination temperature on the methanol production, further IR measurements were made on CuMorS-1 samples, which were ion-exchanged at varied temperature (450–650 ^{o}C). As exchanged Cu species in zeolite can move to other locations upon changing the treatment temperature, the activation of Cu/mordenite for IR analysis must be performed at the same temperature of the former Cu exchange step. The IR bands of CuMorS-1 prepared at 450 ^{o}C with a BAS-MC/BAS-SP ratio of 55%:45% were considered as a reference value for detecting spectroscopic changes of BAS-MC and BAS-SP in the other samples. Increasing the calcination temperature to 550 ^{o}C led to a clear improvement of the Cu exchange in mordenite, i.e. mainly in the side pockets with further 61% of BAS-SP exchanged (Figure 3.12). As can be expected, treatment of a mixture of NH$_4$-Mor-1 and Cu(acac)$_2$ at 650 ^{o}C allowed an almost complete occupation of BAS-SP by Cu^{2+} species while a

significant fraction of acid sites in the main channels (~ 69%) remained unexchanged. These IR results convincingly demonstrated that in solid-state ion exchange, temperature plays an important role in the placement of Cu species at the cation positions. More Cu species in the side pockets could be obtained at higher ion-exchange temperatures, leading to corresponding improvements of methanol production mentioned before.

The study on the influence of activation temperatures on methane-to-methanol conversion was then extended to the CuMorL-1 catalyst, which was conventionally prepared by liquid-phase ion exchange. After activated at 450 $^\circ$C, CuMorL-1 was able to produce 15.3 μmol g_{cat}^{-1} of methanol after treatment with methane at 200 $^\circ$C for 60 min and off-line extraction with 10 ml of water. This yield is in good agreement with the yields found in previous studies under similar experimental conditions. For example, the preparation of Cu/mordenite was also performed in aqueous medium and the temperature of 450 $^\circ$C was typically applied for the activation. Subsequently, methanol produced was quantified by the same method using a GC.[103,104,118,122] Also for CuMorL-1, a clear increase in methanol production to 28.2 μmol g_{cat}^{-1} was observed when the activation step was carried out at 550 $^\circ$C, indicating the positive impact of elevated activation temperature on the methane conversion. Again, it is obvious that a larger number of Cu species activated by O_2 can be achieved by increasing the activation temperature.

It should be noted that performing the catalytic cycle at different temperatures for each step is one of major drawbacks of this stepwise procedure. Very recently, Tomkins *et al.* have introduced the cyclic conversion of methane to methanol over Cu/mordenite under isothermal conditions at 200 $^\circ$C. A high methanol yield, namely 56.2 μmol g_{cat}^{-1}, was obtained; however, a very high methane pressure of 37 bar had to be applied. It was assumed that Cu sites which are almost inactive at low partial pressures of methane are able to react with methane when the pressure is raised. Although technical challenges in developing this protocol are obvious, the given isothermal process at a low temperature with an improved conversion is indeed promising for further studies.

Notably, it was found that CuMorS-1 had a much better catalytic performance for the partial oxidation of methane to methanol than CuMorL-1 under identical conditions even though the Cu loading in CuMorS-1 is significantly lower. Further MS analysis during the online extraction with steam from RT to 200 $^\circ$C shows similar CO_2 amounts produced from two Cu/mordenite catalysts (Table 3.2), proving that CuMorS-1 possesses a larger number of Cu sites, that can

selectively convert methane to methanol, while the formation of unselective Cu sites seems to be independent on the method used to prepare Cu/mordenite.

Table 3.2. Yield of the products over CuMorS-1 and CuMorL-1.

Entry	Catalyst	Cu loading (wt.%)	Product yield ($\mu mol\ g_{cat}^{-1}$)			Selectivity[c] (%)
			MeOH[a]	DME[b]	CO_2[b]	
1	CuMorS-1	2.58	56.0	1.6	9.0	87.7
2	CuMorL-1	3.21	28.2	1.0	8.4	78.2

[a]Methanol was analyzed by GC after off-line extraction with liquid water.

[b]Gas-phase products were analyzed by MS during online extraction with steam.

[c]Selectivity to MeOH and DME = [moles(MeOH) + 2*moles(DME)]/ moles(reacted CH_4)
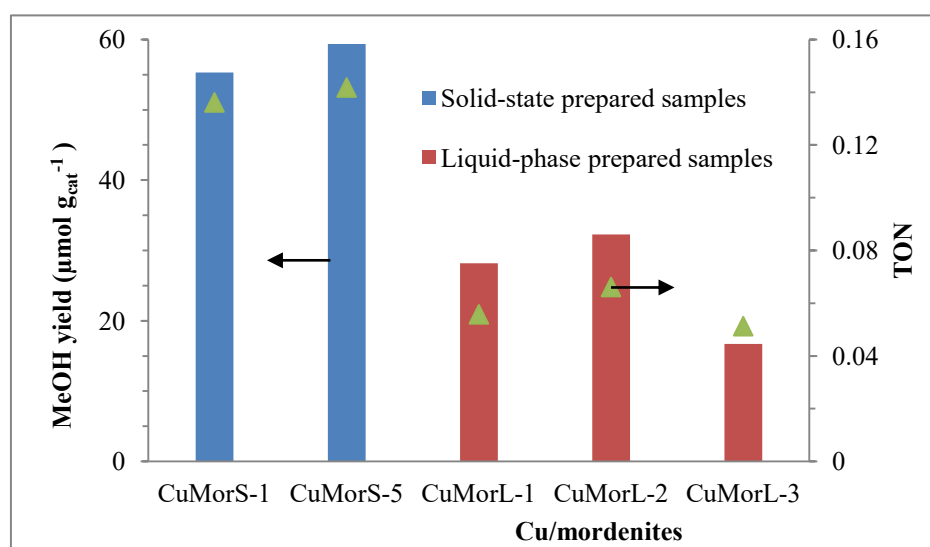
Figure 3.13. Catalytic performances of different mordenites-supported Cu catalysts. Reaction conditions: activation in O_2 at 550 °C for 8 h, reaction with CH_4 at 200 °C for 1 h, collection of MeOH with 10 ml of liquid water at RT.

For a further comparison of these two ion-exchange methods, more Cu/mordenites were prepared using mordenites with different Si/Al ratios. The TON-based activities of Cu/mordenites prepared via the same ion exchange were found to be quite similar under identical conditions, indicating no significant influence of the Si/Al ratio in mordenite on their catalytic performance within this study (Figure 3.13). On the other hand, it is confirmed that solid-state

ion exchange of NH_4-Mor with $Cu(acac)_2$ could produce more active catalysts (CuMorS-1 and CuMorS-5) for the stepwise methane-to-methanol conversion. The high-temperature solid-state reaction under flowing O_2 could promote the metal ion diffusion to all exchangeable charge-balancing sites in the microporous mordenite framework.[171] As the above-mentioned catalyst characterizations including N_2 sorption, PXRD, and TEM measurements show similar results for both CuMorS-1 and CuMorL-1, no explanation for their different catalytic performance can be given from these analytic results.

It should be noted that the temperature for the reduction of metallic species depends on their stability and the accessibility of reducing agents to their location.[171-173] The zeolite structure is complex with many types of cages and channels; supported Cu species located at different positions therefore showed different corresponding reducibility. Accessibility of H_2 to the Cu centers and activation energy for the reduction are dependent on cage size, cage linking and coordination of Cu into the framework, e.g. bulk CuO species on the surface and Cu sites at supercages are more easily reduced than Cu species located at smaller cages.[144,171-178] Cu/mordenites after activation in O_2 were therefore first subjected to temperature-programmed reduction with H_2 (H_2-TPR) to gain insight into type and position of Cu species located in the mordenite framework. Reduction performances of copper oxides were measured as references.
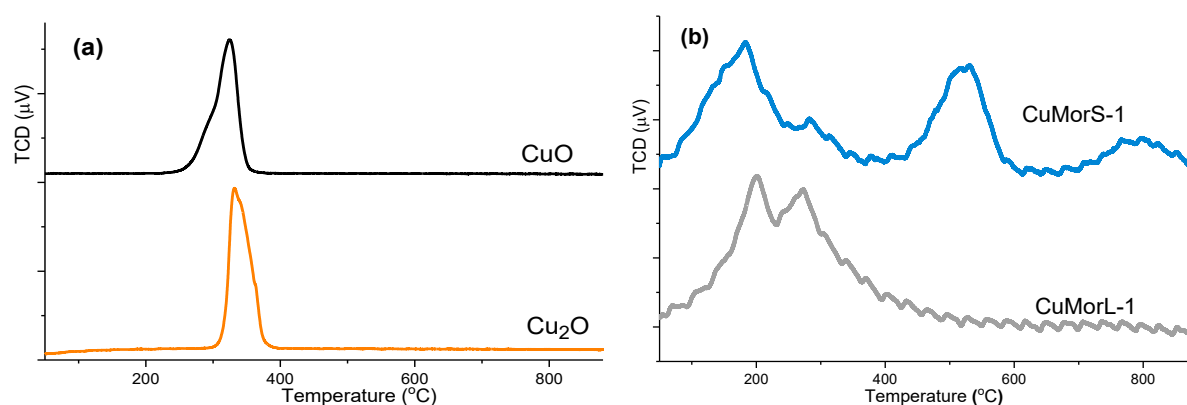
Figure 3.14. H_2-TPR profiles of Cu-based materials, (a) reference copper oxides, (b) O_2-activated Cu/mordenites.

By using the H_2-TPR data of CuO for calibration of the thermal conductivity detector (TCD)-based signals, it was seen that H_2 consumptions for the TPR experiments of CuMorS-1 and CuMorL-1 are close to the stoichiometric ratio for the reduction of Cu^{2+} to Cu^0 (namely, 1.08 and 1.10, respectively). The small deviation compared to the ideal value ($H_2/Cu = 1$) can be explained by the low Cu loadings in mordenite.[179] This result indicates that the Cu species in the

materials are exclusively Cu(II) species, consistent to earlier works.[159,163,180] In addition, the oxidation state of Cu in the samples was also determined by XANES analysis (Figure 3.15). No features of Cu^+ were observed for Cu/mordenite after activation in O_2 and the spectra are completely consistent with those of Cu(II)-containing compounds.
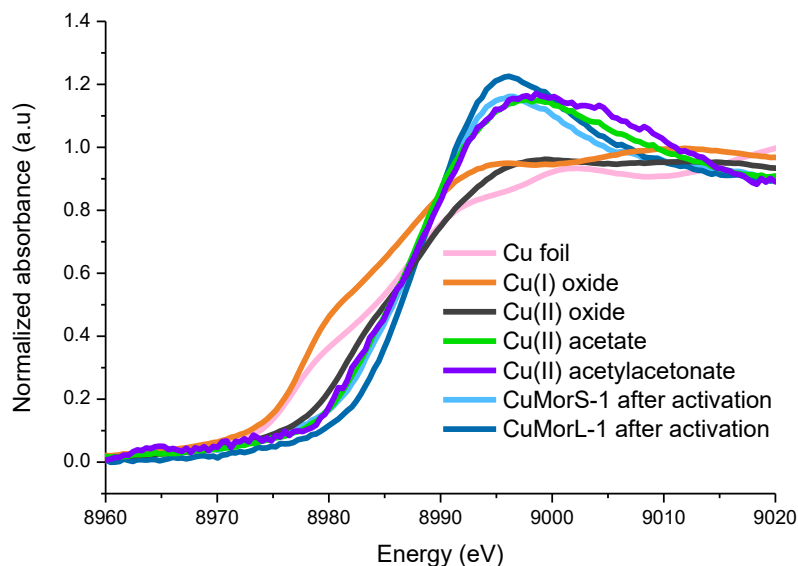
Figure 3.15. XANES spectra of CuMorS-1 and CuMorL-1 after activation in O_2.

The H_2-TPR profiles generally show three H_2 uptake stages in the studied temperature range (RT–900 ^{o}C). The peaks in the first reduction stage from 100 to 300 ^{o}C observed for both CuMorS-1 and CuMorL-1 were attributed to the most accessible Cu species probably on the external zeolite surface and in the largest channel of mordenite, i.e. 12-MR channel (Figure 3.14).[171] It was observed that these reduction peaks appeared at lower temperatures than those found in the H_2-TPR profiles of bulk copper oxides most probably due to the small size and the good dispersion of Cu clusters on mordenite.[171,181,182]

Further H_2 uptakes detected at harsher conditions were assigned to the reduction of the less accessible Cu sites in the smaller channel and linked cages (e.g., 8-MR pores, side pockets), where the active sites can be generated.[171] Particularly, under identical measurement conditions, CuMorL-1 exhibited only a shoulder peak for the second reduction stage at approx. 370 ^{o}C while an intense separate feature at a greatly higher temperature, namely 530 ^{o}C, was observed for CuMorS-1. The difference in this reduction range demonstrates that a significant fraction of Cu species can be loaded into the ion-exchangeable positions of lower accessibility upon solid-state ion exchange in a flowing O_2 stream.

Furthermore, a broad reduction peak observed at the temperature above 750 °C for CuMorS-1 could be attributed to bare Cu cations stabilized in the zeolitic framework that would just be reduced at distinctly high temperatures.[177,180,181,183] Such cationic sites coordinate only with framework oxygen atoms at the small rings (i.e. 5-MR, 6-MR) without any guest oxygen ligands.[117,184-187] In contrast, the H_2 consumption at this temperature range was negligible for CuMorL-1, indicating that much more of these Cu sites existed in CuMorS-1. Although such Cu species have been described to be inactive for activation of C-H bonding,[115,117,188] this result can be considered as a further evidence for the greater efficiency of the solid-state ion exchange method in distributing Cu species to small pores in mordenite. On the other hand, when Cu exchange is carried out in aqueous medium, formed $[Cu(H_2O)_6]^{2+}$ complexes seem to be too large to access the small cages of zeolite. In addition, the presence of sodium cations hampers cation exchange in such narrow spaces. As a result, most of Cu species are located in the large channels after the liquid-phase protocol.
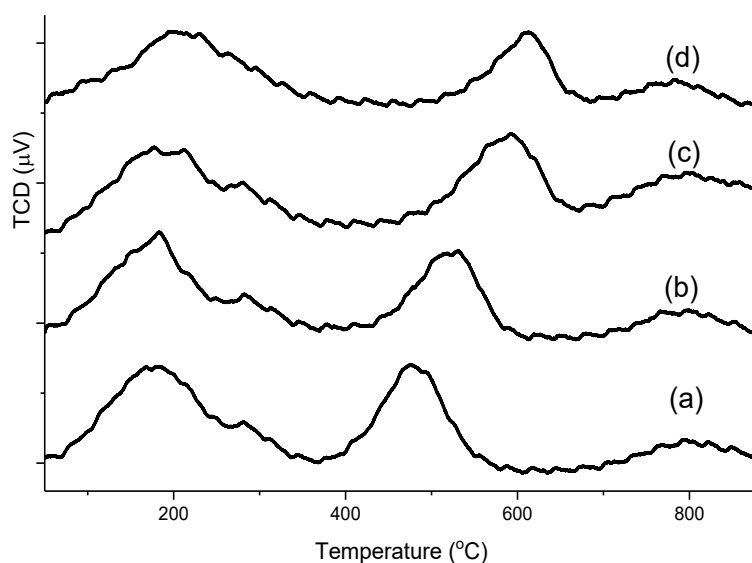
Figure 3.16. H_2-TPR profiles of CuMorS-1 activated at (a) 450 °C, (b) 550 °C, (c) 650 °C, (d) 750 °C.

H_2-TPR analysis was further carried out on CuMorS-1 samples that were activated in O_2 flow at different temperatures to further clarify the enhanced catalytic performance with increasing activation temperature (Figure 3.16). Notably, the measurements showed a clear shift of the second reduction peak to higher temperatures for CuMorS-1 activated from 450 to 650 °C while other reduction stages at ~ 200 °C and 800 °C remained unchanged. This proves that increasing activation temperature up to 650 °C led to an enhanced diffusion of Cu cations to the smaller pores in mordenite. As a result of such enhancements, the methanol yield significantly increased

as showed before. However, the activation of CuMorS-1 performed at 750 $^{\circ}$C yielded only a negligible further improvement in methanol production and indeed also just a small increase in the temperature at which the second reduction occurred was observed for this sample.
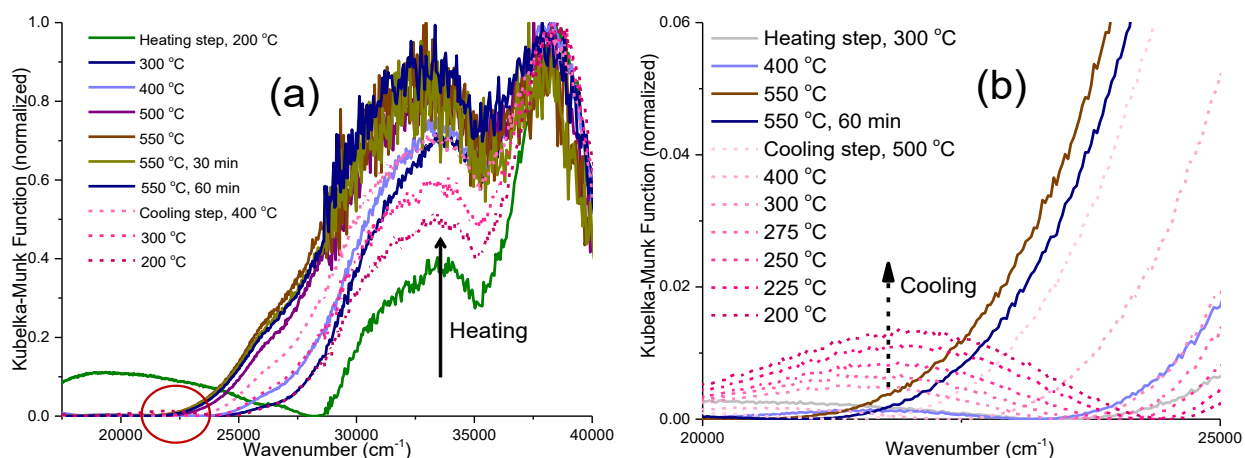
Figure 3.17. *In situ* UV-vis spectra of CuMorS-1 activated under an O_2 flow in the band range of (a) 15 000 40 000 cm^{-1}, (b) 20 000–25 000 cm^{-1} (bands at ~ 33 000 cm^{-1} and 22 200 cm^{-1} are indicated by the arrow).
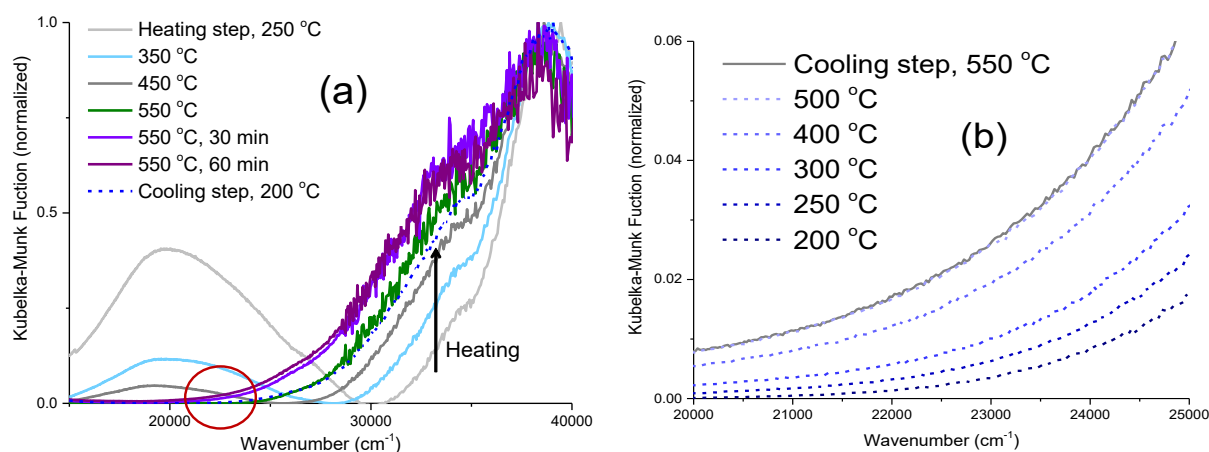
Figure 3.18. *In situ* UV-vis spectra of CuMorL-1 activated under an O_2 flow in the band range of (a) 15000–40000 cm^{-1}, (b) 20000–25000 cm^{-1} (band at ~ 33000 cm^{-1} is indicated by the arrow).

As introduced before, *in situ* UV-vis spectroscopy is currently one of the most efficient analytical methods to propose the active sites in Cu/zeolites and detect their structural changes during the stepwise conversion. The focused spectroscopic region of 20 000–30 000 cm^{-1} is typical for copper species binding to extra-framework oxygen.[75,120] The most well-known band centred at about 22 700 cm^{-1} was first found in the *in situ* UV-vis spectra of Cu/ZSM-5 as the sample was activated in O_2 at high temperatures. The disappearance of the band after treatment

with methane indeed proves that this feature is related to an active Cu site towards the selective oxidation of methane to methanol. Based on the well-defined structures of homogenous Cu complexes, the responsible site was assigned to a bent mono-(μ-oxo)dicopper(II) complex ($[Cu_2(\mu\text{-}O)]^{2+}$) stabilized in the ZSM-5 framework.[75,103,108,120,158,189] An additional absorption feature at 29 000 cm^{-1} was observed on Cu/ZSM-5 and assigned to a μ-(η^2:η^2)peroxo dicopper(II) site, that was proposed to convert into the $[Cu_2(\mu\text{-}O)]^{2+}$ form that is more stable in O_2 but reactive with CH_4.[75,190] Also, an O_2-activated Cu/mordenite showed the same spectroscopic behavior with a band centered between 22 200 cm^{-1} and 22 700 cm^{-1}. [104,112,171,180] However, to date, the structure of active species formed and stabilized in Cu-exchanged zeolites has not been fully determined. Recent further studies showed various results on Cu sites responsible for the methane-to-methanol conversion. Grundner *et al.* described a new broad band at about 31000 cm^{-1} for Cu/mordenite while no band at ~ 22 500 cm^{-1} was observed.[109] The absence of this feature for Cu/mordenite activated at 200 ^{o}C was also reported in another study, in which the active site was then proposed to be a dehydrated copper oxide cluster. Such Cu sites were less active than the mono-(μ-oxo)dicopper(II) site, and only became reactive at a high pressure of methane.[118]

UV-vis diffuse reflectance spectra of CuMorS-1 and CuMorL-1 were collected *in situ* during the sample activation in a 50 Nml min^{-1} O_2 flow. A development of a band at about 32 000 cm^{-1} upon raising temperature was observed for both catalysts (Figures 3.17a and 3.18a). This UV-vis spectral feature is in good agreement with the earlier study, in which the structure of the active clusters in the catalyst was found to be different from those previously reported.[109,114] It should be noted that even though the Cu loading in CuMorS-1 is lower, the intensity of the 33 000 cm^{-1} band is significantly higher than the one observed for CuMorL-1. No bands in the region of 20 000–25 000 cm^{-1} were detected when the materials were heated to 550 ^{o}C and the temperature was held for 1 h. Surprisingly, cooling CuMorS-1 in the same O_2 atmosphere revealed an developement of the 22 200 cm^{-1} band, which is assigned to a mono-(μ-oxo)dicopper(II) core in mordenite. The band at 22 200 cm^{-1} became even more noticeable as the temperature decreased to lower than 300 ^{o}C while a decrease in intensity of the band centred at ~ 33 000 cm^{-1} was observed. These simultaneous changes suggest that a small fraction of the Cu clusters showing the 33 000 cm^{-1} feature in the UV-vis spectra of CuMorS-1 was converted into the $[Cu_2(\mu\text{-}O)]^{2+}$ sites at low activation temperatures (Figures 3.17b). Vaneldegen *et al.* also observed the band at 22 200 cm^{-1} at a 250 ^{o}C and its strong intensity decrease by heating Cu/mordenite to above 330 ^{o}C.[112] The 22 200 cm^{-1} band was however not found for CuMorL-1 during the cooling step

(Figure 3.18b). The *in situ* UV-vis results thus demonstrated that in CuMorS-1, a larger number of different active copper clusters can be formed than in CuMorL-1, resulting in a more efficient catalytic performance for the methane-to-methanol conversion.
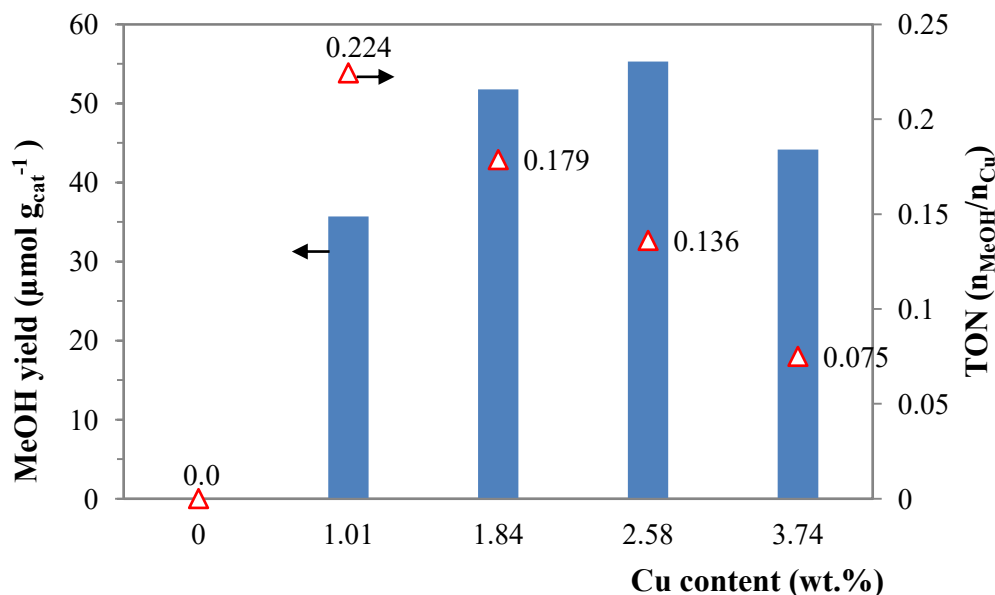
Figure 3.19. Catalytic performance of CuMorS with varied Cu loading. Reaction conditions: activation in O_2 at 550 $^{\circ}$C for 8 h, reaction with CH_4 at 200 $^{\circ}$C for 1 h, collection of MeOH with 10 ml of liquid water at RT.

To evaluate the efficiency of Cu species in CuMorS-1, the influence of the amount of Cu loaded in mordenite via solid-state ion exchange on the methanol production was investigated. No methanol was detected in the cycle using the fresh NH_4-form mordenite, proving that Cu species are indispensable for producing methanol from methane. Excellent performances were obtained even at low Cu loadings in mordenite. Indeed, mordenite loaded with 1.01 and 1.84 wt.% of Cu yielded already 35.7 and 51.8 μmol g_{cat}^{-1} of methanol, respectively (Figure 3.19). Notably, a lower Cu loading led to a great enhancement of catalytic efficiency of Cu/mordenide. The TON per catalytic cycle increased from 0.14 to 0.22 as the Cu content was reduced from 2.58 to 1.01 wt.%. From these values, it can be concluded that 45 % of the Cu sites in CuMorS-2 (1.01 wt.% Cu) are active sites for methane conversion based on the assumption that a mono(μ-oxo)dicopper core is responsible for the catalysis. The proportion of active Cu sites even reaches to 67% when a tricopper species is assumed.[109,112,114]

Increasing the Cu content to 3.74 wt.% not only decreased the TON but also lower methanol yield. It was observed that after calcination in an O_2 flow, Cu/mordenite with such a high Cu content turned grey instead of light blue as usual, which indicates that a significant fraction of

the Cu species was converted to CuO on the mordenite surface.[174] The presence of CuO nanoparticles is obviously not beneficial as they could block the pores, hindering the interaction of more active Cu sites located in the small pores with O_2 and methane, respectively. No differences were detected from TEM and PXRD measurements on Cu/mordenites with different Cu contents; nevertheless, H_2-TPR profiles showed that the temperature at which the second reduction step took place gradually decreased by increasing the Cu loading in the range between 1.01 and 3.74 wt.% (Figure 3.20), indicating an impeded diffusion of Cu species to the smaller pores. The efficiency of Cu/mordenite could be therefore enhanced when low Cu loadings was applied.
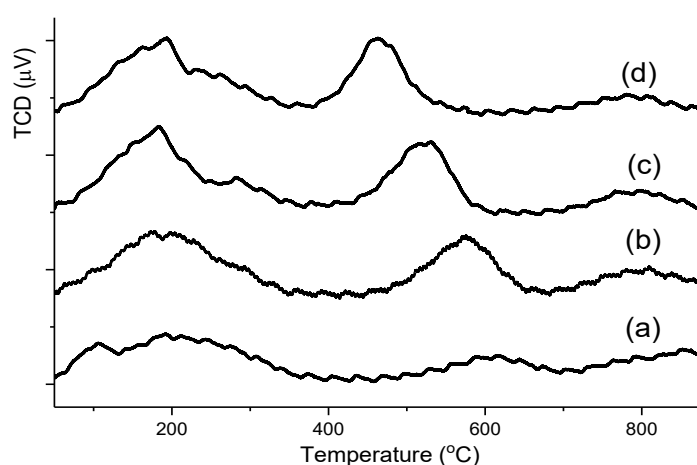
Figure 3.20. H_2-TPR profiles of CuMorS with varied Cu loading (a) 1.01 wt.%, (b) 1.84 wt.%, (c) 3.21 wt.%, (d) 3.74 wt.%.

To investigate the effect of zeolite type on the reaction performance, various commercial NH_4-form zeolites and in lab-synthesized silicalite-1 were used as supports for preparation of Cu-loaded catalysts similar to the Cu/mordenite. The zeolite-based materials contained similar content of Cu and were tested under identical reaction conditions. The zeolite structure was found to strongly affect the catalytic activity (Figure 3.21). Cu/mordernite showed an excellent catalytic performance compared to others. Moderate yields of methanol were obtained over Cu-exchanged ZSM-5 and ferrierite while the reaction using Cu/zeolite β and Cu/zeolite Y produced poor methanol amounts. From these results, it can be concluded that the zeolitic framework of mordenite, ZSM-5, and ferrierite is appropriate to produce the active Cu sites for the stepwise partial oxidation of methane to methanol by O_2. Indeed, the hypothesis of $[Cu_2(\mu\text{-}O)]^{2+}$ as an active site for methane activation was first given based on the 10-MR of ZSM-5. 12-MRs of zeolite β and zeolite Y seem to be too large for the formation of the active Cu species. In the

ferrierite framework, 8-MR channels intersect 10-MR channels, forming cavities that are only accessible through 8-MR windows.[191] Meanwhile, as described before, mordenite also possesses side pockets, of which at the 8-MR window active sites can be generated.

Figure 3.21. Methanol production over Cu/zeolites. Reaction conditions: activation in O_2 at 550 ^{o}C for 8 h, reaction with CH_4 at 200 ^{o}C for 1 h, collection of MeOH with 10 ml of liquid water at RT.
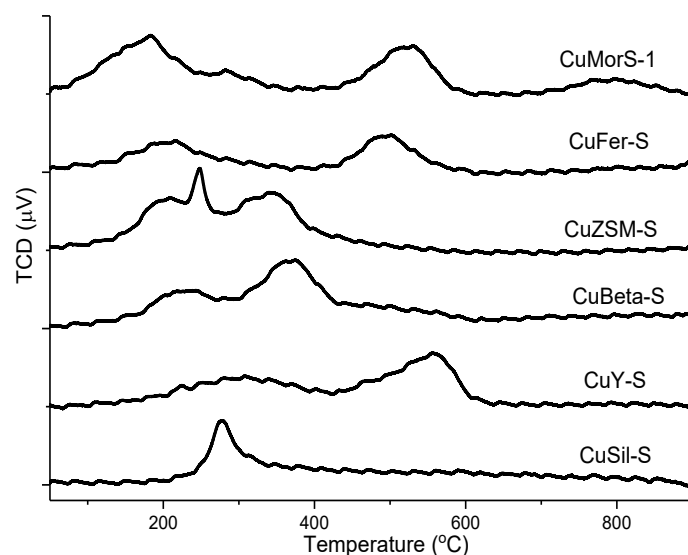
Figure 3.22. H_2-TPR profiles of Cu/zeolites.

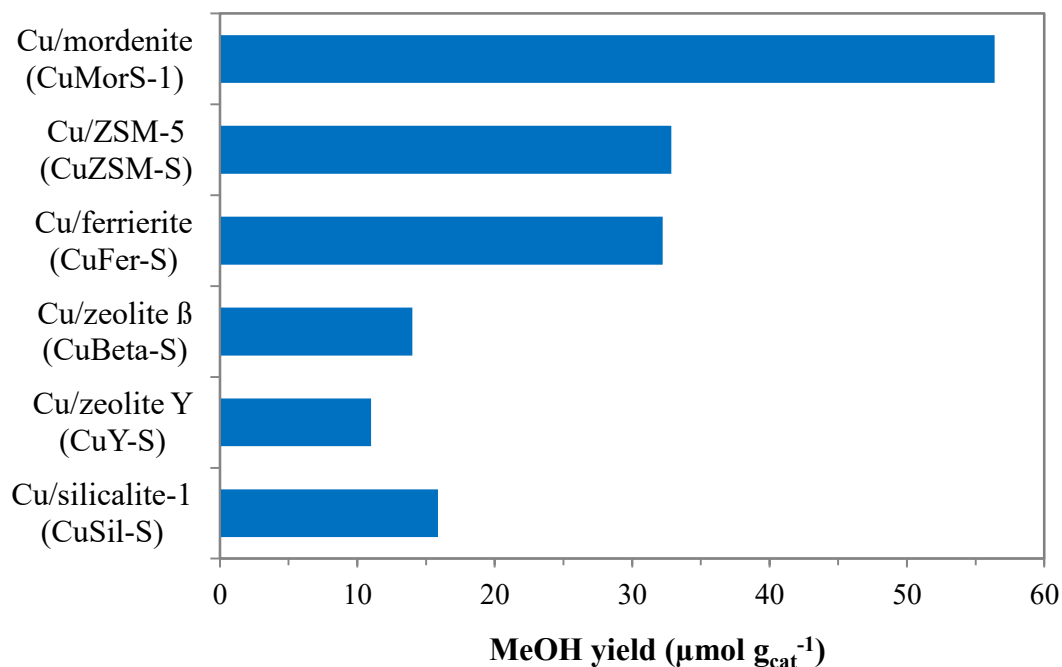The structural resemblance of the Cu/zeolites can be further seen by H_2-TPR analysis (Figure 3.22). Similar profiles were achieved by reducing Cu species in mordenite and ferrierite. Also, the structure consisting of intersecting large channels of ZSM-5 and zeolite β (i.e.,10 MR and 12 MR, respectively) leads to earlier reduction of Cu species by H_2. The H_2-TPR profile of Cu/silicalite-1 showed a single H_2 uptake below 300 ^{o}C, indicating formation of only CuO species via dry impregnation of the Al-free silicalite-1 with $Cu(acac)_2$. A small amount of methanol produced over Cu/silicalite-1 strongly indicates that these CuO clusters can also become reactive with methane. The possible activity of CuO sites would be further investigated in the next chapter.
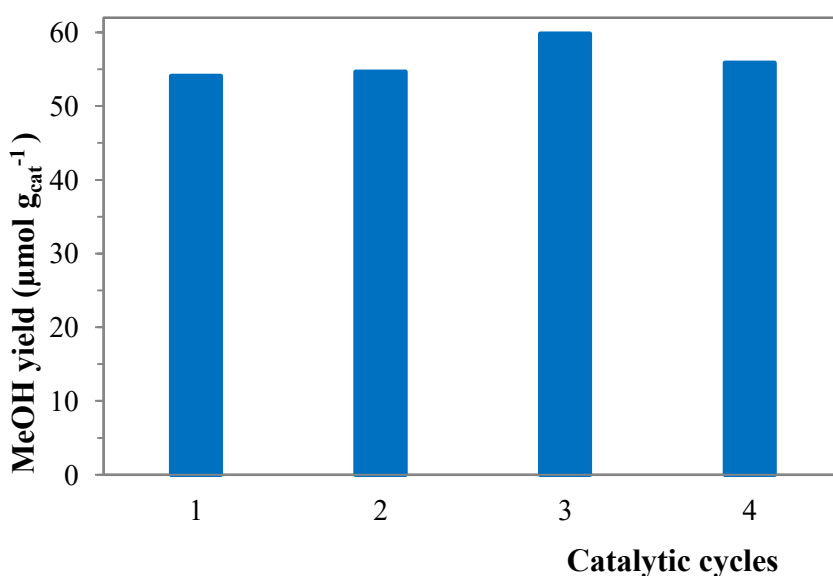
Figure 3.23. Recycling studies on CuMorS-1. Reaction conditions: activation in O_2 at 550 ^{o}C for 8 h, reaction with CH_4 at 200 ^{o}C for 1 h, collection of MeOH with 10 ml of liquid water at RT.

Recoverability and reusability of CuMorS-1 were studied in repeated catalytic cycles. After a multi-step procedure including activation at 550 ^{o}C for 8 h in oxygen, reaction with methane at 200 ^{o}C for 1 h, and finally methanol extraction in water at room temperature, the catalyst was dried at 105 ^{o}C for 12 h and loaded in the reactor for the next cycle. No degradation in catalytic activity was observed with about 55 μmol g_{cat}^{-1} of methanol produced in the successive cycles (Figure 12). ICP analysis showed that the Cu content in mordenite almost remained unchanged after the 4th dispersion in water for off-line collection of methanol. PXRD patterns of the reused catalyst are similar to those of the fresh mordenites and the catalyst activated in O_2. N_2 adsorption measurements of the catalyst after several cycles showed an insignificant change in

surface area (Table S1). These results indicate that the Cu sites loaded in mordenite by solid-state ion exchange are highly stable and can be reactivated for successive catalytic cycles.

3.5 Conclusions

Cu-containing zeolites were prepared via a facile solid-state ion exchange of NH_4-zeolite with $Cu(acac)_2$. The Cu-exchanged zeolites were then used as a biomimetic solid catalyst for the partial oxidation of methane to methanol by molecular O_2 in a stepwise procedure. Based on the online MS analysis, it was confirmed that water is indeed needed for a full conversion of methane to methanol. The detection of CO and CO_2 at different temperatures when the catalyst was heated in a dry He flow demonstrated that more than one intermediate is formed after the reaction of the O_2-activated catalyst with methane.

Mordenite, ferrierite, and ZSM-5 were found to be the best materials of the tested commercial zeolites to prepare Cu/zeolites for methane-to-methanol conversion since 8-MRs and 10-MRs in these zeolites are appropriate for accommodation of Cu^{2+} species, which can be converted into Cu-oxo species active for the methane conversion. Cu^{2+} species supported on zeolite Y and zeolite ß with large 12-MR cages showed poor reaction performances. Interestingly, a small amount of methanol was obtained on Cu/silicalite-1, showing that CuO species formed by impregnating exchangeable sites-free silicalite-1 with $Cu(acac)_2$ can be also active for this reaction.

The methanol production over Cu/morndenite was significantly enhanced by optimizing the conditions of the catalytic cycle, including prolonging the reaction time (to 60 min), adding more water for off-line extraction of methanol (to 10 ml for a batch using 0.6 g of Cu/mordenite), and increasing the activation temperature (to 650 ^{o}C). H_2-TPR and IR measurements showed that at elevated activation temperature, the Cu^{2+} exchange preferentially occurs at the less accessible acid sites, e.g. in 8-MR side pockets, where active Cu-oxo sites are favorably generated. Furthermore, a notable increase of efficiency of Cu/modernite was obtained with decreased Cu loading. This improvement was elucidated by further H_2-TPR analysis showing again a transfer of the Cu^{2+} species to smaller pores as lower Cu contents were applied.

Notably, the activity of solid-state ion-exchanged Cu/mordenites (CuMorS) was greatly higher compared to that of the catalysts prepared conventionally in aqueous medium (CuMorL). This difference was confirmed on mordenites with varied Si/Al ratio and at different activation temperature. H_2-TPR measurements revealed that a significant fraction of Cu^{2+} ions was

exchanged in small pores of mordenite by high-temperature solid-state treatment while for CuMorL, Cu^{2+} species are mostly located on the mordenite surface and in larger cages. Furthermore, in the *in situ* UV-vis spectra of CuMorS, the bands assigned to the active Cu sites were detected with much higher intensity compared to those of CuMorL.

Solid-state ion exchange was applied as an alternative to the conventional route in liquid phase for the preparation of Cu/mordenite. The comparative results on methanol production and characterization of the catalysts demonstrated the great efficiency of solid-state ion exchange to prepare Cu/mordenite with high activity for the direct conversion of methane to methanol. These findings can contribute to a better understanding of Cu species within zeolite and provide synthetic approaches to further enhance the activity of biomimetic Cu-based catalysts for this "dream reaction" under milder conditions.

3.6 Appendix

Table 3.3. N_2 sorption analysis of mordenites and Cu/mordenites.

Sample	Cu content (wt.%)	BET surface area ($m^2 \, g^{-1}$)	Total volume ($cm^3 \, g^{-1}$)
NH_4-Mor-1	-	352.1	0.242
CuMorS-1	2.58	307.0	0.209
CuMorS-1 - after the 4st run	2.58	313.5	0.245
CuMorS-2	1.01	339.7	0.342
CuMorS-3	1.84	328.3	0.243
CuMorS-4	3.74	305.9	0.228
CuMorS-Cl	2.84	327.5	0.255
CuMorS-OA	2.55	334.4	0.275
Na-Mor-2	-	346.9	0.249
CuMorL-1	3.21	327.1	0.275
NH_4-ZSM-5	-	336.9	0.245
CuZSM-S	2.62	307.5	0.246
NH_4-zeolite β	-	497.6	0.737
CuBeta-S	2.66	485.3	0.668
NH_4-zeolite Y	-	626.0	0.458
CuY-S	2.46	548.0	0.374
NH_4-ferrierite	-	278.2	0.204
CuFer-S	2.61	279.6	0.191
As-synthesized silicalite-1	-	321.3	0.278
CuSil-S	2.51	274.7	0.198
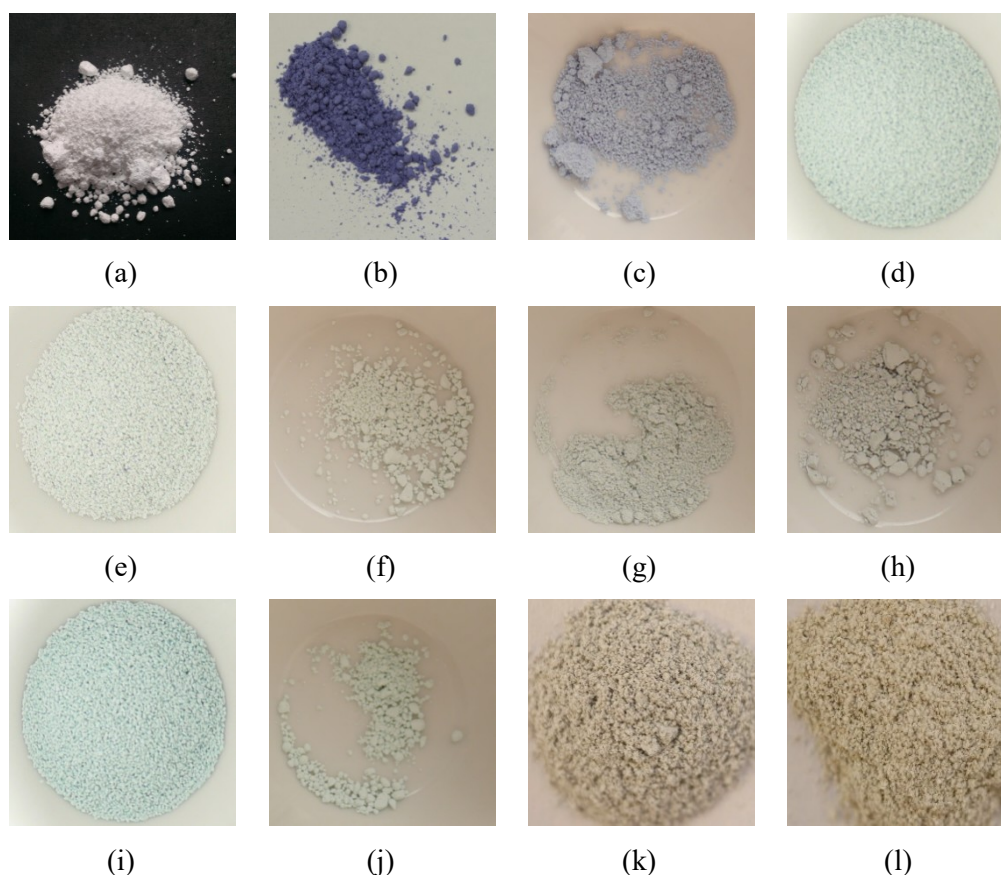
Figure 3.24. Photographs of the materials used in the study (a) NH_4-Mor-1, (b) $Cu(acac)_2$, (c) a well-ground mixture of NH_4-Mor-1 and $Cu(acac)_2$, (d) CuMorS-1, (e) CuMorS-1 after the 1st cycle, (f) CuMorS-1 after the 4th cycle, (g) CuMorS-4, (h) CuMorS-4 after the 1st cycle, (i) calcined CuMorL-1, (j) CuMorL-1 after the 1st cycle, (k) CuMorS-OA, and (l) CuSil-S.
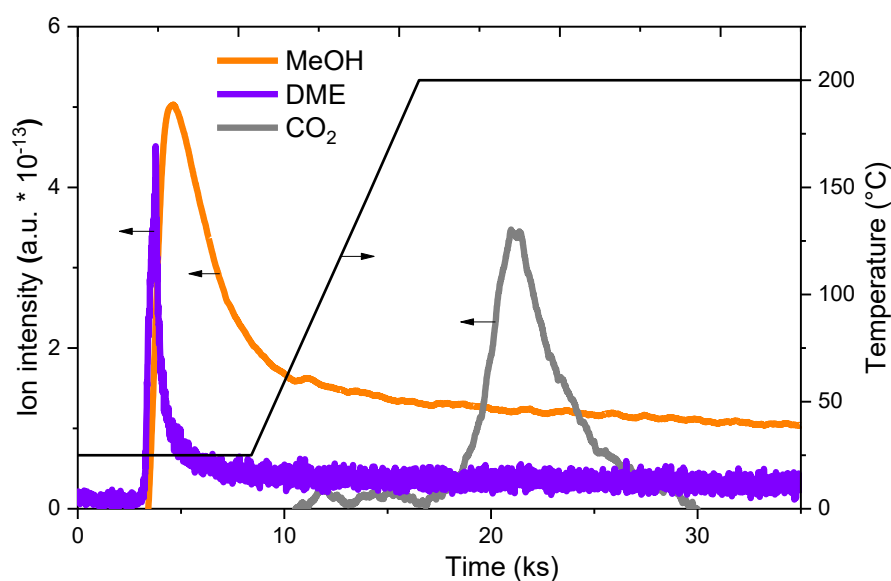
Figure 3.25. Mass spectroscopy-based signal of products during the treatment of CuMorL-1 in a wet He flow.

(a)   (b)   (c)

(d)   (e)
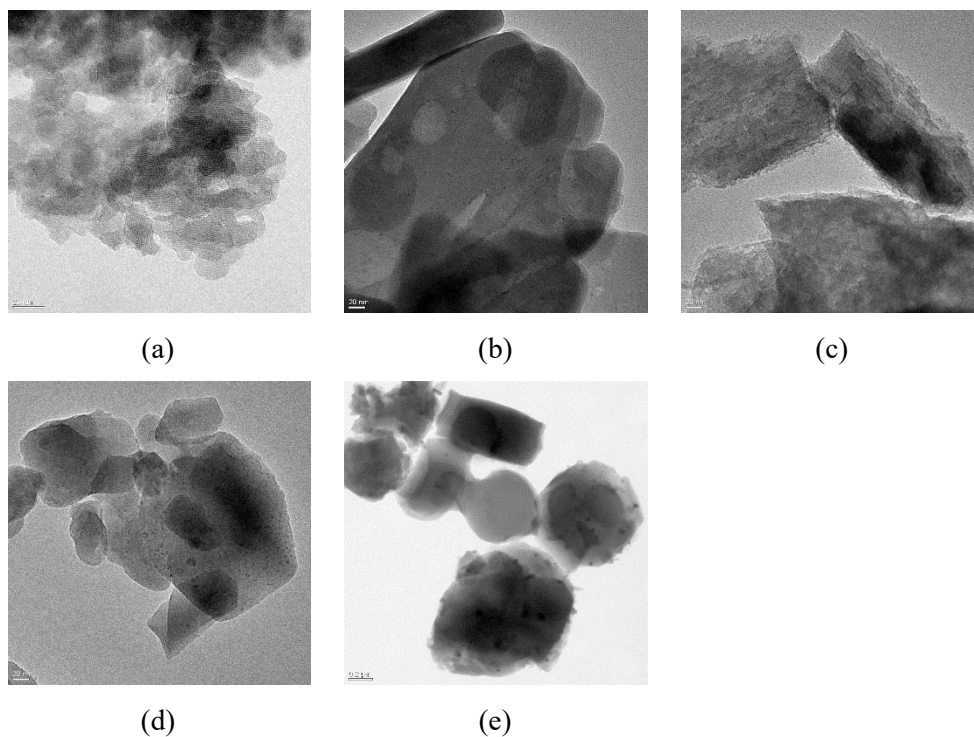
Figure 3.26. TEM images of Cu/zeolites (a) CuBeta-S, (b) CuFer-S, (c) CuY-S, (d) CuZSM-S, (e) CuSil-S, scale bar: 20 nm except for (e): 200 nm.
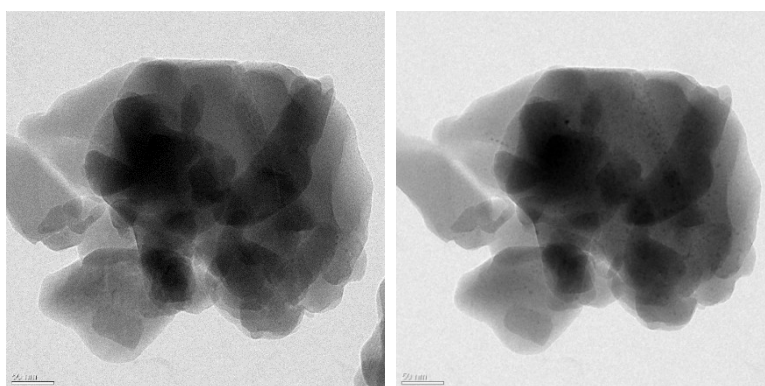
Figure 3.27. Effect of irradiation time on the formation of nanoparticles in TEM analysis, left image: 1-min irradiation, right image: 5-min irradiation, scale bar: 50 nm.

Chapter 4

SBA-15-Supported Cu Catalysts for the Methane-to-Methanol Conversion

4.1 Introduction

Inspired by the prototype natural machines, in the last decade, Cu-, Co- and Fe-exchanged zeolites have been used as heterogeneous catalysts for the methane-to-methanol conversion due to their ability to activate methane at low temperatures and reveal a high selectivity to methanol. This is typically achieved in a stepwise process, in which the catalyst is typically oxidized in O_2 or N_2O at high temperatures (> 250 °C), and then reacts with methane at lower temperatures ($\leq$ 200 °C). The subsequent transformation of the formed intermediate stabilized on the catalyst to methanol is performed via a final treatment with water.[96,103,124] As the so far most active catalysts, Cu/zeolites have been intensively studied to identify the structures of active Cu sites and the catalytic mechanisms to finally develop improved procedures.[105,109,112,114,116,118,119,125]

In the previous chapter, Cu/mordenite was prepared by solid-state ion exchange between NH_4-mordenite and $Cu(acac)_2$, which is more facile and environmentally friendly than the aqueous-phase synthetic route. The resulting material showed a much better activity for the stepped conversion of methane to methanol in comparison with traditional Cu/modernite catalysts. Furthermore, surprisingly, the reaction using Cu/silicalite-1 prepared in a similar approach, yielded a small amount of methanol while CuO particles are supposed as the main phase of Cu species in silicalite-1, which is an Al-free zeolite without any ion-exchangeable site. This result demonstrated that CuO species could become active for the activation of methane.

To further investigate the activity of CuO species in this catalysis, a highly ordered mesoporous silica, i.e. SBA-15, was used as a support for CuO species. In an earlier study, Cu grafted on SBA-15 could catalyze the selective oxidation of methane to formaldehyde by O_2 at 625 °C. A selectivity of up to 96% was obtained while no methanol was produced in such a high-temperature gas-phase oxidation.[53] This chapter would show the first demonstration of direct production of methanol from methane over SBA-15-supported Cu catalysts upon the stepwise procedure. Unlike the Cu-oxo complexes in Cu/zeolites previously proposed as the active sites for the hydroxylation of methane, the catalytic activity of Cu/SBA-15 is attributed to small CuO nanoclusters that are highly dispersed throughout the SBA-15 framework.

The study was further extended to modifying the SBA-15 surface with Cu siloxide complexes synthesized by Dr. F. Schax and M.-L. Wind (AK Limberg, HU Berlin). These compounds contain biomimetic Cu sites binding to siloxane-based ligands as a silica-surface mimic. The functionalized SBA-15 samples were calcined and subsequently tested for the conversion of

methane to methanol. The achieved results are expected to accelerate the development of novel Cu-based catalysts using other supports than zeolites for this "dream reaction".

4.2 Synthesis of materials

4.2.1 Synthesis of SBA-15

SBA-15 was prepared according to the procedure previously described by Zhu *et al.*.[192] Typically, P123 ($EO_{20}PO_{70}EO_{20}$, M_{av} = 5800, 2 g) were dissolved in a mixture of water (30 g) and a 2 M hydrochloric acid solution (60 g) at 35 ^{o}C. After vigorous stirring for 1 h, the solution was added with tetraethoxysilane (4.2 g). The resulting mixture was stirred at the same temperature for 24 h before aged in a Teflon-lined autoclave at 100 ^{o}C for another 24 h. The white solid was then filtered, washed with water, dried at 105 ^{o}C for 12 h, and calcined under static air at 500 ^{o}C (2 ^{o}C min^{-1}) for 4 h.

4.2.2 Synthesis of CuO/SBA-15 by wet impregnation with common Cu sources

A simple Cu-based precursor ($Cu(acac)_2$ or $Cu(OAc)_2$, 0.45 mmol) was added to a mixture of SBA-15 (0.975 g) and absolute ethanol (10 ml). After sonication for 10 min, a slow evaporation of ethanol was performed at 40 ^{o}C under vigorous stirring until a sludge-like phase was obtained. The sample was then dried at 80 ^{o}C for 12 h to remove ethanol. The resulting powder was then pressed into pellets at 100 bar for 60 s, lightly ground, and sieved to a 200-400 μm diameter fraction. Calcination of the material was performed under static air at 550 ^{o}C for 4 h. The Cu content in the materials was determined by inductively coupled plasma-optical emission spectrometry (ICP-OES).

4.2.3 Synthesis of Cu siloxide/SBA-15

Three Cu siloxide precursors denoted as Cu_2Si_2, Cu_2Si_6, and Cu_1Si_4 (Figure 4.9) were synthesized by by Dr. F. Schax and M.-L. Wind (AK Prof. Christian Limberg, HU Berlin). A predetermined amount of a precursor was dissolved in dry toluene (80 ml) in an argon-filled glove box. Calcined SBA-15 (1 g) was then added to the resulting solution. Functionalization of SBA-15 surface by Cu siloxide was performed in 24 h at room temperature under vigorous stirring in argon atmosphere. The solid was filtrated, washed with further 20 ml of toluene, dried under vacuum at 80 ^{o}C overnight, and finally calcined at 550 ^{o}C (2 K min^{-1}) for 4 h in static air. Before catalytic test, the calcined powder was then pressed into pellets at 100 bar for 60 s, lightly ground, and sieved to a 200-400 μm diameter fraction.

4.3 Catalytic studies

Investigation of catalytic activity of the Cu-containing SBA-15 samples was performed as described in Section 3.3 of Chapter 3.

4.4 Results and discussion

4.4.1 CuO/SBA-15 based on common Cu sources

Cu species were first supported on SBA-15 using wet impregnation method. In detail, the catalyst synthesized from $Cu(acac)_2$ was named Cu-AA/SBA while the one obtained using $Cu(OAc)_2$ was named Cu-OA/SBA. Similar Cu loadings (~ 2.7 wt.%) were obtained for both Cu-AA/SBA and Cu-OA/SBA.
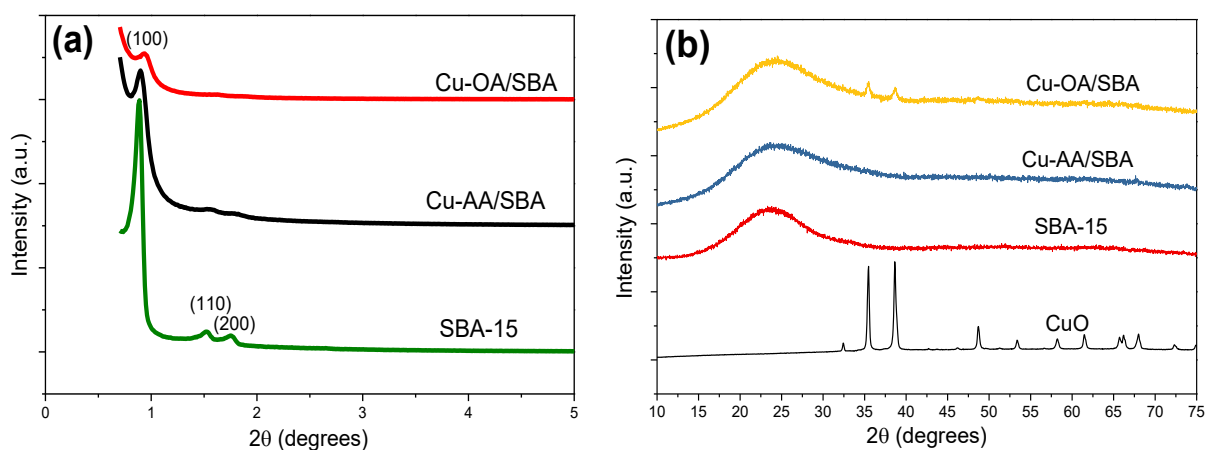
Figure 4.1. PXRD patterns at (a) low angles and (b) wide angles of the materials.

The PXRD pattern at low angles of the unloaded SBA-15 showed three diffraction peaks indexed as (100), (110), and (200) plane corresponding to the well-ordered two-dimensional hexagonal structure of SBA-15 (Figure 4.1a).[192] The (100) diffraction peak was as well observed for both CuO/SBA-15 materials, indicating that the porous structure of the SBA-15 pore was sustained during impregnation. The decreased intensity of the peaks for Cu-containing samples can be attributed to the presence of Cu species in the SBA-15 channels.[193] Wide-angle XRD measurements of the CuO/SBA-15 samples showed different results, depending on the used Cu(II) precursors (Figure 4.1b). No obvious peaks for any crystalline phase are observed for Cu-AA/SBA, showing that the Cu species are well-dispersed throughout the support. In contrast, the diffractogram for Cu-OA/SBA shows to peaks at $2\Theta = 36°$ and $39°$ indicative of the formation of CuO particles on the support.
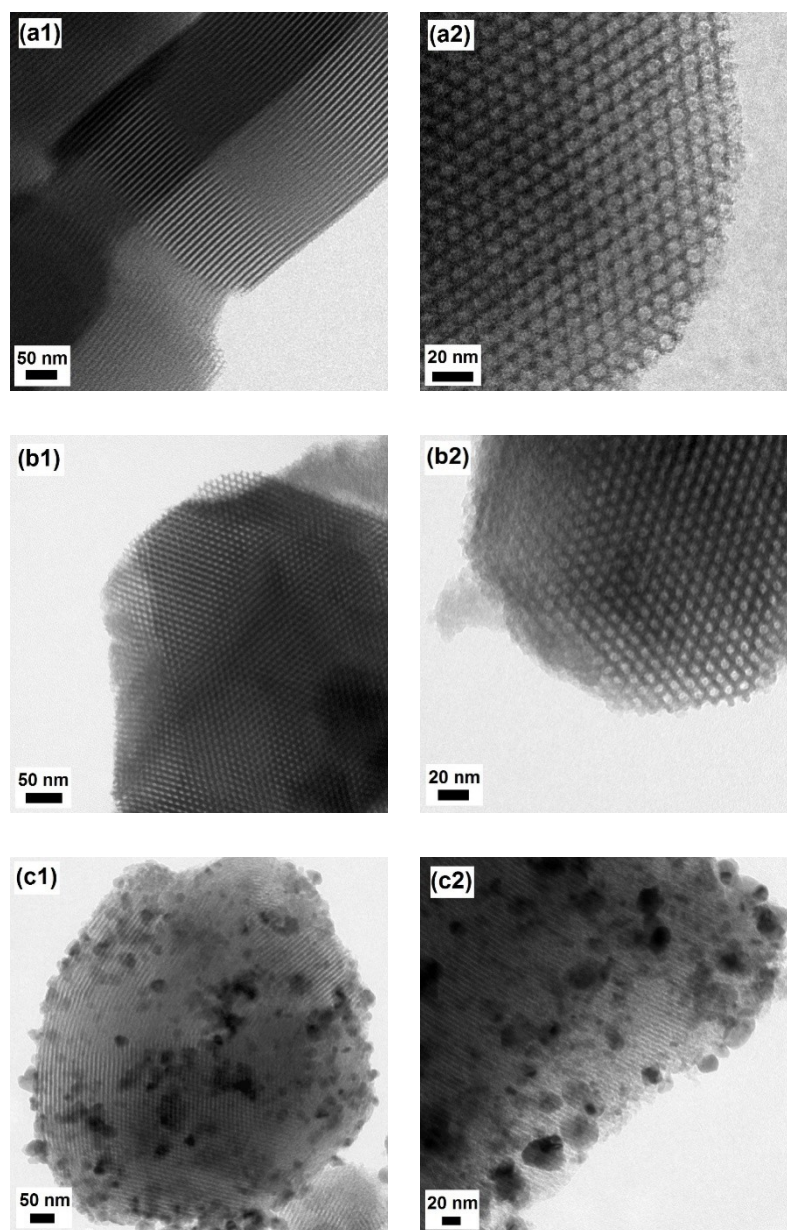
Figure 4.2. TEM images of (a1, a2) pure SBA-15, (b1, b2) calcined Cu-AA/SBA, and (c1, c2) calcined Cu-OA/SBA.

The structure of the CuO/SBA-15 samples was further investigated by TEM measurements. Regular hexagonal mesochannels are seen for all samples, before and after impregnation and calcination (Figure 4.2). No nanoparticles are detected in the TEM images of Cu-AA/SBA (Figure 4.2b) while nanoparticles with various sizes (10–50 nm) are obviously seen for the Cu-OA/SBA sample (Figure 4.2c). Nitrogen sorption measurements show a decrease of surface area and total pore volume after the impregnation of the Cu species into SBA-15, which is found to be more significant for Cu-AA/SBA (Table 4.1). In addition, both mesopore and micropore volumes of Cu-AA/SBA are lower than those of Cu-OA/SBA, respectively. In combination with

TEM and XRD results, it can be concluded that Cu species are indeed mainly located within the pores of Cu-AA/SBA while for Cu-OA/SBA larger CuO nanoparticles are also located on the outer surface of SBA-15.

Table 4.1. Textural properties of SBA-15-based materials.

Sample	Cu loading (wt.%)	SA^a $(m^2 g^{-1})$	PA^b (nm)	V_{meso}^b $(cm^3 g^{-1})$	V_{micro}^b $(cm^3 g^{-1})$	V_{total}^c $(cm^3 g^{-1})$
SBA-15	-	899.1	5.7	0.90	0.18	1.19
Cu-AA/SBA	2.71	508.8	4.0	0.45	0.10	0.64
Cu-OA/SBA	2.78	588.5	3.8	0.53	0.12	0.82

^{a}SA = surface area calculated by the BET method.

^{b}P$_a$ = average pore size, V$_{meso}$ = mesoporous volume, and V$_{micro}$ = microporous volume calculated by the NLDFT method.

^{c}V$_{total}$ = total pore volume calculated at p/p$_0$ = 0.99.

The catalytic activity of the CuO/SBA-15 materials was investigated for the selective oxidation of methane to methanol according to the well-known stepwise procedure first reported by Groothaert *et al.*[103] Typically, the catalyst was activated in O_2 at 550 °C, then allowed to interact with methane at 200 °C. The last step for extraction of methanol could be performed with either liquid water (off-line extraction) or steam (online extraction). For a catalytic comparison, Cu/mordenite with a Cu loading of ~ 2.6 wt.% prepared by previously reported solid-state ion exchange between NH_4-mordenite and $Cu(acac)_2$ was applied as a reference zeolite-based catalyst.[125]

After the extraction with water, methanol was detected in calatytic cycles over both CuO/SBA-15 catalysts indicating that methane was indeed activated by Cu sites in SBA-15 at low temperature (200 °C) and then converted to methanol upon the treatment with water (Table 4.2). Cu-AA/SBA yielded 30.2 µmol g_{cat}^{-1} of methanol (Table 4.2, Entry 1) while a lower methanol amount of 11 µmol g_{cat}^{-1} was produced over Cu-OA/SBA (Table 4.2, Entry 3). The increased production of methanol over Cu-AA/SBA is attributed to the high dispersion of Cu species in the SBA-15 framework. Similar to our previous report on Cu/mordenite, CO_2 was observed when the extraction was performed over 100 °C (Figure 4.3). Notably, the selectivity toward methanol

in the reaction using the CuO/SBA-15 catalysts (> 84%) is comparable to the results obtained with Cu/mordenite.

Table 4.2. Catalytic performances of the Cu-based catalysts.

Entry	Catalyst	Cu loading (wt.%)	Product yield (μmol g_{cat}^{-1})			Oxidized methane[c] (μmol g_{cat}^{-1})	TON[d]	Selectivity to MeOH & DME[e] (%)
			MeOH[a]	DME[b]	CO_2[b]			
1	Cu-AA/SBA	2.71	30.2	0	3.4	33.6	0.079	89.9
2	Cu-AA/SBA[f]		31.7	0	5.8	37.5	0.088	84.5
3	Cu-OA/SBA	2.78	11.1	0	1.0	12.1	0.028	91.7
4	Cu/mordenite	2.58	56.0	1.6	9.0	68.2	0.167	87.7

[a]Methanol was analyzed by GC after off-line extraction with liquid water.

[b]Gas-phase products were analyzed by MS during online extraction with steam.

[c]Amount of oxidized methane was = moles(MeOH) + 2*moles(DME) + moles(CO_2).

[d]Turnover number (TON) = moles(oxidized methane)/moles(Cu)

[e]Selectivity to MeOH and DME = [moles(MeOH) + 2*moles(DME)]/ moles(reacted CH_4)

[f]Reused catalyst for the second cycle.

DME could be considered as a side product by acidic zeolite-catalyzed dehydration of methanol as the extraction with steam is performed at an elevated temperature ($\geq$ 135 $^{\circ}$C).[96,109] However, our earlier study with the Cu/mordenite catalyst showed that both methanol and DME were detected at room temperature, suggesting that different intermediates were generated on the catalyst surface, which would be transformed into methanol and DME, respectively, by the treatment of the catalyst with steam.[125] In this study, no DME was produced over CuO/SBA-15 catalysts compared to 1.6 μmol g_{cat}^{-1} of DME obtained in the catalytic cycle using Cu/mordenite (Table 4.2, Entry 4). To investigate the mechanism of formation of DME on the Cu-based catalysts, an online extraction of the samples with a methanol-saturated He flow at room temperature was performed after their interaction with methane (Figure 4.4).
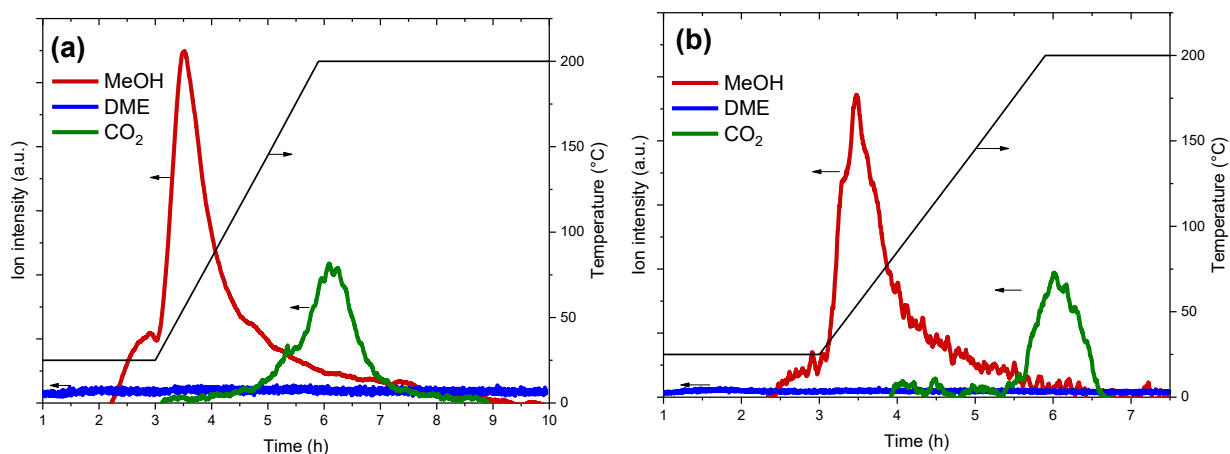
Figure 4.3. Mass-spectral signal of products in the online extraction of (a) Cu-AA/SBA and (b) Cu-OA/SBA with water.
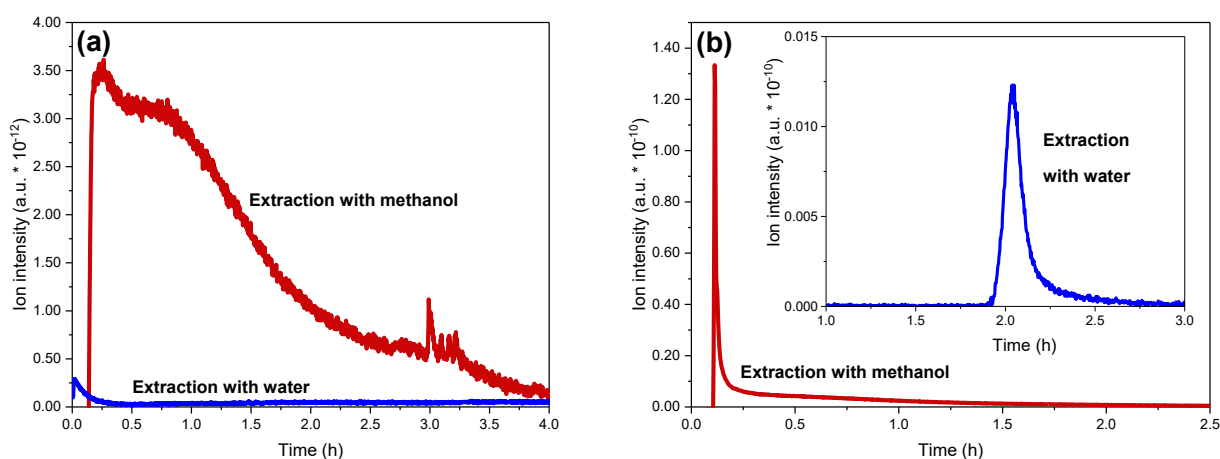
Figure 4.4. Comparison of mass-spectral signals of DME extracted from (a) Cu-AA/SBA and (b) Cu/mordenite in the online stage at RT using different solvents.

Notably, 27.6 µmol g_{cat}^{-1} of DME were achieved with Cu-AA/SBA after the treatment with methanol vapor (Table 4.3). Also, the production of DME on Cu/mordenite was remarkably increased to 48.6 µmol g_{cat}^{-1}. These DME yields are close to the methanol amounts produced upon the water-mediated extraction, indicating that DME obtained in the experiment with a methanol-saturated inert flow is a product of the reaction between methanol molecules and bound intermediate species. It can be thus concluded that the intermediate is indeed a methoxy species stabilized on the catalyst surface after the reaction of active Cu species with methane (Figure 4.5). The rate of such a reaction could be significantly enhanced by acidic sites, which are abundantly available in zeolite catalysts. The MS detected signals of DME with ~ 30 times higher intensities for Cu/mordenite after its contact with methanol vapor compared to the results obtained from Cu-AA/SBA (Figure 4.4, red curves). DME can be also produced in an online

extraction stage with water due to the attack of *in situ*-produced methanol on unreacted intermediate species. Such as-formed methanol species would be retained for a longer time within the zeolite framework mainly possessing micropores in comparison with the mesoporous SBA-15 material. This can explain the small amount of DME generated along with methanol over Cu/mordenite in the steam-assisted extraction step at room temperature.

Table 4.3. Production of DME by the online extraction at room temperature with different solvents.

Entry	Catalyst	DME amount produced[a] ($\mu mol\ g_{cat}^{-1}$)	
		Online extraction with steam	Online extraction with methanol vapor
1	Cu-AA/SBA	0	27.6
2	Cu/mordenite	1.6	48.6
[a]Analyzed by MS.			
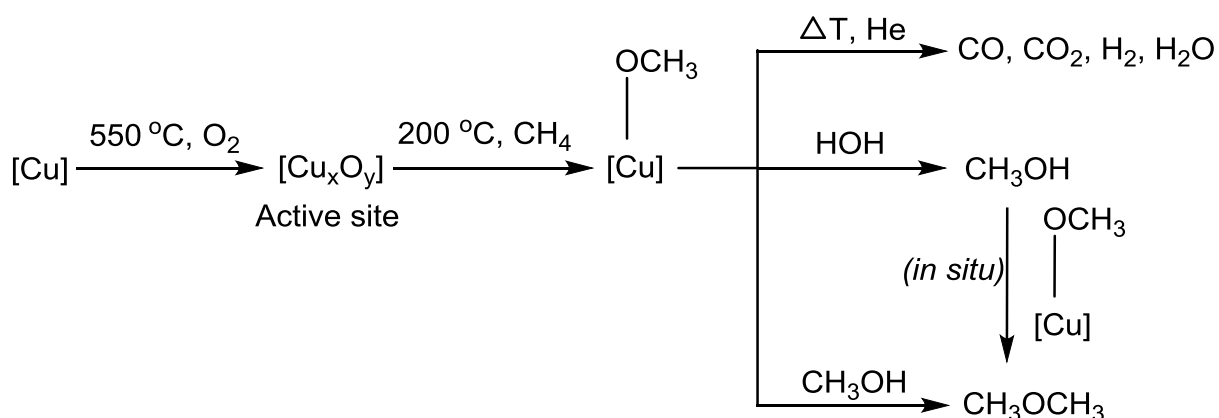
Figure 4.5. Proposed formation of products on the Cu-based catalyst based on the former studies[119,125,163] and mass spectrometry.

To gain more insight into the location of the Cu sites in SBA-15, H_2-TPR measurements were performed for CuO/SBA-15 materials in comparison with the H_2-TPR results of Cu oxide standards. The first reduction stage for CuO/SBA-15 samples is observed from 200 to 300 ^oC, which is attributed to CuO nanoparticles on the surface and at the facilely accessible mesopores of SBA-15 (Figure 4.6). Most of the Cu species in Cu-OA/SBA-15 were reduced by H_2 in this temperature range, consistent with above characterization results that large CuO nanoparticles are the main phase of Cu in this sample. Besides, further H_2 reduction steps at 350 °C and 500

°C are found for the Cu-AA/SBA sample, indicating that Cu species can be distributed at less accessible sites of SBA-15, namely micropores in the main-channel wall, by using $Cu(acac)_2$ for the preparation of CuO/SBA-15. It is therefore suggested that the formation of smaller CuO clusters in Cu-AA/SBA led to its better catalytic performance compared to the result obtained with Cu-OA/SBA. Calculation of H_2 consumption in the TPR measurements further indicates that after activated in O_2, the samples indeed contain Cu(II) species only, as found in Cu/zeolites, which are responsible for activation of methane in the earlier studies (Table 4.4).[105,109,125,189]
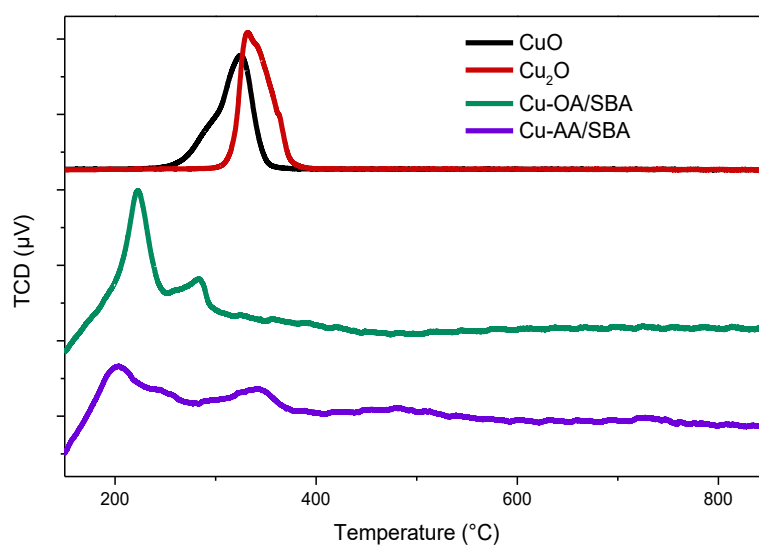
Figure 4.6. H_2-TPR profiles of Cu oxides, calcined Cu-OA/SBA and calcined Cu-AA/SBA.

Table 4.4. Comparison of the Cu loading vs. the H_2 uptake.

Entry	Sample	Cu content[a] (mmol g^{-1})	H_2 uptake[b] (mmol g^{-1})	Molar ratio of Cu to H_2
1	Cu-AA/SBA	0.426	0.431	0.988
2	Cu-OA/SBA	0.437	0.433	1.009
[a]ICP-OES analysis				
[b]H_2-TPR analysis				

Since the first report on the stepwise manner for the gas-phase direct production of methanol from methane over Cu-exchanged zeolites,[103] only zeolites and zeotypes have been used to prepare Cu-based catalysts. In spite of many attempts over the last decade, the nature of the active species in the Cu/zeolite catalysts is still unknown.[119] Based on both theoretical and spectroscopic analyses, several different structures of Cu sites, which can be activated in O_2 and

subsequently be able to react with methane molecules, have been suggested using a zeolitic model with cation-exchangeable frameworks.[116,194-196] *In situ* UV-vis analysis is known as one of the essential characterization techniques to yield useful information on the activated Cu sites. In earlier studies, UV-vis spectra of O_2-activated Cu/ZSM-5 and Cu/mordenite showed a band at ~ 22 500 cm^{-1}, whose intensity is rapidly decreasing when methane was purged to the samples.[103,111,112] This band is assigned to an active site of monooxo-dicopper ($[\mu-Cu_2O]^{2+}$).[108] Notably, several studies have recently reported the absence of this band for Cu/mordenite during the O_2-activation step.[109,118,119] Grundner *et al.* instead reported another broad band at ~ 31 000 cm^{-1} which was stable in O_2 and disappeared after 30 min contact with methane.[109] Also in this study, a $[Cu_3(\mu-O)_3]^{2+}$ core was suggested to be responsible for the activation of methane. A similar result was further found in the very recent work by Kim *et al.*[113] In addition, several other Cu sites embedded in the zeolite channels have been proposed as potential cores for the activation of methane, namely a simple monocopper site,[117] larger Cu-oxo clusters such as $[Cu_4O_4]^{2+}$ and $[Cu_5O_5]^{2+},$[116] and even small/ultrasmall CuO clusters.[118,119]

It should be noted that SBA-15 is known as a porous silica material without ion-exchangeable positions. Therefore, the formation of the isolated Cu-oxo species, which are defined as active sites for Cu/zeolites, in SBA-15 seems to be impossible. After the O_2 activation up to 550 °C, indeed no band in the region of 20 000–25 000 cm^{-1} was found in the *in situ* UV-vis spectra of CuO/SBA-15, demonstrating the absence of the mono-μ-oxo dicopper site. The spectra of the samples activated in O_2 show an absorption band centered at ~ 13 000 cm^{-1}, that is assignable to d-d transitions of Cu(II) ions.[120,122,180,197] Interestingly, similar to the results recently reported for Cu/mordenite,[109,113] a considerable development of the broad band centered at ~ 32 000 cm^{-1} was observed for both Cu-AA/SBA and Cu-OA/SBA during the activation step (Figures 4.7a and 4.8a). It should be noted that the ~ 32 000 cm^{-1} absorption commonly appears in UV-vis spectra of Cu-based materials due to a charge transfer of $O^{2-} \rightarrow Cu^{2+}$ in CuO clusters.[197-200] This increasing feature observed in the UV-vis spectra of CuO/SBA-15 samples is therefore assigned to activated CuO species deposited on SBA-15. As can be expected, in the next step for interaction with methane at 200 °C, the intensity of the 32 000 cm^{-1} band started decreasing as methane was sent to the sample (Figures 4.7b and 4.8b), proving that the O_2-activated CuO species are reactive with methane. Importantly, analyzing the outlet stream with the MS during the contact of the samples with methane revealed that water which is typically generated upon the simple reduction of CuO in the presence of methane at higher temperatures (> 500 °C),[201-203] and methanol were not detected. Such a decrease in the 32 000 cm^{-1} band intensity is therefore

attributed to the activation of methane by CuO species at 200 °C, which yields the corresponding intermediate stabilized on the catalyst surface. However, the incomplete disappearance of the band after 2 h interaction with methane, which is more significantly observed for Cu-OA/SBA, showed that the CuO species in the samples consist of both active and inactive sites. In combination with the better production of methanol observed for Cu-AA/SBA and an earlier study on inactive larger CuO nanoparticles (30–60 nm) supported in pure silica,[119] we therefore conclude that well-dispersed small CuO nanoparticles located within the SBA-15 framework are more active for the methane-to-methanol conversion. Also, according to the in situ UV-vis spectroscopy results of Cu/mordenite catalysts previously reported,[113,118,125] it is suggested that Cu/zeolites may possess both different active sites including extra-framework Cu-oxo complexes and small CuO nanoclusters.
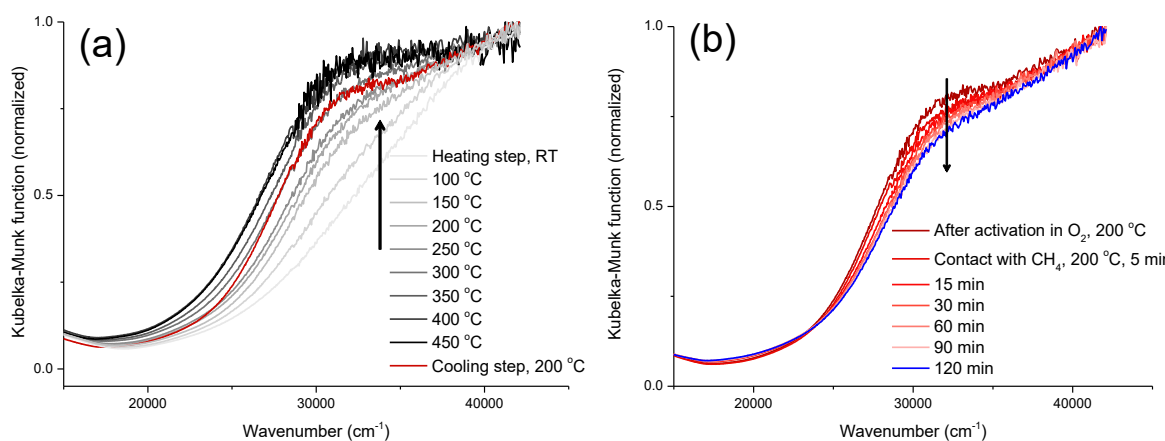

Figure 4.7. *In situ* UV-vis spectra of Cu-AA/SBA (a) after activation in O_2 and (b) subsequent reaction with methane at 200 °C.
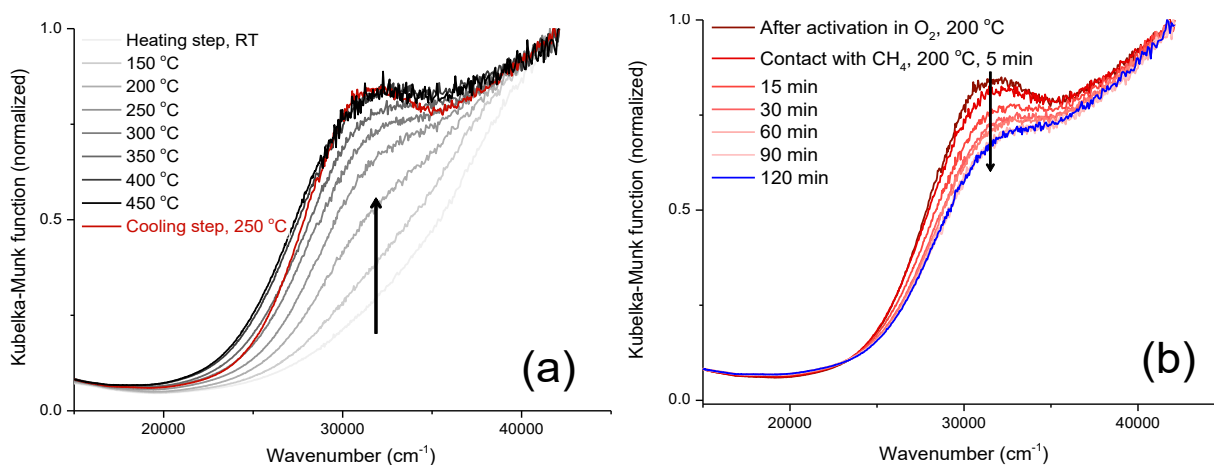

Figure 4.8. *In situ* UV-vis spectra of Cu-OA/SBA (a) after activation in O_2 and (b) subsequent reaction with methane at 200 °C.
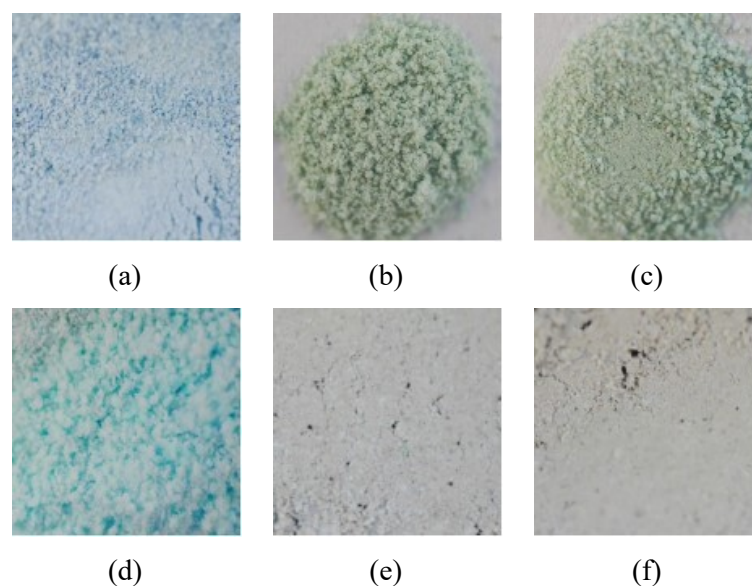
| (a) | (b) | (c) |
| (d) | (e) | (f) |

Figure 4.9. Photographs of Cu/SBA-15, top: Cu-AA/SBA-15 (a) before calcination, (b) after calcination, and (c) after the first catalyst cycle; bottom: Cu-OA-SBA/15 (d) before calcination, (e) after calcination, and (f) after the first catalyst cycle.

In the second catalytic cycle, Cu-AA/SBA was able to produce a similar amount of methanol under the identical conditions. The mass-spectrometric analysis during the online extraction of products with steam also showed similar results to those of the first run. No considerable changes in structure and morphology of the used catalyst were found based on TEM, XRD, and N_2-sorption measurements. Therefore, it can be concluded that CuO species are stable in SBA-15 and can be reactivated after the first cycle.

4.4.2 Cu siloxide/SBA-15

Cu/SBA-15 materials prepared via wet impregnation of SBA-15 with Cu(acac)$_2$ or Cu(OAc)$_2$) were found to be active for the direct conversion of methane to methanol. The performance of the catalysts is proposed to be dependent on location, dispersion, and size of CuO species in the SBA-15 framework. Inspired by the findings on active sites in pMMO and in Cu/zeolite for the hydroxylation of methane under milder conditions, Limberg *et al.* have recently introduced a series of compounds containing copper in siloxide coordination spheres, which may not only form biomimetic dicopper units but also represent low-molecular-weight analogues for hydroxylated silica surfaces.[204] It is therefore expected that modification of the SBA-15 surface with such Cu siloxide complexes can improve the activity of SBA-15-based catalysts.

Cu siloxides used in the study (Figure 4.10) were provided by Dr. F. Schax and M.-L. Wind (AK Limberg, HU Berlin). These compounds are sensitive to O_2 and moisture; the immobilization

procedure was therefore carried out in argon atmosphere. The solutions of Cu_2Si_2, Cu_2Si_6, and Cu_1Si_4 in dry toluene were light yellow, green, and blue, respectively, while the filtrates after the immobilization procedure were colourless and the calcined solids turned from white (colour of fresh SBA-15) to blue, indicating a successful immobilization of Cu-containing complexes onto SBA-15 (Figure 4.11).

(Cu₂Si₂)   (Cu₂Si₆)   (Cu₁Si₄)
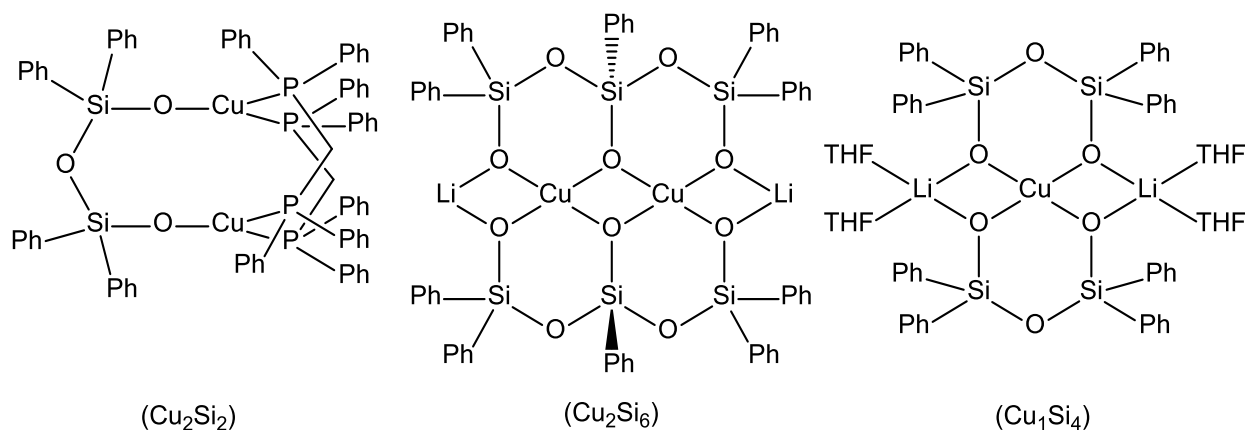
Figure 4.10. Cu siloxides used in the study.

(a)   (b)   (c)   (d)
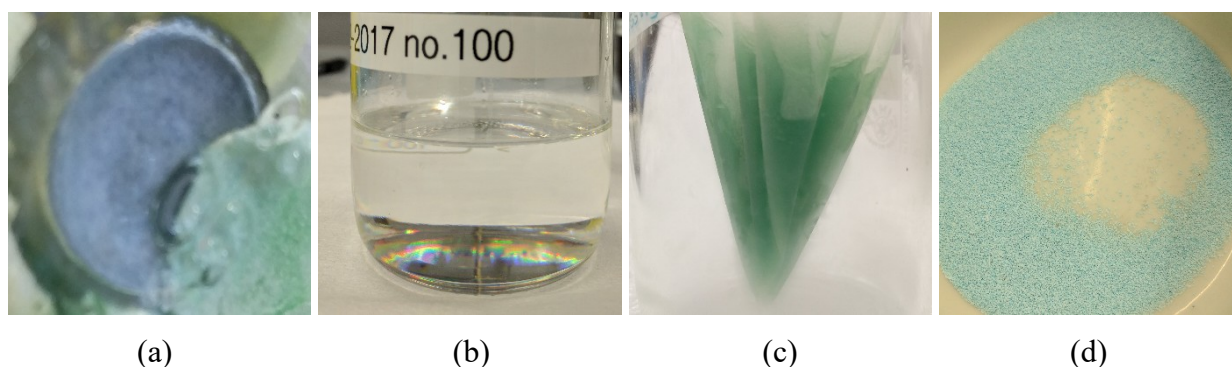
Figure 4.11. Photographs of (a) as-synthesized Cu_2Si_6 precursor, (b) filtrate, (c) Cu_2Si_6/SBA-15 after filtration, and (d) Cu_2Si_6/SBA-15 after calcination.

The TGA analysis in air showed a large weight loss in the temperature region of 200–700 $^{\circ}$C for all vacuum-dried Cu siloxide/SBA-15 samples, most probably due to the decomposition of siloxide species and removal of the organic substituent by O_2. Similar Cu loadings were obtained based on calculating the TGA weight loss and ICP-OES analysis (Table 4.4). These values were also close to the nominal Cu contents, demonstrating that most of the Cu siloxide species were supported on SBA-15. The efficient immobilization in toluene can be explained by the an exchange of the siloxane-based ligands in Cu siloxides by the hydroxyl groups of the silica support, which should yield highly dispersed Cu-species on the surface. It should be noted that the mesopores of SBA-15 have a diameter of ~ 6-nm large while the size of the used Cu

siloxides is about 2 nm. The inner large surface area of the SBA channels will therefore be fully accessible for the Cu siloxide precursors.

Table 4.5. Details on immobilization of Cu siloxide on SBA-15.

Entry	Cu siloxide (Cu content, wt.%) – Amount used (g)	SBA-15 amount (g)	Nominal Cu loading (wt.%)	Calculated Cu loading[a] (wt.%)	Actual Cu loading[b] (wt.%)
1	Cu_2Si_2 (9.71)		2.10	2.19	2.07
2	Cu_2Si_6 (10.26)	1.00	2.50	2.58	2.44
3	Cu_1Si_4 (5.34)		2.25	2.07	2.14
[a]Based on TGA					
[b]ICP-OES analysis					

Table 4.6. Textural properties of the calcined materials.

Sample	Cu loading (wt.%)	SA^a ($m^2\,g^{-1}$)	PA^b (nm)	V_{meso}^b ($cm^3\,g^{-1}$)	V_{micro}^b ($cm^3\,g^{-1}$)	V_{total}^c ($cm^3\,g^{-1}$)
SBA-15	-	880.6	5.7	0.90	0.17	1.18
Cu_2Si_6/SBA-15	2.44	329.7	3.8	0.27	0.05	0.38
Cu_1Si_4/SBA-15	2.14	379.6	4.8	0.49	0.04	0.60

^{a}SA = surface area calculated by the BET method.

^{b}PA = average pore size, V_{meso} = mesoporous volume, and V_{micro} = microporous volume calculated by the NLDFT method.

^{c}V$_{total}$ = total pore volume calculated at $p/p_0 = 0.99$.

PXRD measurements showed that the typical structure of SBA-15 was preserved after impregnation and no large crystalline Cu oxide species were formed (Figure 4.12). These are further seen by TEM images, in which the hexagonal channels of SBA-15 can be observed without the presence of any recognizable nanoparticles for all calcined Cu siloxide/SBA-15 samples (Figure 4.13). On the other hand, the peaks for Cu could be detected throughout the channels in additional EDX measurement, confirming a high dispersion of Cu in the SBA-15 framework. N$_2$-sorption isotherms show a decrease in surface area from 880 $m^2\,g^{-1}$ for pure SBA-15 to ~ 350 $m^2\,g^{-1}$ for Cu-loaded ones (Table 4.6). With considerable decreases found for

both microporous and mesoporous volumes calculated from these isotherms by the NLDFT method, it can be concluded that the Cu species are present at both micropores and mesopores of SBA-15.
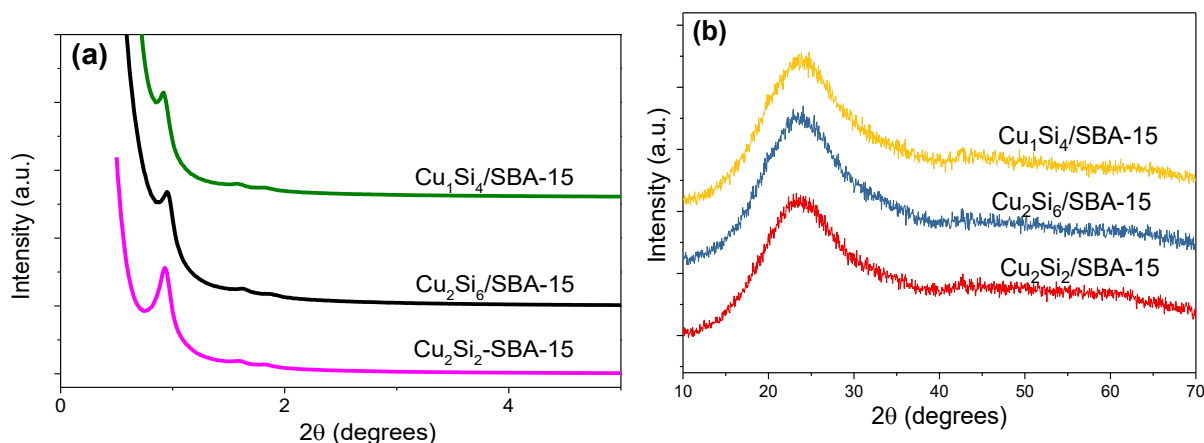
Figure 4.12. Small-angle XRD patterns of the SBA-15-based samples.
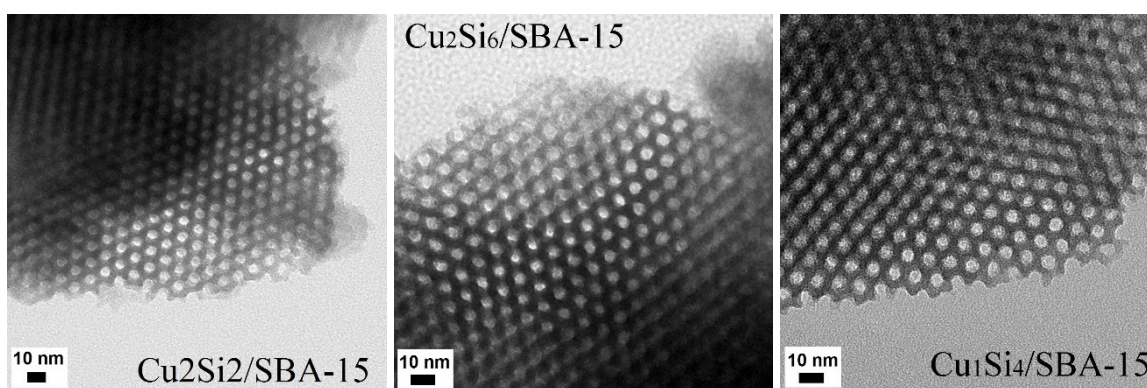
Figure 4.13. TEM images of Cu siloxide/SBA-15 after calcination in static air.

Table 4.7. Methanol production over Cu siloxide/SBA-15.

Entry	Cu siloxide/SBA-15	Cu content, wt.%	MeOH yield ($\mu mol\ g_{cat}^{-1}$)
1	Cu_2Si_2/SBA-15	2.07	3.7
2	Cu_2Si_6/SBA-15	2.44	0.1
3	Cu_1Si_4/SBA-15	2.14	0.0
[a] ICP-OES analysis.			
[b] Analyzed by GC after off-line extraction with liquid water.			

The calcined Cu siloxide/SBA-15 materials were then applied toward the direct synthesis of methanol from methane. Unfortunately, the activity of the materials was negligible with poor methanol productions obtained (Table 4.7). The best performance of 3.7 μmol g_{cat}^{-1} of methanol over Cu_2Si_2/SBA-15 was even lower than the results obtained from the above-mentioned CuO/SBA-15 catalysts. The experiments using the online MS analysis showed similar catalytic results (Figure 4.14). No significantly emerging signals of methanol ($m/z = 31$) were detected for Cu_2Si_6/SBA-15 and Cu_1Si_4/SBA-15 compared to the baseline during the online extraction.
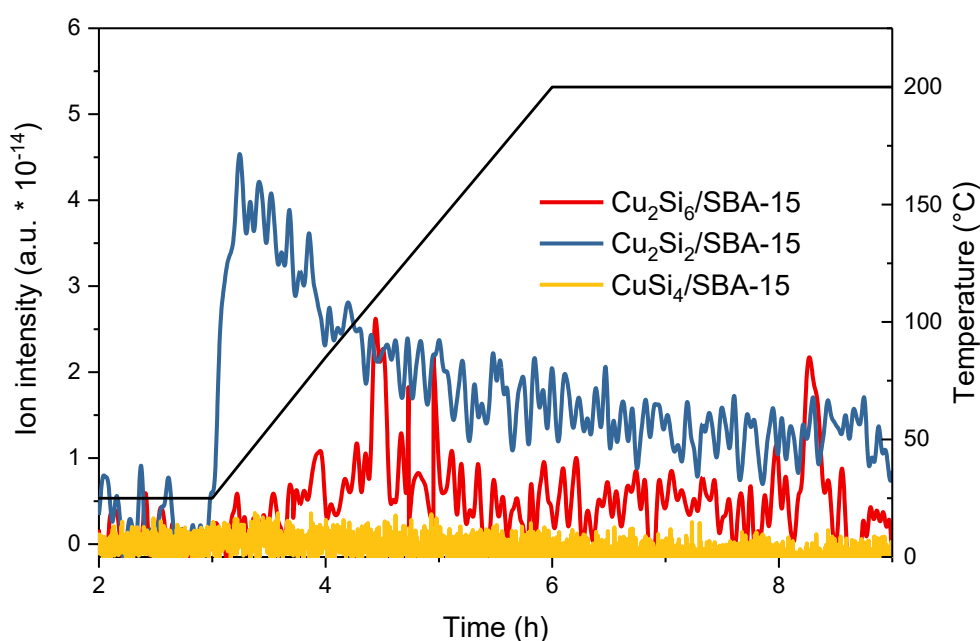
Figure 4.14. Mass-spectral signal of methanol in the online extraction of Cu siloxide/SBA-15 with water.
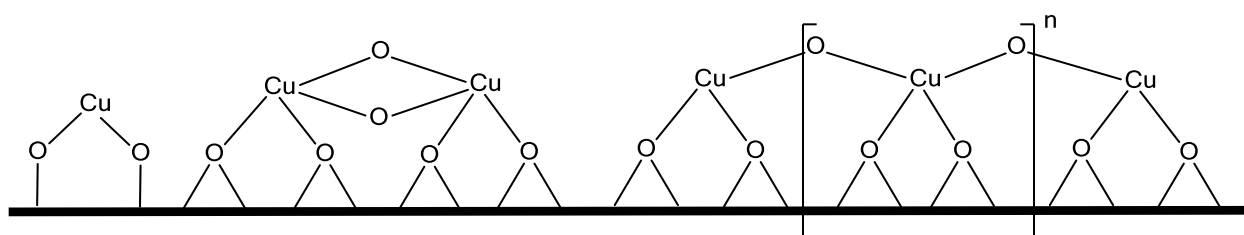
Figure 4.15. Potential Cu species supported on SBA-15, including monomer, dimer and oligomeric species.[200]

As mentioned above, various supported Cu(II) species such as monocopper site, di-/tricopper-oxo complexes, small CuO clusters are proposed to be active for the activation of methane. Cu siloxides were used as molecular models and precursors with the aim of producing highly active cores on the SBA/15 surface (Figure 4.15). It should be noted that Cu_2Si_2 contains Cu(I) species

while Cu(II) cores are found in Cu_2Si_6 and Cu_1Si_4. However, after calcination in O_2, Cu(I) species supported on porous silica would be facilely oxidized to Cu(II) species, which is able to catalyze the methane-to-methanol oxidation. It can be seen that a Cu atom coordinating to only a chelating siloxide ligand as in Cu_2Si_2 has the greatest potential for formation of a dicopper-oxo species due to their flexibility and intermediate oxidation state and indeed the only activity was found from a catalyst from this precursor. This activity is unfortunately much lower than that for Cu-OA/SBA-15 with large CuO particles. Given the catalytic performance of CuO/SBA-15 within this thesis and findings from recently reported works, active Cu sites for the methane-to-methanol conversion seem to be more complex, including tri- and larger Cu-oxo complexes and small/ultrasmall CuO clusters,[109,116,118] while the here-applied precursors probably yielded a too uniform dispersion of the Cu species, i.e. avoiding the formation of any larger cluster than the dicopper site.

4.5 Conclusions

CuO species on SBA-15 were prepared by wet impregnation of SBA-15 with simple precursors such as $Cu(OAc)_2$ and $Cu(acac)_2$ and tested for the partial oxidation of methane to methanol via a three-step manner. Our study showed that methanol was indeed produced on CuO/SBA-15, indicating that SBA-15-supported Cu species activated in O_2 can react with methane at low temperature (200 °C). This conclusion was further supported by *in situ* UV-vis measurements, in which the intensity of the band centered at 32 000 cm^{-1}, attributed to CuO clusters, increased during O_2-activation and subsequently considerably decreased after the contact with methane.

The catalyst prepared from $Cu(acac)_2$ revealed a better catalytic performance due to the high dispersion of small/ultra-small CuO species in the SBA-15 framework compared to the $Cu(OAc)_2$-based sample. H_2-TPR and TEM measurements also confirmed that CuO species could be found at the smaller pores of SBA-15 in Cu-AA/SBA-15, while the CuO species in Cu-OA/SBA-15 are mostly located on the external surface and in the mesopores of SBA-15. Further studies on CuO/SBA-15 will be needed to determine the size of the active clusters and improve their activity.

The reaction using the Cu/mordenite catalyst yielded a minor amount of DME upon the online extraction with steam; however, no DME was obtained in the presence of CuO/SBA-15. In the extraction step, replacing water with methanol resulted in a great improvement in producing DME for both catalysts at room temperature. I propose that DME is generated via the reaction of methanol with the methoxy-like intermediate stabilized on the catalyst surface, which could be

promoted by acid sites. Therefore, in a water-using cycle catalysed by Cu/mordenite, as-formed methanol species could react with the intermediate at room temperature, producing DME as a by-product.

In a further work, Cu siloxides were immobilized on SBA-15 to prepare materials possessing bioinspired Cu sites well dispersed on the surface. The analytic results indicated that Cu siloxides could be sufficiently accommodated within the SBA-15 framework. Unfortunately, only minor activities were observed for Cu siloxide/SBA-15, showing low reactivity of Cu sites with methane, probably because the low-temperature hydroxylation of methane over a Cu-based material requires a catalytic cluster consisting of more than two Cu atoms.

4.6 Appendix
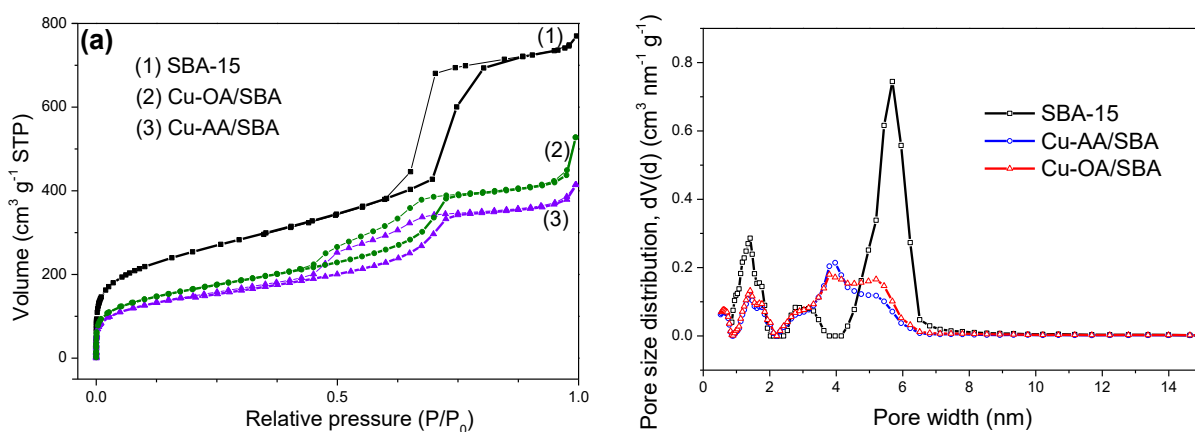
Figure 4.16. (a) N_2-sorption isotherms and (b) pore size distribution of as-synthesized SBA-15, calcined Cu-AA/SBA, and calcined Cu-OA/SBA.
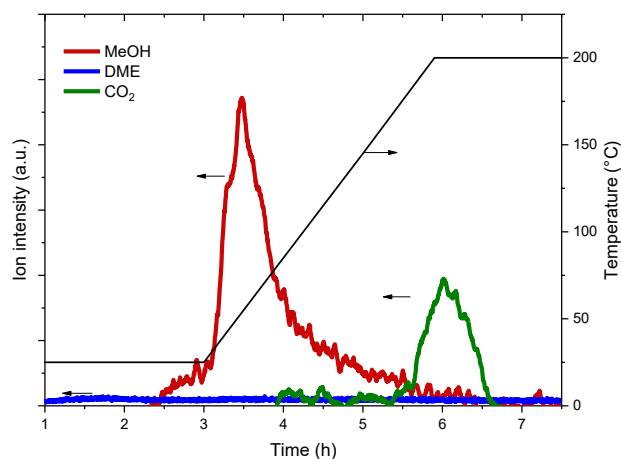
Figure 4.17. Mass-spectral signal of products in the online extraction of Cu-OA/SBA with water.

Table 4.8. Textural properties of CuO/SBA-15 catalysts after the first cycle.

Sample	SA[a] ($m^2 g^{-1}$)	PA[b] (nm)	V_{meso}[b] ($cm^3 g^{-1}$)	V_{micro}[b] ($cm^3 g^{-1}$)	V_{total}[c] ($cm^3 g^{-1}$)
Cu-OA/SBA	647.8	3.8	0.58	0.12	0.88
Cu-AA/SBA	515.6	3.8	0.49	0.09	0.72

[a] SA = surface area calculated by the BET method.

[b] PA = average pore size, V_{meso} = mesoporous volume, and V_{micro} = microporous volume calculated by the NLDFT method.

[c] V_{total} = total pore volume calculated at p/p_o = 0.99.
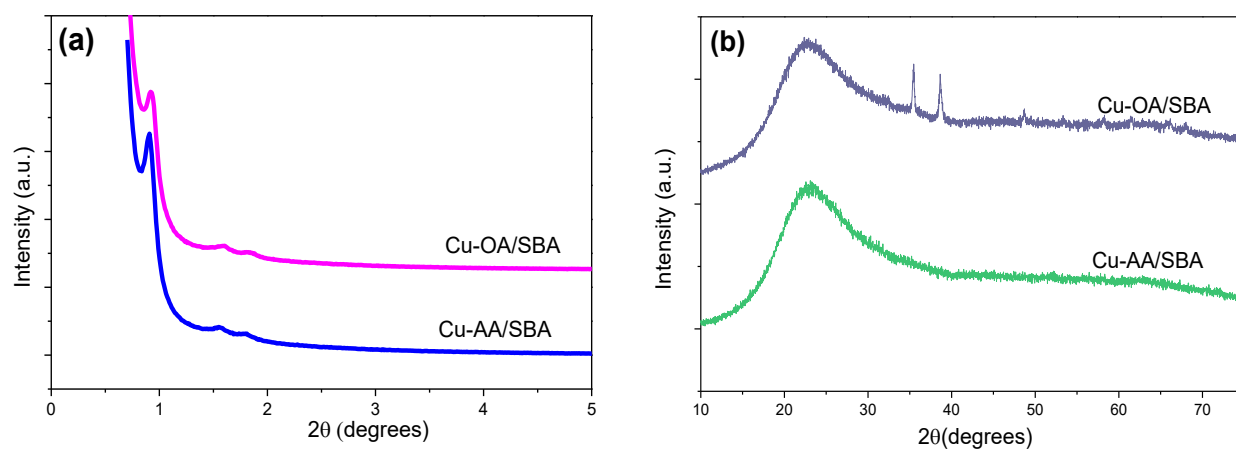
Figure 4.18. (a) Small-angle and (b) wide-angle XRD patterns of Cu-AA/SBA and Cu-OA/SBA after the first cycle.
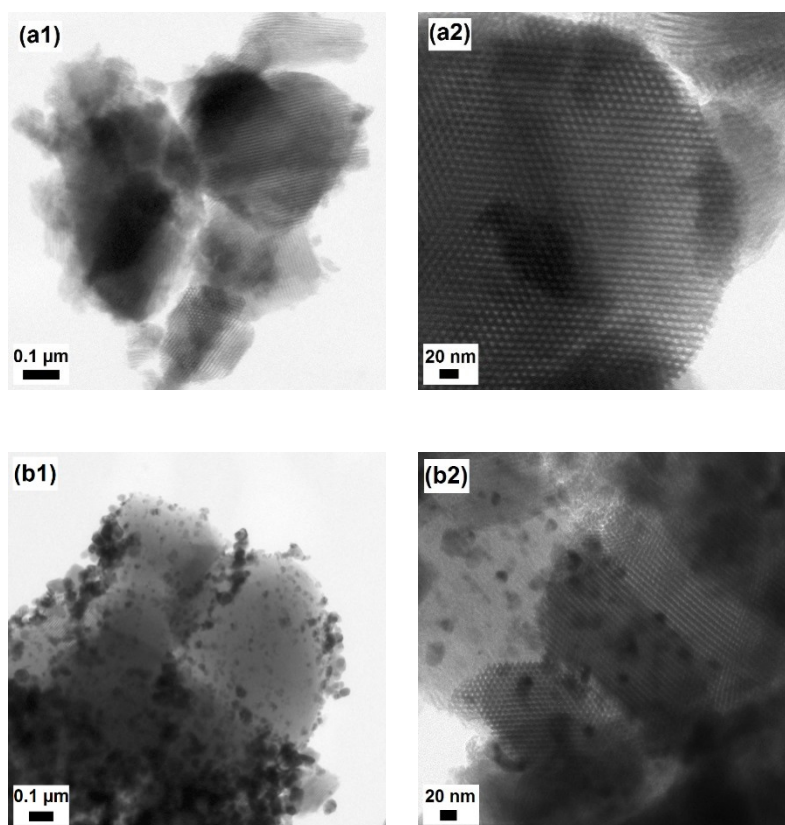
Figure 4.19. TEM images of (a1, a2) Cu-AA/SBA and (b1, b2) Cu-OA/SBA after the first catalytic cycle.

(a) (b) (c)
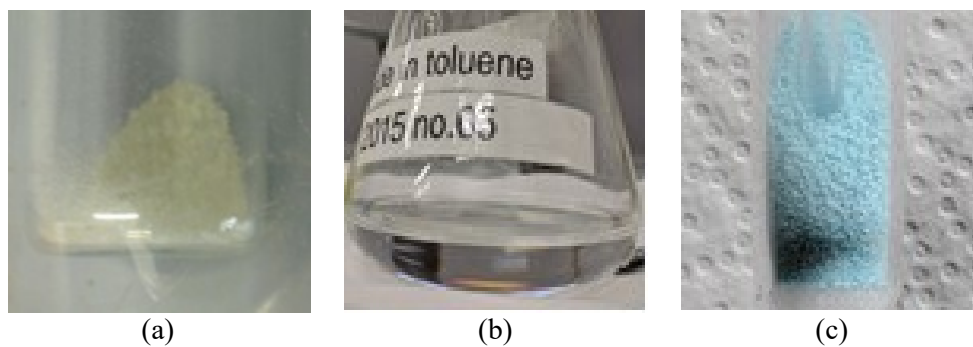
Figure 4.20. Photographs of (a) as-synthesized Cu_2Si_2 precursor, (b) filtrate after isolation of Cu_2Si_2/SBA-15, and (c) Cu_2Si_2/SBA-15 after calcination.

(a) (b) (c) (d)
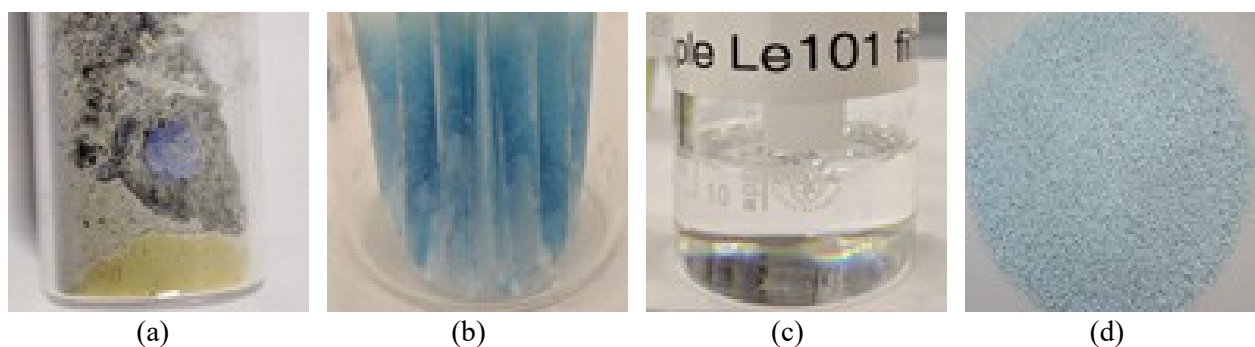
Figure 4.21. Photographs of (a) as-synthesized Cu_1Si_4 precursor, (b) Cu_1Si_4/SBA-15 after filtration, (c) filtrate, (d) Cu_1Si_4/SBA-15 after calcination.
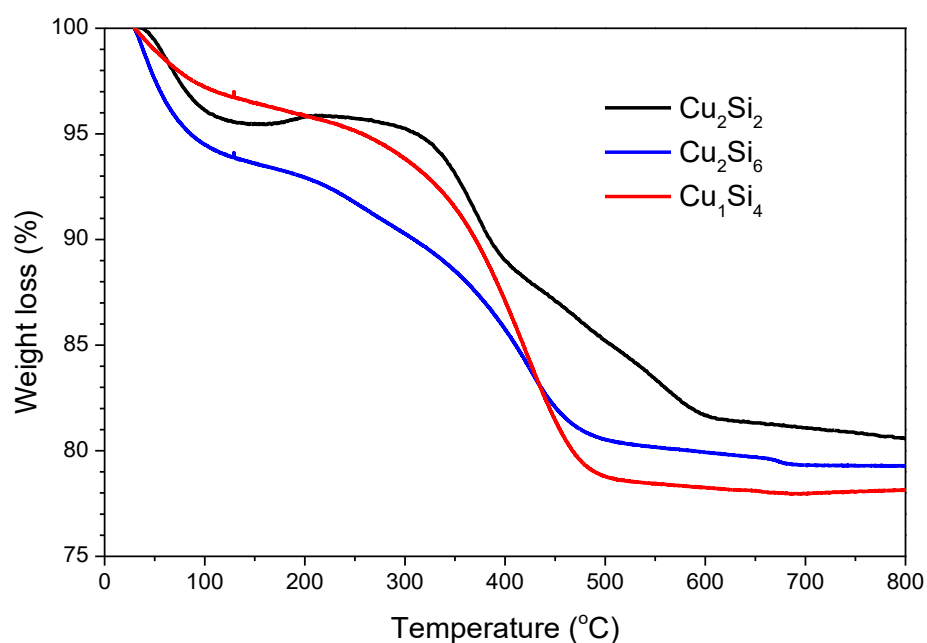
Figure 4.22. TGA results of the SBA-15 samples functionalized with Cu siloxides after vacuum drying.

Chapter 5

Conclusions and Outlook

5.1 Conclusions

The Fe- and Cu-dependent performances of MMOs have opened up great opportunities for developing novel methane-to-methanol conversion processes with improved efficiency. In this work, the use of bioinspired solid catalysts in two main routes with either H_2O_2 or O_2 to oxidize methane to methanol under mild conditions was critically studied.

Although consumption of H_2O_2 to produce methanol is not regarded as a commercially viable strategy, this process is of fundamental significance to mechanistic understanding of methane oxidation to methanol. A high-pressure batch reactor was installed to perform the aqueous-phase hydroxylation of methane catalyzed by Fe- and Cu-containing zeolites, which were prepared via hydrothermal treatment or solid-state ion exchange. It was indicated that extra-framework Fe species are responsible for the methane-to-methanol conversion while supported Cu species are inactive sites. Elevated pressure of methane is essential to facilitate the heterogeneous catalysis of zeolite-bound Fe clusters. On the other hand, to enhance the methanol yield, Fe/ZSM-5- and Fe-silicalite-1-mediated systems required different reaction conditions. For the reaction using the Fe/ZSM-5 (2.28 wt.%) catalyst, as proposed in earlier studies, the activation of methane mainly occurs at a diiron-oxo core, yielding methyl hydroperoxide as the primary product, which is subsequently catalytically decomposed to methanol. Methyl hydroperoxide can also be oxidized by highly reactive OH· radicals to formic acid and CO_2. Under milder reaction conditions and in the presence of Cu species, the formation of the free radicals can be constrained, leading to a significant improvement in the methanol yield. By contrast, the activity of Fe-silicalite-1, in which Fe species mainly exist as isolated sites, is suggested to be dependent on the OH· radicals. As expected, more methanol was obtained by increasing reaction temperature and H_2O_2 concentration while the addition of Cu/zeolites to the reaction inhibited the methanol production compared to the Fe-silicalite-1-only system.

When O_2 was used to oxidize methane to methanol in a stepwise procedure, Cu species supported on zeolites showed much higher activity than the Fe-based catalyst. Solid-state Cu exchange was shown to be a potential and feasible alternative to the liquid-phase route to produce Cu/zeolites with improved activity. UV-vis spectroscopy and H_2-TPR analysis led to the conclusion that under solid-state conditions, a large fraction of Cu ions are preferentially exchanged at the small pores of mordenite such as the side pockets, producing more active Cu sites. Combining catalytic tests and IR measurements, it can be confirmed that the Cu exchange in the side pockets can be improved at elevated calcination temperature, thereby yielding more

methanol. These findings can guide practical and efficient approaches to improve the methanol production over the Cu-exchanged zeolites.

Instead of zeolites, a mesoporous silica, namely SBA-15, was used as the support for Fe and Cu catalysts for the hydroxylation of methane. No methanol was produced over Fe_2O_3/SBA-15 in the H_2O_2-mediated reaction, excluding the role of Fe_2O_3 clusters. Surprisingly, CuO/SBA-15 materials showed the ability to stepwise convert methane to methanol with a comparable selectivity. From *in situ* UV-vis and H_2-TPR measurements, it is concluded that the activity of CuO/SBA-15 is attributed to small/ultrasmall CuO clusters well-dispersed throughout the silica framework.

The stepwise conversion of methane to methanol over the active Cu sites was intensely investigated. Based on the online MS spectrometry, it was shown that the reaction of O_2-activated Cu species with methane produces at least two intermediates with different stabilities. One of them was defined to be a methoxy species, which requires additional water molecules to subsequently hydrolyze to methanol. Formation of CO_2 observed from ~ 150 ^{o}C is attributed to another intermediate and independent on the presence of water. A small amount of DME could be produced not only from dehydrated methanol at high temperatures (> 130 ^{o}C) but also from the reaction of as-formed methanol with remaining methoxy species, which is facilitated by acidic sites in modernite.

The results presented in this thesis are expected to contribute understanding to synthesis, application, and characterization of bioinspired heterogeneous catalysts for the direct production of methanol from methanol. With undeniable advantages of the use of O_2 to oxidize methane, the high selectivity, and the mild reaction conditions, Cu-based catalytic systems will be further improved to satisfy the requirements of industrial application.

5.2 Outlook

The hypothesis on different mechanisms applied to different Fe/zeolite systems needs to be further studied. The role of free radicals in the methanol production can be defined by using an alternative radical scavenger (e.g., Na_2SO_3) instead of supported Cu species. Other oxygenated products than methanol should be analyzed to determine the selectivity to methanol.

For the low-temperature oxidation of methanol over Cu/zeolites, the possibility of operating improved procedures including isothermal multistep route with elevated methane pressure, continuous methanol production from a feed stream of water, methane, and O_2, and anaerobic

oxidation of methane by water, has very recently been demonstrated. Such highly promising strategies can be used for solid-state ion-exchanged Cu/modernite to further simplify the present protocol with the retained high activity.
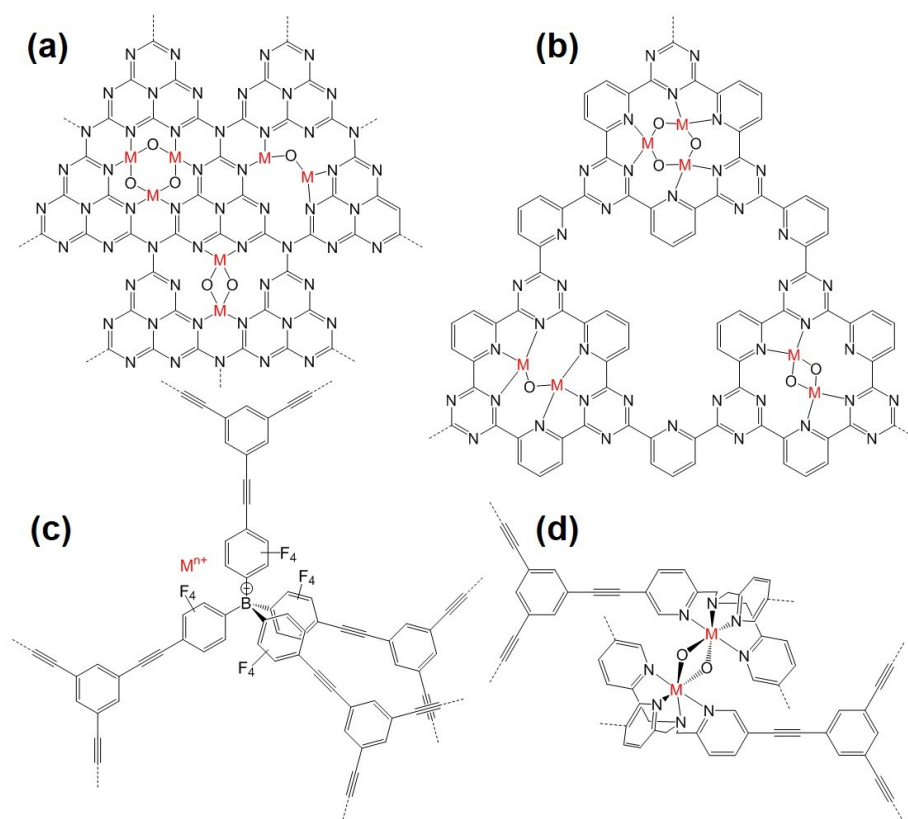
Figure 5.1. Promising porous materials for accommodation of active Fe and Cu sites toward the hydroxylation of methane including (a) carbon nitride, (b) covalent triazine framework, (c) ionic polymer, and (d) functional polymer.

The liquid-phase oxidation under above-described conditions (Section 2.3) using a carbon nitride-supported Fe catalyst (Fe/CN$_x$) has been performed. A significant amount of methanol (~ 13.4 μmol of methanol for 15% wt.% Fe/CN$_x$) was detected, proving that active Fe sites are present in carbon nitride. Notably, Ikuno *et al.* have reported production of methanol over Cu-oxo clusters stabilized in a water-stable Zr-based metal-organic framework (NU-1000) in the temperature range of 150–200 ^{o}C.[205] Therefore, porous materials such as carbon nitrides, covalent triazine frameworks (CTFs) or porous polymers can be promising alternatives to zeolites and silica for preparation of novel Cu- and Fe-containing catalysts for the hydroxylation of methane at low temperatures.

Chapter 6

Characterization of Materials

6.1 Transmission electron microscopy (TEM)

TEM and energy dispersive X-ray spectroscopy (EDX) measurements were recorded on a TECNAI G²20 S-TWIN electron microscope. The microscope is operated at 200 kV, equipped with an EDAX EDX system (Si(Li)) SUTW detector, energy resolution of 136 eV (for MnK(α)). To prepare a sample for TEM measurement, a drop of the material dispersed in ethanol was deposited onto a carbon-coated grid *via* evaporation. TEM grids made of nickel were used for Cu-containing materials while other materials were deposited on cupric grids.

6.2 N$_2$ sorption analysis

N$_2$ sorption analysis was performed at 77 K using a QUADRASORB SI equipped with automated surface area analyzer. Before analysis, samples were degassed at 150 °C overnight. Specific surface areas were determined over a 0.05–0.30 P/P$_o$ range by Brunauer–Emmett–Teller (BET) method. Total pore volume of samples was collected at P/P$_o$ = 0.99. Average pore width was calculated based on non-local density functional theory (NLDFT) method.

6.3 Powder X-ray Diffraction (XRD)

Powder XRD measurements were performed with a Bruker-AXS D8 Advanced diffractometer with DAVINCI design using CuKα radiation (λ = 1.5418 Å) equipped with a Lynx Eye detector.

6.4 Inductively coupled plasma (ICP)

Metal content was measured using a Varian ICP optical emission spectrometer (Version 715 ES) with sample gas flow 0.863 L min^{-1} and plasma power 1350 W.

6.5 *In situ* UV-visible (UV-vis) spectroscopy

UV-visible diffuse reflectance spectra were measured on a Cary 5000 spectrometer (Agilent) equipped with a Harrick Praying Mantis™ diffuse reflectance attachment (DRP-P72) and a reaction chamber (HVC-VUV). The *in situ* cell was connected to a gas delivery system for operation under flow conditions. Spectralon® was used as a white standard. Spectra were taken in the 200-800 nm range with a step size of 1 nm every 3 min during the treatment of materials. Results are shown in the Kubelka-Munk function (F(R)), which are calculated from the recorded reflectance data.

The *in situ* cell was heated to 550 °C with a rate of 10 °C min^{-1} in a 50 Nml min^{-1} flow of O$_2$. The sample was held at 550 °C for 60 min, and then cooled to 200 °C with a rate of 10 °C min^{-1} under

the same flow. After O_2 removal by a 50 Nml min^{-1} flow of He for 5 min, a mixture of 15 Nml min^{-1} CH_4 and 15 Nml min^{-1} He was sent to the cell for 120 min at 200 ^{o}C.

6.6 Temperature-programmed reduction by hydrogen (H$_2$-TPR)

H_2-TPR experiments were conducted on a BELCAT II instrument (Version 0.4.5.13). Prior to measurements, Cu/mordenites were pretreated in a 40 NmL min^{-1} flow of O_2 at 550 ^{o}C for 3 h, and then cooled to 40 ^{o}C. H_2-TPR profiles of the samples were recorded in a 30 NmL min^{-1} flow of 5% H_2/N_2 at a heating rate of 3 ^{o}C min^{-1} up to 900 ^{o}C.

6.7 Infrared (IR) spectroscopy

The IR spectra of self-supporting wafers containing a small amount of the samples and dry KBr were collected on a Varian 640-IR spectrometer over a range of 4000–400 cm^{-1} at a resolution of 2 cm^{-1}.

6.8 Advanced IR spectroscopy

The sample was calcined in O_2 at a predetermined temperature (450–650 ^{o}C) before measured on an IR device. Firstly, the sample prepared as a self-supporting wafer was activated in vacuum (~ 5.0 x 10^{-7} mbar) for 1 h at the same temperature of the previous calcination step. The measurements were performed by Maike Hashagen (FHI). IR spectra of the activated sample were then recorded at room temperature on a Perkin Elmer PE 100 spectrometer equipped with a mercury cadmium telluride (MCT) detector at a resolution of 2 cm^{-1}. 256 scans were collected for each measurement.

6.9 Thermogravimetric analysis (TGA)

TGA was performed on a TGA 1 instrument from Mettler Toledo. The sample was heated to 900 ^{o}C (5 K min^{-1}) under O_2 atmosphere.

6.10 X-ray absorption spectroscopy (XAS)

X-ray absorption measurements were carried out by Christopher Schlesiger (AK Kanngießer, TUB) on a novel self-developed wavelength dispersive spectrometer in von Hamos geometry. The spectrometer is equipped with a microfocus X-ray tube, a curved Highly Annealed Pyrolytic Graphite mosaic crystal and a charge coupled device (CCD) camera with a pixel size of 13.5 μm x 13.5 μm. The tube was operated with a high voltage of 13.5 kV and a current of 870 μA. The samples were prepared as powders on scotch tape and constantly moved during the

measurements to minimize effects of local thickness inhomogeneity. The beam size on the samples is around 3 mm x 3 mm. The gathered spectral range is covering the Cu K absorption edge at 8980 eV.

6.11 X-ray photoelectron spectroscopy (XPS)

XPS analysis was performed at room temperature using a Thermo Scientific K-Alpha$^+$ X-ray Photoelectron Spectrometer with Al Kα radiation. C 1s (284.6 eV) was used to calibrate the binding energies of the elements.

References

(1) Smith, P.; Reay, D.; Van Amstel, A. In *Methane and climate change*, Smith, P.; Reay, D.; Van Amstel, A., Eds.; Earthscan, 2010, pp 1-13.

(2) Villa, P. L.; Rapagnà, S. In *Catalytic activation and functionalisation of light alkanes: advances and challenges*, Derouane, E. G.; Haber, J.; Lemos, F.; Ribeiro, F. R.; Guisnet, M., Eds.; Springer: Dordrecht, 1998, pp 3-34.

(3) Farsi, A.; Moradi, A.; Ghader, S.; Shadravan, V.; Manan, Z. A. *J. Nat. Gas. Sci. Eng.* **2010**, *2*, 270-274.

(4) Spivey, J. J.; Hutchings, G. *Chem. Soc. Rev.* **2014**, *43*, 792-803.

(5) Saha, D.; Grappe, H. A.; Chakraborty, A.; Orkoulas, G. *Chem. Rev.* **2016**, *116*, 11436-11499.

(6) Haynes, C. A.; Gonzalez, R. *Nat. Chem. Biol.* **2014**, *10*, 331-339.

(7) Horn, R.; Schlögl, R. *Catal. Lett.* **2014**, *145*, 23-39.

(8) Latimer, A. A.; Aljama, H.; Kakekhani, A.; Yoo, J. S.; Kulkarni, A.; Tsai, C.; Garcia-Melchor, M.; Abild-Pedersen, F.; Norskov, J. K. *Phys. Chem. Chem. Phys.* **2017**, *19*, 3575-3581.

(9) Ge, X.; Yang, L.; Sheets, J. P.; Yu, Z.; Li, Y. *Biotechnol. Adv.* **2014**, *32*, 1460-1475.

(10) Eekert, M. H. A. v.; Dooren, H. J. v.; Lexmond, M.; Zeeman, G. In *Methane and climate change*, Smith, P.; Reay, D.; Van Amstel, A., Eds.; Earthscan, 2010, pp 151-174.

(11) Pakhare, D.; Spivey, J. *Chem. Soc. Rev.* **2014**, *43*, 7813-7837.

(12) Hwang, I. Y.; Lee, S. H.; Choi, Y. S.; Park, S. J.; Na, J. G.; Chang, I. S.; Kim, C.; Kim, H. C.; Kim, Y. H.; Lee, J. W.; Lee, E. Y. *J. Microbiol. Biotechnol.* **2014**, *24*, 1597-1605.

(13) Zakaria, Z.; Kamarudin, S. K. *Renew. Sust. Energy. Rev.* **2016**, *65*, 250-261.

(14) Usman, M.; Wan Daud, W. M. A.; Abbas, H. F. *Renew. Sust. Energy. Rev.* **2015**, *45*, 710-744.

(15) Wang, V. C.; Maji, S.; Chen, P. P.; Lee, H. K.; Yu, S. S.; Chan, S. I. *Chem. Rev.* **2017**, *117*, 8574-8621.

(16) Chong, Z. R.; Yang, S. H. B.; Babu, P.; Linga, P.; Li, X.-S. *Appl. Energy* **2016**, *162*, 1633-1652.

(17) International Energy Agency (Licence: www.iea.org/t&c), World Energy Outlook 2013, 2013, https://www.iea.org/publications/freepublications/publication/WEO2013.pdf,

(18) Global Gas Flaring Reduction Partnership, Guidance Document - Flaring Estimates Produced by Satellite Observations, 2012, http://siteresources.worldbank.org/INTGGFR/Resources/Guidance_Document_Flaring_Estimates_Produced_by_Satellite_Observations.pdf, (Accessed August 22, 2017).

(19) Wood, D. A.; Nwaoha, C.; Towler, B. F. *J. Nat. Gas. Sci. Eng.* **2012**, *9*, 196-208.

(20) Global Gas Flaring Reduction Partnership, The News Flare Issue No. 13 November 2011 - August 2012. GGFR Partners Mark 10th Anniversary by Scaling up Flaring Reduction Efforts, 2012, http://siteresources.worldbank.org/INTGGFR/Resources/GGFR_Gas_Flaring_Aug2012_a6.pdf, (Accessed August 22, 2017).

(21) Gunsalus, N. J.; Koppaka, A.; Park, S. H.; Bischof, S. M.; Hashiguchi, B. G.; Periana, R. A. *Chem. Rev.* **2017**, *117*, 8521-8573.

(22) Hammond, C.; Conrad, S.; Hermans, I. *ChemSusChem* **2012**, *5*, 1668-1686.

(23) Tang, P.; Zhu, Q.; Wu, Z.; Ma, D. *Energy Environ. Sci.* **2014**, *7*, 2580-2591.

(24) Ravi, M.; Ranocchiari, M.; van Bokhoven, J. A. *Angew. Chem., Int. Ed.* **2017**.

(25) Schwach, P.; Pan, X.; Bao, X. *Chem. Rev.* **2017**, *117*, 8497-8520.

(26) Tomkins, P.; Ranocchiari, M.; van Bokhoven, J. A. *Acc. Chem. Res.* **2017**, *50*, 418-425.

(27) Wang, B.; Albarracín-Suazo, S.; Pagán-Torres, Y.; Nikolla, E. *Catal. Today* **2017**, *285*, 147-158.

(28) Guo, Z.; Liu, B.; Zhang, Q.; Deng, W.; Wang, Y.; Yan, Y. *Chem. Soc. Rev.* **2014**, *43*, 3480-3524.

(29) Olivos-Suarez, A. I.; Szécsényi, À.; Hensen, E. J. M.; Ruiz-Martinez, J.; Pidko, E. A.; Gascon, J. *ACS Catal.* **2016**, 2965-2981.

(30) Gupta, M.; Spivey, J. J. In *New and Future Developments in Catalysis*; Elsevier: Amsterdam, 2013, pp 87-126.

(31) Baltrusaitis, J.; Luyben, W. L. *ACS Sustainable Chem. Eng.* **2015**, *3*, 2100-2111.

(32) da Silva, M. J. *Fuel Process. Technol.* **2016**, *145*, 42-61.

(33) Riaz, A.; Zahedi, G.; Klemeš, J. J. *J. Cleaner Prod.* **2013**, *57*, 19-37.

(34) Galadima, A.; Muraza, O. *J. Nat. Gas. Sci. Eng.* **2015**, *25*, 303-316.

(35) Bian, Z.; Das, S.; Wai, M. H.; Hongmanorom, P.; Kawi, S. *ChemPhysChem* **2017**.

(36) Christian Enger, B.; Lødeng, R.; Holmen, A. *Appl. Catal., A* **2008**, *346*, 1-27.

(37) Holmen, A. *Catal. Today* **2009**, *142*, 2-8.

(38) Holmen, A.; Rokstad, O. A.; Solbakken, A. *Ind. Eng. Chem. Process Des. Dev.* **1976**, *15*, 439-444.

(39) Aschi, M.; Brönstrup, M.; Diefenbach, M.; Harvey, J. N.; Schröder, D.; Schwarz, H. *Angew. Chem., Int. Ed.* **1998**, *37*, 829-832.

(40) Stünkel, S.; Trivedi, H.; Godini, H.-R.; Jašo, S.; Holst, N.; Arndt, S.; Steinbach, J.; Schomäcker, R. *Chem. Ing. Tech.* **2012**, *84*, 1989-1996.

(41) Kondratenko, E. V.; Baerns, M. In *Handb. Heterog. Catal.*; Wiley-VCH Verlag GmbH & Co. KGaA, 2008.

(42) Karakaya, C.; Kee, R. J. *Prog. Energy Combust. Sci.* **2016**, *55*, 60-97.

(43) Zavyalova, U.; Holena, M.; Schlögl, R.; Baerns, M. *ChemCatChem* **2011**, *3*, 1935-1947.

(44) Farrell, B. L.; Igenegbai, V. O.; Linic, S. *ACS Catal.* **2016**, *6*, 4340-4346.

(45) Kondratenko, E. V.; Peppel, T.; Seeburg, D.; Kondratenko, V. A.; Kalevaru, N.; Martin, A.; Wohlrab, S. *Catal. Sci. Technol.* **2017**, *7*, 366-381.

(46) Sadjadi, S.; Simon, U.; Godini, H. R.; Görke, O.; Schomäcker, R.; Wozny, G. *Chem. Eng. J.* **2015**, *281*, 678-687.

(47) Salehi, M.-S.; Askarishahi, M.; Godini, H. R.; Görke, O.; Wozny, G. *Ind. Eng. Chem. Res.* **2016**, *55*, 3287-3299.

(48) Gerceker, D.; Motagamwala, A. H.; Rivera-Dones, K. R.; Miller, J. B.; Huber, G. W.; Mavrikakis, M.; Dumesic, J. A. *ACS Catal.* **2017**, *7*, 2088-2100.

(49) Ohnishi, R.; Liu, S.; Dong, Q.; Wang, L.; Ichikawa, M. *J. Catal.* **1999**, *182*, 92-103.

(50) Wang, L.; Tao, L.; Xie, M.; Xu, G.; Huang, J.; Xu, Y. *Catal. Lett.* **1993**, *21*, 35-41.

(51) Wang, Y.; Otsuka, K. *J. Chem. Soc., Chem. Commun.* **1994**, 2209-2210.

(52) Gesser, H. D.; Hunter, N. R.; Prakash, C. B. *Chem. Rev.* **1985**, *85*, 235-244.

(53) An, D.; Zhang, Q.; Wang, Y. *Catal. Today* **2010**, *157*, 143-148.

(54) Otsuka, K.; Wang, Y. *Appl. Catal., A* **2001**, *222*, 145-161.

(55) Ali, K. A.; Abdullah, A. Z.; Mohamed, A. R. *Renew. Sust. Energy. Rev.* **2015**, *44*, 508-518.

(56) Amouroux, J.; Siffert, P.; Pierre Massué, J.; Cavadias, S.; Trujillo, B.; Hashimoto, K.; Rutberg, P.; Dresvin, S.; Wang, X. *Prog. Nat. Sci.: Mater. Int.* **2014**, *24*, 295-304.

(57) Jadhav, S. G.; Vaidya, P. D.; Bhanage, B. M.; Joshi, J. B. *Chem. Eng. Res. Des.* **2014**, *92*, 2557-2567.

(58) Olah, G. A. *Angew. Chem., Int. Ed.* **2005**, *44*, 2636-2639.

(59) Olsbye, U.; Svelle, S.; Bjørgen, M.; Beato, P.; Janssens, T. V. W.; Joensen, F.; Bordiga, S.; Lillerud, K. P. *Angew. Chem., Int. Ed.* **2012**, *51*, 5810-5831.

(60) Behrens, M.; Studt, F.; Kasatkin, I.; Kühl, S.; Hävecker, M.; Abild-Pedersen, F.; Zander, S.; Girgsdies, F.; Kurr, P.; Kniep, B.-L.; Tovar, M.; Fischer, R. W.; Nørskov, J. K.; Schlögl, R. *Science* **2012**, *336*, 893-897.

(61) Labinger, J. A. *J. Mol. Catal. A: Chem.* **2004**, *220*, 27-35.

(62) Merkx, M.; Kopp, D. A.; Sazinsky, M. H.; Blazyk, J. L.; Müller, J.; Lippard, S. J. *Angew. Chem., Int. Ed.* **2001**, *40*, 2782-2807.

(63) Sazinsky, M. H.; Lippard, S. J. In *Sustaining Life on Planet Earth: Metalloenzymes Mastering Dioxygen and Other Chewy Gases. Metal Ions in Life Sciences*, Kroneck, P. M. H.; Torres, M. E. S., Eds.; Springer: Cham, 2015, pp 205-256.

(64) Lawton, T. J.; Rosenzweig, A. C. *J. Am. Chem. Soc.* **2016**, *138*, 9327-9340.

(65) Strong, P. J.; Xie, S.; Clarke, W. P. *Environ. Sci. Technol.* **2015**, *49*, 4001-4018.

(66) Tinberg, C. E.; Lippard, S. J. *Acc. Chem. Res.* **2011**, *44*, 280-288.

(67) Friedle, S.; Reisner, E.; Lippard, S. J. *Chem. Soc. Rev.* **2010**, *39*, 2768-2779.

(68) Banerjee, R.; Proshlyakov, Y.; Lipscomb, J. D.; Proshlyakov, D. A. *Nature* **2015**, *518*, 431-434.

(69) Yao, S.; Herwig, C.; Xiong, Y.; Company, A.; Bill, E.; Limberg, C.; Driess, M. *Angew. Chem., Int. Ed.* **2010**, *49*, 7054-7058.

(70) Balasubramanian, R.; Rosenzweig, A. C. *Acc. Chem. Res.* **2007**, *40*, 573-580.

(71) Bollinger Jr, J. M. *Nature* **2010**, *465*, 40-41.

(72) Culpepper, M. A.; Cutsail, G. E., 3rd; Hoffman, B. M.; Rosenzweig, A. C. *J. Am. Chem. Soc.* **2012**, *134*, 7640-7643.

(73) Balasubramanian, R.; Smith, S. M.; Rawat, S.; Yatsunyk, L. A.; Stemmler, T. L.; Rosenzweig, A. C. *Nature* **2010**, *465*, 115-119.

(74) Shiota, Y.; Yoshizawa, K. *Inorg. Chem.* **2009**, *48*, 838-845.

(75) Smeets, P. J.; Hadt, R. G.; Woertink, J. S.; Vanelderen, P.; Schoonheydt, R. A.; Sels, B. F.; Solomon, E. I. *J. Am. Chem. Soc.* **2010**, *132*, 14736-14738.

(76) Chan, S. I.; Wang, V. C.; Lai, J. C.; Yu, S. S.; Chen, P. P.; Chen, K. H.; Chen, C. L.; Chan, M. K. *Angew. Chem., Int. Ed.* **2007**, *46*, 1992-1994.

(77) Chan, S. I.; Yu, S. S. F. *Acc. Chem. Res.* **2008**, *41*, 969-979.

(78) Takeguchi, M.; Miyakawa, K.; Okura, I. *J. Mol. Catal. A: Chem.* **1998**, *132*, 145-153.

(79) Choi, D.-W.; Kunz, R. C.; Boyd, E. S.; Semrau, J. D.; Antholine, W. E.; Han, J.-I.; Zahn, J. A.; Boyd, J. M.; Arlene, M.; DiSpirito, A. A. *J. Bacteriol.* **2003**, *185*, 5755-5764.

(80) Semrau, J. D.; DiSpirito, A. A.; Yoon, S. *FEMS Microbiol. Rev.* **2010**, *34*, 496-531.

(81) Martinho, M.; Choi, D. W.; DiSpirito, A. A.; Antholine, W. E.; Semrau, J. D.; Münck, E. *J. Am. Chem. Soc.* **2007**, *129*, 15783-15785.

(82) Culpepper, M. A.; Rosenzweig, A. C. *Crit. Rev. Biochem. Mol. Biol.* **2012**, *47*, 483-492.

(83) Bordeaux, M.; Galarneau, A.; Drone, J. *Angew. Chem., Int. Ed.* **2012**, *51*, 10712-10723.

(84) Chan, S. I.; Lu, Y.-J.; Nagababu, P.; Maji, S.; Hung, M.-C.; Lee, M. M.; Hsu, I. J.; Minh, P. D.; Lai, J. C. H.; Ng, K. Y.; Ramalingam, S.; Yu, S. S. F.; Chan, M. K. *Angew. Chem., Int. Ed.* **2013**, *52*, 3731-3735.

(85) Liu, C.-C.; Mou, C.-Y.; Yu, S. S. F.; Chan, S. I. *Energy Environ. Sci.* **2016**, *9*, 1361-1374.

(86) Siewert, I.; Limberg, C. *Chem. - Eur. J.* **2009**, *15*, 10316-10328.

(87) Yuan, Q.; Deng, W.; Zhang, Q.; Wang, Y. *Adv. Synth. Catal.* **2007**, *349*, 1199-1209.

(88) Hammond, C.; Forde, M. M.; Ab Rahim, M. H.; Thetford, A.; He, Q.; Jenkins, R. L.; Dimitratos, N.; Lopez-Sanchez, J. A.; Dummer, N. F.; Murphy, D. M.; Carley, A. F.; Taylor, S. H.; Willock, D. J.; Stangland, E. E.; Kang, J.; Hagen, H.; Kiely, C. J.; Hutchings, G. J. *Angew. Chem., Int. Ed.* **2012**, *51*, 5129-5133.

(89) Hammond, C.; Jenkins, R. L.; Dimitratos, N.; Lopez-Sanchez, J. A.; ab Rahim, M. H.; Forde, M. M.; Thetford, A.; Murphy, D. M.; Hagen, H.; Stangland, E. E.; Moulijn, J. M.; Taylor, S. H.; Willock, D. J.; Hutchings, G. J. *Chem. - Eur. J.* **2012**, *18*, 15735-15745.

(90) Hammond, C.; Dimitratos, N.; Jenkins, R. L.; Lopez-Sanchez, J. A.; Kondrat, S. A.; Hasbi ab Rahim, M.; Forde, M. M.; Thetford, A.; Taylor, S. H.; Hagen, H.; Stangland, E. E.; Kang, J. H.; Moulijn, J. M.; Willock, D. J.; Hutchings, G. J. *ACS Catal.* **2013**, *3*, 689-699.

(91) Hammond, C.; Dimitratos, N.; Lopez-Sanchez, J. A.; Jenkins, R. L.; Whiting, G.; Kondrat, S. A.; ab Rahim, M. H.; Forde, M. M.; Thetford, A.; Hagen, H.; Stangland, E. E.; Moulijn, J. M.; Taylor, S. H.; Willock, D. J.; Hutchings, G. J. *ACS Catal.* **2013**, *3*, 1835-1844.

(92) Hutchings, G. J. *Top. Catal.* **2016**, *59*, 658-662.

(93) Xu, J.; Armstrong, R. D.; Shaw, G.; Dummer, N. F.; Freakley, S. J.; Taylor, S. H.; Hutchings, G. J. *Catal. Today* **2016**, *270*, 93-100.

(94) Forde, M. M.; Armstrong, R. D.; McVicker, R.; Wells, P. P.; Dimitratos, N.; He, Q.; Lu, L.; Jenkins, R. L.; Hammond, C.; Lopez-Sanchez, J. A.; Kiely, C. J.; Hutchings, G. J. *Chem. Sci.* **2014**, *5*, 3603-3616.

(95) Armstrong, R. D.; Freakley, S. J.; Forde, M. M.; Peneau, V.; Jenkins, R. L.; Taylor, S. H.; Moulijn, J. A.; Morgan, D. J.; Hutchings, G. J. *J. Catal.* **2015**, *330*, 84-92.

(96) Starokon, E. V.; Parfenov, M. V.; Pirutko, L. V.; Abornev, S. I.; Panov, G. I. *J. Phys. Chem. C* **2011**, *115*, 2155-2161.

(97) Starokon, E. V.; Parfenov, M. V.; Arzumanov, S. S.; Pirutko, L. V.; Stepanov, A. G.; Panov, G. I. *J. Catal.* **2013**, *300*, 47-54.

(98) Dubkov, K. A.; Ovanesyan, N. S.; Shteinman, A. A.; Starokon, E. V.; Panov, G. I. *J. Catal.* **2002**, *207*, 341-352.

(99) Snyder, B. E.; Vanelderen, P.; Bols, M. L.; Hallaert, S. D.; Bottger, L. H.; Ungur, L.; Pierloot, K.; Schoonheydt, R. A.; Sels, B. F.; Solomon, E. I. *Nature* **2016**, *536*, 317-321.

(100) Sobolev, V. I.; Dubkov, K. A.; Panna, O. V.; Panov, G. I. *Catal. Today* **1995**, *24*, 251-252.

(101) Wood, B. *J. Catal.* **2004**, *225*, 300-306.

(102) Parfenov, M. V.; Starokon, E. V.; Pirutko, L. V.; Panov, G. I. *J. Catal.* **2014**, *318*, 14-21.

(103) Groothaert, M. H.; Smeets, P. J.; Sels, B. F.; Jacobs, P. A.; Schoonheydt, R. A. *J. Am. Chem. Soc.* **2005**, *127*, 1394-1395.

(104) Alayon, E. M.; Nachtegaal, M.; Ranocchiari, M.; van Bokhoven, J. A. *Chem. Commun.* **2012**, *48*, 404-406.

(105) Sushkevich, V. L.; Palagin, D.; Ranocchiari, M.; van Bokhoven, J. A. *Science* **2017**, *356*, 523-527.

(106) Groothaert, M. H.; van Bokhoven, J. A.; Battiston, A. A.; Weckhuysen, B. M.; Schoonheydt, R. A. *J. Am. Chem. Soc.* **2003**, *125*, 7629-7640.

(107) Groothaert, M. H.; Lievens, K.; Leeman, H.; Weckhuysen, B. M.; Schoonheydt, R. A. *J. Catal.* **2003**, *220*, 500-512.

(108) Woertink, J. S.; Smeets, P. J.; Groothaert, M. H.; Vance, M. A.; Sels, B. F.; Schoonheydt, R. A.; Solomon, E. I. *Proc. Natl. Acad. Sci.* **2009**, *106*, 18908-18913.

(109) Grundner, S.; Markovits, M. A. C.; Li, G.; Tromp, M.; Pidko, E. A.; Hensen, E. J. M.; Jentys, A.; Sanchez-Sanchez, M.; Lercher, J. A. *Nat. Commun.* **2015**, *6*, 7546.

(110) Alayon, E. M. C.; Nachtegaal, M.; Kleymenov, E.; van Bokhoven, J. A. *Microporous Mesoporous Mater.* **2013**, *166*, 131-136.

(111) Vanelderen, P.; Hadt, R. G.; Smeets, P. J.; Solomon, E. I.; Schoonheydt, R. A.; Sels, B. F. *J. Catal.* **2011**, *284*, 157-164.

(112) Vanelderen, P.; Snyder, B. E. R.; Tsai, M.-L.; Hadt, R. G.; Vancauwenbergh, J.; Coussens, O.; Schoonheydt, R. A.; Sels, B. F.; Solomon, E. I. *J. Am. Chem. Soc.* **2015**, *137*, 6383-6392.

(113) Kim, Y.; Kim, T. Y.; Lee, H.; Yi, J. *Chem. Commun.* **2017**, *53*, 4116-4119.

(114) Li, G.; Vassilev, P.; Sanchez-Sanchez, M.; Lercher, J. A.; Hensen, E. J. M.; Pidko, E. A. *J. Catal.* **2016**, *338*, 305-312.

(115) Markovits, M. A. C.; Jentys, A.; Tromp, M.; Sanchez-Sanchez, M.; Lercher, J. A. *Top. Catal.* **2016**, *59*, 1554-1563.

(116) Palagin, D.; Knorpp, A. J.; Pinar, A. B.; Ranocchiari, M.; van Bokhoven, J. A. *Nanoscale* **2017**, *9*, 1144-1153.

(117) Kulkarni, A. R.; Zhao, Z.-J.; Siahrostami, S.; Nørskov, J. K.; Studt, F. *ACS Catal.* **2016**, *6*, 6531-6536.

(118) Tomkins, P.; Mansouri, A.; Bozbag, S. E.; Krumeich, F.; Park, M. B.; Alayon, E. M. C.; Ranocchiari, M.; van Bokhoven, J. A. *Angew. Chem., Int. Ed.* **2016**, *55*, 5467–5471.

(119) Narsimhan, K.; Iyoki, K.; Dinh, K.; Román-Leshkov, Y. *ACS Cent. Sci.* **2016**, *2*, 424-429.

(120) Wulfers, M. J.; Teketel, S.; Ipek, B.; Lobo, R. F. *Chem. Commun.* **2015**, *51*, 4447-4450.

(121) Pappas, D. K.; Borfecchia, E.; Dyballa, M.; Pankin, I. A.; Lomachenko, K. A.; Martini, A.; Signorile, M.; Teketel, S.; Arstad, B.; Berlier, G.; Lamberti, C.; Bordiga, S.; Olsbye, U.; Lillerud, K. P.; Svelle, S.; Beato, P. *J. Am. Chem. Soc.* **2017**, *139*, 14961-14975.

(122) Narsimhan, K.; Michaelis, V. K.; Mathies, G.; Gunther, W. R.; Griffin, R. G.; Román-Leshkov, Y. *J. Am. Chem. Soc.* **2015**, *137*, 1825-1832.

(123) Grundner, S.; Luo, W.; Sanchez-Sanchez, M.; Lercher, J. A. *Chem. Commun.* **2016**, *52*, 2553-2556.

(124) Beznis, N. V.; van Laak, A. N. C.; Weckhuysen, B. M.; Bitter, J. H. *Microporous Mesoporous Mater.* **2011**, *138*, 176-183.

References

(125) Le, H. V.; Parishan, S.; Sagaltchik, A.; Göbel, C.; Schlesiger, C.; Malzer, W.; Trunschke, A.; Schomäcker, R.; Thomas, A. *ACS Catal.* **2017**, *7*, 1403-1412.

(126) Berlier, G.; Spoto, G.; Fisicaro, P.; Bordiga, S.; Zecchina, A.; Giamello, E.; Lamberti, C. *Microchem. J.* **2002**, *71*, 101-116.

(127) Pérez-Ramírez, J.; Mul, G.; Kapteijn, F.; Moulijn, J. A.; Overweg, A. R.; Doménech, A.; Ribera, A.; Arends, I. W. C. E. *J. Catal.* **2002**, *207*, 113-126.

(128) Battiston, A. *J. Catal.* **2003**, *218*, 163-177.

(129) Bordiga, S.; Buzzoni, R.; Geobaldo, F.; Lamberti, C.; Giamello, E.; Zecchina, A.; Leofanti, G.; Petrini, G.; Tozzola, G.; Vlaic, G. *J. Catal.* **1996**, *158*, 486-501.

(130) Ratnasamy, P.; Kumar, R. *Catal. Today* **1991**, *9*, 329-416.

(131) Perezramirez, J.; Groen, J.; Bruckner, A.; Kumar, M.; Bentrup, U.; Debbagh, M.; Villaescusa, L. *J. Catal.* **2005**, *232*, 318-334.

(132) Phu, N. H.; Hoa, T. T. K.; Tan, N. V.; Thang, H. V.; Ha, P. L. *Appl. Catal., B* **2001**, *34*, 267-275.

(133) Dükkancı, M.; Gündüz, G.; Yılmaz, S.; Yaman, Y. C.; Prikhod'ko, R. V.; Stolyarova, I. V. *Appl. Catal., B* **2010**, *95*, 270-278.

(134) Szostak, R.; Nair, V.; Thomas, T. L. *J. Chem. Soc., Faraday Trans. 1* **1987**, *83*, 487-494.

(135) Berlier, G.; Spoto, G.; Bordiga, S.; Ricchiardi, G.; Fisicaro, P.; Zecchina, A.; Rossetti, I.; Selli, E.; Forni, L.; Giamello, E.; Lamberti, C. *J. Catal.* **2002**, *208*, 64-82.

(136) Yuranov, I.; Bulushev, D.; Renken, A.; Kiwiminsker, L. *J. Catal.* **2004**, *227*, 138-147.

(137) Edwards, E. R.; Antunes, E. F.; Botelho, E. C.; Baldan, M. R.; Corat, E. J. *Appl. Surf. Sci.* **2011**, *258*, 641-648.

(138) Yamashita, T.; Hayes, P. *Appl. Surf. Sci.* **2008**, *254*, 2441-2449.

(139) Pu, M.; Ma, Y.; Wan, J.; Wang, Y.; Wang, J.; Brusseau, M. L. *Catal Sci Technol* **2017**, *7*, 1129-1140.

(140) Biesinger, M. C.; Payne, B. P.; Grosvenor, A. P.; Lau, L. W. M.; Gerson, A. R.; Smart, R. S. C. *Appl. Surf. Sci.* **2011**, *257*, 2717-2730.

(141) Yue, Y.; Liu, H.; Yuan, P.; Yu, C.; Bao, X. *Sci. Rep.* **2015**, *5*, 9270.

(142) Graat, P. C. J.; Somers, M. A. J. *Applied Surface Science* **1996**, *100-101*, 36-40.

(143) Roosendaal, S. J.; van Asselen, B.; Elsenaar, J. W.; Vredenberg, A. M.; Habraken, F. H. P. M. *Surface Science* **1999**, *442*, 329-337.

(144) Gentry, S. J.; Hurst, N. W.; Jones, A. *J. Chem. Soc., Faraday Trans. 1* **1979**, *75*, 1688-1699.

(145) Lobree, L. J.; Hwang, I.-C.; Reimer, J. A.; Bell, A. T. *J. Catal.* **1999**, *186*, 242-253.

(146) Kalamaras, C.; Palomas, D.; Bos, R.; Horton, A.; Crimmin, M.; Hellgardt, K. *Catal. Lett.* **2016**, *146*, 483-492.

(147) Tano, T.; Sugimoto, H.; Fujieda, N.; Itoh, S. *Eur. J. Inorg. Chem.* **2012**, *2012*, 4099-4103.

(148) Brandenberger, S.; Kröcher, O.; Tissler, A.; Althoff, R. *Appl. Catal., A* **2010**, *373*, 168-175.

(149) Taboada, J.; Overweg, A.; Kooyman, P.; Arends, I.; Mul, G. *J. Catal.* **2005**, *231*, 56-66.

(150) Garrido-Ramírez, E. G.; Theng, B. K. G.; Mora, M. L. *Appl. Clay Sci.* **2010**, *47*, 182-192.

(151) Navalon, S.; Alvaro, M.; Garcia, H. *Appl. Catal., B* **2010**, *99*, 1-26.

(152) Cele, M. N.; Friedrich, H. B.; Bala, M. D. *J. Mol. Catal. A: Chem.* **2017**, *427*, 39-44.

(153) Palkovits, R.; von Malotki, C.; Baumgarten, M.; Müllen, K.; Baltes, C.; Antonietti, M.; Kuhn, P.; Weber, J.; Thomas, A.; Schüth, F. *ChemSusChem* **2010**, *3*, 277-282.

(154) Palkovits, R.; Antonietti, M.; Kuhn, P.; Thomas, A.; Schüth, F. *Angew. Chem., Int. Ed.* **2009**, *48*, 6909-6912.

(155) Periana, R. A. *Science* **1998**, *280*, 560-564.

(156) Que, L.; Tolman, W. B. *Nature* **2008**, *455*, 333-340.

(157) Haack, P.; Limberg, C. *Angew. Chem., Int. Ed.* **2014**, *53*, 4282-4293.

(158) Sheppard, T.; Hamill, C. D.; Goguet, A.; Rooney, D. W.; Thompson, J. M. *Chem. Commun.* **2014**, *50*, 11053-11055.

(159) Bozbag, S. E.; Alayon, E. M. C.; Pecháček, J.; Nachtegaal, M.; Ranocchiari, M.; van Bokhoven, J. A. *Catal. Sci. Technol.* **2016**, *6*, 5011-5022.

(160) Abu-Zied, B. M.; Schwieger, W.; Unger, A. *Appl. Catal., B* **2008**, *84*, 277-288.

(161) Karge, H. G.; Wichterlova, B.; Beyer, H. K. *J. Chem. Soc., Faraday Trans.* **1992**, *88*, 1345-1351.

(162) Beznis, N. V.; Weckhuysen, B. M.; Bitter, J. H. *Catal. Lett.* **2010**, *138*, 14-22.

(163) Alayon, E. M. C.; Nachtegaal, M.; Bodi, A.; van Bokhoven, J. A. *ACS Catal.* **2014**, *4*, 16-22.

(164) Shah, R.; Gale, J. D.; Payne, M. C. *J. Phys. Chem.* **1996**, *100*, 11688-11697.

(165) Mirth, G.; Lercher, J. A.; Anderson, M. W.; Klinowski, J. *J. Chem. Soc., Faraday Trans.* **1990**, *86*, 3039-3044.

(166) Baerlocher, C.; McCusker, L. B.; Olson, D. H. In *Atlas of Zeolite Framework Types (Sixth Edition)*; Elsevier Science B.V.: Amsterdam, 2007, pp 218-219.

(167) Liu, K.-L.; Kubarev, A. V.; Van Loon, J.; Uji-i, H.; De Vos, D. E.; Hofkens, J.; Roeffaers, M. B. J. *ACS Nano* **2014**, *8*, 12650-12659.

(168) Zhao, Z.-J.; Kulkarni, A.; Vilella, L.; Nørskov, J. K.; Studt, F. *ACS Catal.* **2016**, *6*, 3760-3766.

(169) Veefkind, V. A.; Smidt, M. L.; Lercher, J. A. *Appl. Catal., A* **2000**, *194–195*, 319-332.

(170) Makarova, M. A.; Wilson, A. E.; van Liemt, B. J.; Mesters, C. M. A. M.; de Winter, A. W.; Williams, C. *J. Catal.* **1997**, *172*, 170-177.

(171) Sainz-Vidal, A.; Balmaseda, J.; Lartundo-Rojas, L.; Reguera, E. *Microporous Mesoporous Mater.* **2014**, *185*, 113-120.

(172) Ma, L.; Cheng, Y.; Cavataio, G.; McCabe, R. W.; Fu, L.; Li, J. *Chem. Eng. J.* **2013**, *225*, 323-330.

(173) Sultana, A.; Nanba, T.; Sasaki, M.; Haneda, M.; Suzuki, K.; Hamada, H. *Catal. Today* **2011**, *164*, 495-499.

(174) Pereda-Ayo, B.; De La Torre, U.; Illán-Gómez, M. J.; Bueno-López, A.; González-Velasco, J. R. *Appl. Catal., B* **2014**, *147*, 420-428.

(175) Liu, J.; Song, W.; Xu, C.; Liu, J.; Zhao, Z.; Wei, Y.; Duan, A.; Jiang, G. *RSC Adv.* **2015**, *5*, 104923-104931.

(176) Qin, J.-X.; Wang, Z.-M.; Liu, X.-Q.; Li, Y.-X.; Sun, L.-B. *J. Mater. Chem. A* **2015**, *3*, 12247-12251.

(177) Richter, M.; Fait, M.; Eckelt, R.; Schneider, M.; Radnik, J.; Heidemann, D.; Fricke, R. *J. Catal.* **2007**, *245*, 11-24.

(178) Valverde, J.; Dorado, F.; Sánchez, P.; Asencio, I.; Romero, A. In *Interfacial Applications in Environmental Engineering*, Keane, M. A., Ed.; CRC Press: New York, 2002.

(179) Tkachenko, O. P.; Klementiev, K. V.; van den Berg, M. W. E.; Koc, N.; Bandyopadhyay, M.; Birkner, A.; Wöll, C.; Gies, H.; Grünert, W. *J. Phys. Chem. B* **2005**, *109*, 20979-20988.

(180) Vanelderen, P.; Vancauwenbergh, J.; Tsai, M. L.; Hadt, R. G.; Solomon, E. I.; Schoonheydt, R. A.; Sels, B. F. *ChemPhysChem* **2014**, *15*, 91-99.

(181) Wang, L.; Li, W.; Qi, G.; Weng, D. *J. Catal.* **2012**, *289*, 21-29.

(182) Luo, M.-F.; Fang, P.; He, M.; Xie, Y.-L. *J. Mol. Catal. A: Chem.* **2005**, *239*, 243-248.

(183) Bulánek, R.; Wichterlová, B.; Sobalík, Z.; Tichý, J. *Appl. Catal., B* **2001**, *31*, 13-25.

(184) Sklenak, S.; Andrikopoulos, P. C.; Whittleton, S. R.; Jirglova, H.; Sazama, P.; Benco, L.; Bucko, T.; Hafner, J.; Sobalik, Z. *J. Phys. Chem. C* **2013**, *117*, 3958-3968.

(185) Göltl, F.; Sautet, P.; Hermans, I. *Angew. Chem., Int. Ed.* **2015**, *54*, 7799-7804.

(186) Liu, X. In *Zeolite Characterization and Catalysis*, Chester, A. W.; Derouane, E. G., Eds.; Springer: Dordrecht, 2009, pp 197-222.

(187) Delabie, A.; Pierloot, K.; Groothaert, M. H.; Weckhuysen, B. M.; Schoonheydt, R. A. *Phys. Chem. Chem. Phys.* **2002**, *4*, 134-145.

(188) Paolucci, C.; Parekh, A. A.; Khurana, I.; Di Iorio, J. R.; Li, H.; Albarracin Caballero, J. D.; Shih, A. J.; Anggara, T.; Delgass, W. N.; Miller, J. T.; Ribeiro, F. H.; Gounder, R.; Schneider, W. F. *J. Am. Chem. Soc.* **2016**, *138*, 6028-6048.

(189) Himes, R. A.; Karlin, K. D. *Proc. Natl. Acad. Sci.* **2009**, *106*, 18877-18878.

(190) Vanelderen, P.; Vancauwenbergh, J.; Sels, B. F.; Schoonheydt, R. A. *Coord. Chem. Rev.* **2013**, *257*, 483-494.

(191) Pinar, A. B.; Gómez-Hortigüela, L.; McCusker, L. B.; Pérez-Pariente, J. *Chem. Mater.* **2013**, *25*, 3654-3661.

(192) Zhu, J.; Kailasam, K.; Xie, X.; Schomaecker, R.; Thomas, A. *Chem. Mater.* **2011**, *23*, 2062-2067.

(193) Yang, Q.; Gu, F.; Tang, Y.; Zhang, H.; Liu, Q.; Zhong, Z.; Su, F. *RSC Adv.* **2015**, *5*, 26815-26822.

(194) Mahyuddin, M. H.; Staykov, A.; Shiota, Y.; Miyanishi, M.; Yoshizawa, K. *ACS Catal.* **2017**, *7*, 3741-3751.

(195) Smeets, P. J.; Groothaert, M. H.; Schoonheydt, R. A. *Catal. Today* **2005**, *110*, 303-309.

(196) Mahyuddin, M. H.; Staykov, A.; Shiota, Y.; Yoshizawa, K. *ACS Catal.* **2016**, *6*, 8321-8331.

(197) Liu, C.-H.; Lai, N.-C.; Lee, J.-F.; Chen, C.-S.; Yang, C.-M. *J. Catal.* **2014**, *316*, 231-239.

(198) de Carvalho, M. C. N. A.; Passos, F. B.; Schmal, M. *Appl. Catal., A* **2000**, *193*, 265-276.

(199) Ismagilov, Z. R.; Yashnik, S. A.; Anufrienko, V. F.; Larina, T. V.; Vasenin, N. T.; Bulgakov, N. N.; Vosel, S. V.; Tsykoza, L. T. *Appl. Surf. Sci.* **2004**, *226*, 88-93.

(200) Nauert, S. L.; Schax, F.; Limberg, C.; Notestein, J. M. *J. Catal.* **2016**, *341*, 180-190.

(201) Monazam, E. R.; Siriwardane, R.; Breault, R. W.; Tian, H.; Shadle, L. J.; Richards, G.; Carpenter, S. *Energy Fuels* **2012**, *26*, 2779-2785.

(202) Adánez, J.; Gayán, P.; Celaya, J.; de Diego, L. F.; García-Labiano, F.; Abad, A. *Ind. Eng. Chem. Res.* **2006**, *45*, 6075-6080.

(203) Guilhaume, N.; Primet, M. *J. Chem. Soc., Faraday Trans.* **1994**, *90*, 1541-1545.

(204) Schax, F.; Limberg, C.; Mügge, C. *Eur. J. Inorg. Chem.* **2012**, *2012*, 4661-4668.

(205) Ikuno, T.; Zheng, J.; Vjunov, A.; Sanchez-Sanchez, M.; Ortuno, M. A.; Pahls, D. R.; Fulton, J. L.; Camaioni, D. M.; Li, Z.; Ray, D.; Mehdi, B. L.; Browning, N. D.; Farha, O. K.; Hupp, J. T.; Cramer, C. J.; Gagliardi, L.; Lercher, J. A. *J. Am. Chem. Soc.* **2017**.

Publications and Presentations

Publications

Ha Vu Le, Samira Parishan, Anton Sagaltchik, Caren Göbel, Christopher Schlesiger, Wolfgang Malzer, Annette Trunschke, Reinhard Schomäcker, and Arne Thomas, *'Solid-state ion-exchanged Cu/mordenite catalysts for the direct conversion of methane to methanol'*, ACS Catalysis, 2017, 7(2), 1403-1412.

Ha Vu Le, Samira Parishan, Anton Sagaltchik, Hamideh Ahi, Annette Trunschke, Reinhard Schomäcker, and Arne Thomas, *'Stepwise methane-to-methanol conversion on CuO/SBA-15'*, submitted.

Ha Vu Le, Maximilian Neumann, Reinhard Schomäcker, Arne Thomas, *'Fe-zeolites as solid catalysts for the hydroxylation of methane with hydrogen peroxide*, to be submitted.

Oral presentation

Ha Vu Le, Samira Parishan, Anton Sagaltchik, Maike Hashagen, Annette Trunschke, Reinhard Schomäcker, and Arne Thomas, *'Activity and characterization of solid-state ion-exchanged Cu/mordenite for direct production of methanol from methane and oxygen'*, 8th World Congress on Oxidation Catalysis, 09/2017, Krakow, Poland.

Poster presentations

Ha Vu Le, Samira Parishan, Anton Sagaltchik, Caren Göbel, Christopher Schlesiger, Wolfgang Malzer, Annette Trunschke, Reinhard Schomäcker, and Arne Thomas, '*Enhanced production of methanol from methane over Cu/mordenites prepared by solid-state ion exchange*', 50. Jahrestreffen Deutscher Katalytiker, 03/2017, Weimar, Germany.

Ha V. Le, Samira Parishan, Caren Göbel, Annette Trunschke, Reinhard Schomäcker, Arne Thomas, '*A more efficient Cu-containing zeolite catalyst for direct conversion of methane to methanol*', 11th Natural Gas Conversion Symposium, 06/2016, Tromsø, Norway.

Ha Vu Le, Reinhard Schomäcker, Arne Thomas, '*Fe- and Cu-containing zeolites as solid catalysts for partial oxidation of methane to methanol by hydrogen peroxide*', 49. Jahrestreffen Deutscher Katalytiker, 03/2016, Weimar, Germany.

Curriculum Vitae

Full name: Ha Vu Le

Date of birth: 20/11/1987

Place of birth: Quang Ngai, Vietnam

Education

10/2013 – present: Ph.D. in chemistry, Technische Universität Berlin, Germany

Supervisors: Prof. Dr. Arne Thomas and Prof. Dr. Reinhard Schomäcker

Thesis: Bioinspired solid catalysts for the hydroxylation of methane

08/2010 – 06/2012: M.Eng. in chemical engineering, Ho Chi Minh City University of Technology, Vietnam.

Supervisors: Prof. Dr. Nam Phan

Thesis: Greener synthesis of pravadoline using imidazolium-based ionic liquids as recyclable solvents

09/2005 – 04/2010: B.Eng. in chemical engineering, Ho Chi Minh City University of Technology, Vietnam.

Supervisors: Prof. Dr. Nam Phan

Thesis: Magnetic nanoparticles-supported palladium catalyst for the Sonogashira reaction